

# The Mediterranean forecasting system.

## Part I: evolution and performance

Giovanni Coppini<sup>1,\*</sup>, Emanuela Clementi<sup>2</sup>, Gianpiero Cossarini<sup>3</sup>, Stefano Salon<sup>3</sup>, Gerasimos Korres<sup>4</sup>, Michalis Ravdas<sup>4</sup>, Rita Lecci<sup>1</sup>, Jenny Pistoia<sup>2</sup>, Anna Chiara Goglio<sup>2</sup>, Massimiliano Drudi<sup>1</sup>, Alessandro Grandi<sup>1</sup>, Ali Aydogdu<sup>2</sup>, Romain Escudier<sup>2,5</sup>, Andrea Cipollone<sup>2</sup>, Vladislav Lyubartsev<sup>1</sup>, Antonio Mariani<sup>1</sup>, Sergio Creti<sup>1</sup>, Francesco Palermo<sup>1</sup>, Matteo Scuro<sup>1</sup>, Simona Masina<sup>2</sup>, Nadia Pinardi<sup>6,7</sup>, Antonio Navarra<sup>6,8</sup>, Damiano Delrosso<sup>9</sup>, Anna Teruzzi<sup>3</sup>, Valeria Di Biagio<sup>3</sup>, Giorgio Bolzon<sup>3</sup>, Laura Feudale<sup>3</sup>, Gianluca Coidessa<sup>3</sup>, Carolina Amadio<sup>3</sup>, Alberto Brosich<sup>3</sup>, Arnau Miró<sup>10</sup>, Eva Alvarez<sup>3</sup>, Paolo Lazzari<sup>3</sup>, Cosimo Solidoro<sup>3</sup>, Charikleia Oikonomou<sup>4</sup>, Anna Zacharioudaki<sup>4</sup>

<sup>1</sup> Ocean Predictions and Applications Division, Fondazione Centro Euro-Mediterraneo sui Cambiamenti Climatici (CMCC), Italy

<sup>2</sup> Ocean Modeling and Data Assimilation Division, Centro Euro-Mediterraneo sui Cambiamenti Climatici (CMCC), Italy

<sup>3</sup> Istituto Nazionale di Oceanografia e di Geofisica Sperimentale (OGS), Italy

<sup>4</sup> Hellenic Centre for Marine Research (HCMR), Greece

<sup>5</sup> Mercator Océan International, France

<sup>6</sup> Centro Euro-Mediterraneo sui Cambiamenti Climatici (CMCC), Bologna, Italy

<sup>7</sup> Department of Physics and Astronomy, Università di Bologna, Bologna, Italy

<sup>8</sup> Department of Biological, Geological and Environmental Sciences (BIGEA), Università di Bologna, Bologna, Italy

<sup>9</sup> Istituto Nazionale di Geofisica e Vulcanologia (INGV), Italy

<sup>10</sup> Barcelona Supercomputing Center, Barcelona (BSC), Spain

Correspondence to: Giovanni Coppini [giovanni.coppini@cmcc.it](mailto:giovanni.coppini@cmcc.it)

**Abstract.** The Mediterranean Forecasting System produces operational analyses, reanalyses and 10-day forecasts for many Essential Ocean Variables (EOVs), from currents, temperature, salinity, sea level to wind waves and pelagic biogeochemistry. The products are available at a horizontal resolution of 1/24 degrees (approximately 4 km) and 141 unevenly spaced vertical levels.

The core of the Mediterranean Forecasting System is constituted by the physical (PHY), the biogeochemical (BIO) and the wave (WAV) components, consisting of both numerical models and data assimilation modules. The 3 components together constitute the so-called Mediterranean Monitoring and Forecasting Center (Med-MFC) of the Copernicus Marine Service.

Daily 10-day forecasts are produced by the PHY, BIO and WAV operational systems as well as analyses, while reanalyses are produced for the past 30 years about every ~3 years and extended (yearly). The modelling systems, their coupling strategy and evolutions are illustrated in detail. For the first time, the quality of the products is documented in terms of skill metrics evaluated on a common three-year period (2018-2020), giving the first complete assessment of uncertainties for all the Mediterranean environmental variable analyses.

Formatted: Font colour: Text 1

Formatted: Font colour: Text 1

Deleted: Systems

Deleted: coupled offline

Deleted: Med-MFC

Deleted: components

Deleted: evolution is

39 **1 Introduction**

40 Ocean analysis and forecasting systems are now available for the global and world ocean regional seas at different spatial  
41 scales and with different numbers of Essential Ocean Variables (EOV) considered (Tonani et al., 2015). The societal drivers  
42 for the operational products stemming out of the ocean analysis and forecasting products are the safety of maritime transport,  
43 multiple coastal hazards and climate anomalies. Moreover, the operational products are at the basis of new understanding of  
44 the dynamics of the ocean circulation (Pinardi et al., 2015), its linked biogeochemical cycles, among others, carbon uptake and  
45 eutrophication (Melaku Kanu et al., 2015; von Schuckmann et al., 2020) and extreme storm surge events (Giesen et al., 2021).  
46 The ocean analysis and forecasting system for the entire Mediterranean Sea was set up in the past 15 years (Pinardi and  
47 Coppini, 2010; Pinardi et al., 2017; Lazzari et al., 2010; Salon et al., 2019; Ravdas et al., 2018; Katsafados et al., 2016) and  
48 in 2015 it became operational in the framework of the Copernicus Marine Service which is the marine component of the  
49 Copernicus Programme European Union service for a sustainable use of the ocean providing free, regular and systematic  
50 information on the state of the Blue (physical), White (sea ice) and Green (biogeochemical) ocean on the global and regional  
51 scales. The Copernicus Marine service in Europe has shown the strength of a state-of-the-art operational service implemented  
52 by hundreds of experts and teams, distributed throughout Europe, coming from public and private sectors, from operational  
53 and research organisations, from different countries, from diverse cultures and relations to the ocean (Le Traon et al., 2017;  
54 Alvarez Fanjul et al., 2022). In this paper we give an overview of the “core” components of the system, i.e., the numerical  
55 models and the data assimilation modules that represent the eddy-resolving ocean general circulation, the biogeochemical  
56 tracers and the wind waves. Furthermore, we will document the quality of EOV products using goodness indices (Brassington  
57 et al., 2017). The core components constitute the so-called Mediterranean Monitoring and Forecasting Center (Med-MFC) of  
58 Copernicus Marine Service (Le Traon et al., 2019). The integrated approach of Med-MFC system represents a unique  
59 opportunity for the users who are able to access state-of-the-art data coupled and provided in a uniform manner (e.g., same  
60 grid, unique format, unique point of access).

61 This ocean analysis and forecasting system, hereafter Med-MFC, produces analyses, 10 days forecasts and reanalysis (Adani  
62 et al., 2011; Pinardi et al., 2015; von Schuckmann et al., 2016; von Schuckmann et al., 2018; von Schuckmann et al., 2019;  
63 Terzic et al., 2021; Simoncelli et al., 2016; Simoncelli et al., 2019; Ravdas et al., 2018; Escudier et al., 2020; Escudier et al.,  
64 2021; Cossarini et al., 2021).

65 An essential task of the production activities concerns the continuous assessment of the quality of the products (Sotillo et al.,  
66 2021; Alvarez Fanjul et al., 2022) which is achieved at two levels: (i) the pre-qualification of the systems before delivering a  
67 new release, including an extensive scientific validation of the products, published in the Quality Information Documents  
68 (QUIDs) available on the Copernicus Marine Product Catalogue; (ii) the operational evaluation of the skill metrics during  
69 operations, made available through the Copernicus Marine Product Quality Dashboard Website (<https://pqd.mercator-ocean.fr>), as well as through the Mediterranean regional validation websites implemented at the level of the Med-MFC  
70 production units (PHY: <https://medfs.cmcc.it/>, WAV: <http://Med-MFC-wav.hcmr.gr/>, BIO: [www.medeaf.ogs.it/NRT-](http://www.medeaf.ogs.it/NRT-)

Deleted: ,

Formatted: Font: (Default) Times New Roman, Font colour: Text 1

Formatted: Font: (Default) Times New Roman, Font colour: Text 1

Formatted: Font: (Default) Times New Roman, Font colour: Text 1

Deleted: Katsafados et al. 2016).

Deleted: Med-MFC

Deleted: PY

Deleted: MED-MFC

Deleted: Med-MFC

Deleted: von Schekumann

Deleted: von Schekumann

Deleted: von Schekumann

Formatted: Font: (Default) Times New Roman, Font colour: Text 1

Formatted: Font: (Default) Times New Roman, Font colour: Text 1

Formatted: Font: (Default) Times New Roman, Font colour: Text 1

Deleted: ,

Deleted: ).

Formatted: Font: (Default) Times New Roman, Font colour: Text 1

Formatted: Font: (Default) Times New Roman, Font colour: Text 1

Formatted: Font: (Default) Times New Roman, Font colour: Text 1

83 validation). All the delivered variables are thus validated with respect to satellite and in-situ observations using Copernicus  
84 Marine observational datasets, as well as additional datasets, climatologies or literature information when needed.

85 The Mediterranean Sea is a semi-enclosed basin with an anti-estuarine circulation corresponding to a 0.9/0.8 ±0.06 Sv  
86 baroclinic inflow/outflow at the Strait of Gibraltar. positive energy inputs by the winds, net buoyancy losses inducing a  
87 vigorous overturning circulation (Cessi et al., 2014; Pinardi et al., 2019). The basin scale circulation is dominated by mesoscale  
88 and sub-mesoscales variability (Pinardi et al., 2016; Bergamasco et al., 2010; Pinardi et al., 2006; Robinson et al., 2001; Ayoub  
89 et al., 1998), the former subdivided into semi-permanent and synoptic mesoscales with a spatial scale larger than 4-6 times the  
90 local Rossby radius of deformation. The stratification is large during summer in the first 50 meters and during winter the water  
91 column is practically unstratified. The Mediterranean Sea is an oligotrophic basin (Siokou-Frangou et al., 2010) with a west-  
92 to-east decreasing productivity gradient (Lazzari et al., 2012) and relatively high primary productivity in open ocean areas  
93 where winter mixing increases surface nutrients (Cossarini et al., 2019). The wave conditions are driven by the winter  
94 storminess, while summer is characterised by low significant wave height values and higher value scatter (Ravdas et al., 2018).

95 The yearly mean wave period, as estimated from available wave buoys over the Mediterranean Sea, amounts to 3.82 s with  
96 typical deviations of 0.92 s, while the mean significant wave height is 0.82 m (1.28 m as estimated by satellite observations)  
97 with typical deviations of 0.67 m/67m (0.77 m for satellite data).

98 In this paper we describe the final set up of the Med-MFC core components for the period 2017-2020. The Med-MFC  
99 modelling systems share the same grid resolution (1/24°), bathymetry and use the same atmospheric and river forcing fields.  
100 Moreover, daily mean fields evaluated by the physical model are used to force the wave component (surface currents) and the  
101 transport-biogeochemical model (temperature, salinity, horizontal and vertical velocities, sea level, diffusivity). This allows  
102 several model parametrizations to be calibrated to obtain the best result in term of the specific environmental variable  
103 considered by each component. In the Copernicus Marine Service the approach of forcing waves and biogeochemistry models  
104 with information from the hydrodynamic models is used and represents a standard which is also applied for the other MFCs.  
105 Several MFCs also foreseen the online coupling between physics and waves models and between physics and biogeochemical  
106 models. Furthermore, this weakly coupled system ensures an efficient development of the data assimilation modules connected  
107 to each numerical model modules and specific input data sets. It is a distributed system that shares information when and how  
108 it is required by relevant processes, with efficiency and effectiveness. Due its rather unique structure and the quality of its  
109 products the system described could be used as a basic standard for new systems to be developed.

110 The paper is organised as follows. Section 2 overviews the technical specifications of the Med-MFC components, Section 3  
111 describes the quality of the system for a reference period from 2018 to 2020 and of the forcing, Section 4 concludes the paper  
112 and presents future perspectives.

113 The Part II (or the second part) of the paper will demonstrate the capacities of the Med-MFC components in describing the  
114 Medicane effects on the ocean. In particular, the Med-MFC physics, biogeochemistry and waves components will be used to  
115 describe the effects of Medicane Zorbas (27-30 September 2018) on the ocean variables.

**Formatted:** Font: (Default) Times New Roman, Font colour: Text 1

**Formatted:** Font: (Default) Times New Roman, Font colour: Text 1

**Deleted:** The Mediterranean Sea is a semi-enclosed basin with an anti-estuarine circulation corresponding to a 0.9/0.8 Sv baroclinic inflow/outflow at the Strait of Gibraltar,

**Deleted:** (Terzic et al., 2021).

**Deleted:** the

**Formatted:** Font: (Default) Times New Roman, Font colour: Text 1

**Deleted:** Mean wave periods are around 5 s and mean significant wave height is 3 m.

**Formatted:** Font: (Default) Times New Roman, Font colour: Text 1

**Formatted:** Font: (Default) Times New Roman, Font colour: Text 1

**Deleted:** Med-MFC

**Formatted:** Font: (Default) Times New Roman, Font colour: Text 1

**Formatted:** Font: (Default) Times New Roman, Font colour: Text 1

**Deleted:** The PHY component is offline coupled daily to the biochemical and wave components.

**Formatted:** Font: (Default) Times New Roman, Font colour: Text 1

**Deleted:** Med-MFC

## 2. Description of the Med-MFC core components

The structure of the Med-MFC core components is shown in Figure 1: the physical component (PHY) is composed of the NEMO general circulation model (Madec et al., 2019) coupled to the WaveWatch-III (WW3) wave model (Clementi et al., 2017a) and the ocean data assimilation OceanVar 3DVAR (Dobricic and Pinardi, 2008 and Storto et al., 2015); the biogeochemical component (BIO) is composed of the Biogeochemical Flux Model (BFM), the tracer transport (OGSTM) and a data assimilation scheme (Lazzari et al., 2012; Lazzari et al., 2016; Cossarini et al., 2015; Vichi et al., 2020), forced daily by the daily mean of the PHY component fields; the wave component (WAV) is composed of the wave model WAM (WAMDL Group, 1988) and its assimilation scheme, forced daily by the daily mean of the PHY component fields. Daily 10 days forecasts are produced with all PHY, BIO and WAVE components as well as analyses and reanalyses as described below.

Each component of the Med-MFC has its own data assimilation system, so that important effort was made to extract the most relevant information from satellite and in-situ observations to produce analysis and correct initial conditions for the forecast in order to benefit the forecasting skills. The main goal of the paper is to present the current quality of the operational system components by comparing the analysis and - for specific variables, such as significant wave height - the background (simulation) with observations, in-situ and/or satellites. The skill of the wave and biogeochemical models is assessed by considering inter-comparisons of the model solution during the 24-h analysis phase with in-situ and remotely sensed observations. As the latter are ingested into the model through data assimilation, the first guess model fields (i.e. model background) are used instead of analyses.

### 2.1. The general circulation model component

#### 2.1.1. Numerical model description

The PHY numerical model component comprises a two-way coupled current-wave model based on NEMO and WW3 implemented over the whole Mediterranean basin and extended into the Atlantic Sea in order to better resolve the exchanges with the Atlantic Ocean (Figure 2). The model horizontal grid resolution is  $1/24^\circ$  (ca. 4 km) and is resolved along 141 unevenly spaced vertical levels (Clementi et al., 2017b; Clementi et al., 2019). The topography is an interpolation of the GEBCO 30 arc second grid (Weatherall et al., 2015) filtered and specifically modified in critical areas such as: the Eastern Adriatic coastal areas (to avoid instabilities in circulation due to the presence of a large number of small islands), Gibraltar and Messina straits (to better represent the transports), Atlantic edges external border (to avoid large bathymetric inconsistencies with respect to the Copernicus Global Analysis and Forecast product in which the model is nested). All the numerical model choices are documented in Table A1.

The general circulation model considers the non-linear free surface formulation and vertical z-star coordinates. The numerical scheme uses the time-splitting formulation to solve the free surface and the barotropic equations with a (100 times) smaller time step with respect to the one used to evaluate the prognostic 3D variables (240 seconds). The active tracers (temperature and salinity) advection scheme is a mixed up-stream/MUSCL (Monotonic Upwind Scheme for Conservation Laws; Levy et

**Deleted:** Med-MFC

**Deleted:** Med-MFC

**Deleted:** (ref)

**Deleted:** coupled

**Deleted:** to

**Deleted:** AMDI

**Deleted:** coupled

**Deleted:** to

**Deleted:** components

**Formatted:** Font: (Default) Times New Roman, Font colour: Text 1

**Formatted:** Font: (Default) Times New Roman, Font colour: Text 1

**Formatted:** Font: (Default) Times New Roman, Font colour: Text 1

**Deleted:** The topography is an interpolation of the

**Deleted:** GEBCO 30arc-second grid ([http://www.gebco.net/data\\_and\\_products/gridded\\_bathymetry\\_data/gebco\\_30\\_second\\_grid/](http://www.gebco.net/data_and_products/gridded_bathymetry_data/gebco_30_second_grid/)), filtered and specifically modified in critical areas such as: the Eastern Adriatic coastal areas, Gibraltar and Messina straits, Atlantic external border.

174 al., 2001) as modified in Oddo et al. (2009). The vertical diffusion and viscosity terms are defined as a function of the  
175 Richardson number, following Pacanowski and Philander (1981). The air-sea surface fluxes of momentum, mass, and heat are  
176 computed using bulk formulae described in Pettenuzzo et al. (2010) and the Copernicus satellite gridded SST data (Buongiorno  
177 Nardelli et al., 2013) is used to correct the non-solar heat flux using a relaxation constant of  $110 \text{ Wm}^{-2}\text{K}^{-1}$  centred at midnight.  
178 A detailed description of other specific features of the model implementations can be found in Tonani et al. (2008), Oddo et  
179 al. (2009), and Oddo et al. (2014).

180 The wave model WW3 is discretized by means of 24 directional bins ( $15^\circ$  resolution) and 30 frequency bins (ranging between  
181  $0.05 \text{ Hz}$  and  $0.7931 \text{ Hz}$ ) to represent the wave spectral distribution. The wave model is implemented using the same bathymetry  
182 and grid of the hydrodynamic model and uses the surface currents to evaluate the wave refraction, but assumes no interactions  
183 with the ocean bottom. The Mediterranean implementation of WW3 follows WAM cycle4 model physics (Gunter et al., 1993);  
184 the wind input and dissipation terms are based on Janssen's quasi-linear theory for wind-wave generation (Jansen, 1989;  
185 Jansen, 1991), the wave dissipation term is based on Hasselmann (1974) whitecapping theory according to Komen et al. (1984)  
186 and the non-linear wave-wave interaction is modelled using the Discrete Interaction Approximation (DIA, Hasselmann et al.,  
187 1985). The exchanges between the circulation and wave models are performed using an online two-way coupling between  
188 NEMO and WW3. The models are forced by the same atmospheric fields (high resolution ECMWF analysis and forecast  
189 winds) and are two-way coupled at hourly intervals exchanging the following fields: NEMO sends to WW3 the sea surface  
190 currents and temperature which are then used to evaluate the wave refraction and the wind speed stability parameter,  
191 respectively. The neutral drag coefficient computed by WW3 is passed to NEMO to compute the surface wind stress.

192 The NEMO-WW3 coupled system is intended to provide the representation of current-wave interaction processes in the ocean  
193 general circulation. At the moment the feedback is considered only for the surface wind stress drag coefficient and more details  
194 on this wave-current model coupling can be found in Clementi et al. (2017a).

### 195 2.1.2. Model initialization, external forcing and boundary conditions

196 The PHY component was initialised in January 2015 using temperature and salinity winter climatological fields from WOA13  
197 V2 (World Ocean Atlas 2013 V2, <https://www.nodc.noaa.gov/OC5/woa13/woa13data.html>). The atmospheric forcing fields  
198 for both NEMO and WW3 models are from the  $1/8^\circ$  horizontal resolution at 6 hours temporal frequency (3 hours frequency is  
199 used to force the first 3 days of forecast) operational analysis fields from the European Centre for Medium-Range Weather  
200 Forecast (ECMWF) Integrated Forecasting System (IFS), a higher spatial resolution of  $1/10^\circ$  (with higher forecast temporal  
201 frequency of 1-3-6 hours according to the forecast leading time) is used starting from year 2020.  
202 The circulation model's lateral open boundary conditions (LOBC) in the Atlantic Ocean are provided by the Copernicus Global  
203 Analysis and Forecast product (Lellouche et al., 2018) at  $1/12^\circ$  horizontal resolution and 50 vertical levels. Daily mean fields  
204 are used, and the numerical schemes applied at the open boundaries are the Flather (1976) radiation scheme for the barotropic  
205 velocity and the Orlanski (1976) radiation condition (normal projection of oblique radiation case) with adaptive nudging  
206 (Marchesiello et al., 2001) for the baroclinic velocity and the tracers. The nesting technique is detailed in Oddo et al. (2009),

Deleted: .,

Deleted: ),

Deleted: The exchanges between the hydrodynamic and wave models are performed using an online hourly two-way coupling which provides to WW3 the air-sea temperature difference and the surface currents evaluated by NEMO, while the neutral drag coefficient estimated in WW3 is sent to NEMO to evaluate the surface wind stress.

Formatted: Font: (Default) Times New Roman, Font colour: Text 1

Deleted: 2017

Formatted: Font colour: Text 1

Deleted: The atmospheric forcing fields for both NEMO and WW3 models are from 6 hours (3 hours for the first 3 days of forecast),  $0.125^\circ$  horizontal resolution operational analysis and forecast fields from the European Centre for Medium-Range Weather Forecast (ECMWF); a higher spatial ( $0.1^\circ$  in horizontal) and temporal resolution dataset is used starting from year 2020.

222 who also show a marked improvement in the salinity characteristics of the Modified Atlantic Water and in the Mediterranean  
 223 sea level seasonal variability. The Dardanelles Strait boundary conditions (Delrosso, 2020) consist of a merge between the  
 224 Copernicus global ocean products and daily climatology derived from a Marmara Sea box model (Maderich et al., 2015). The  
 225 WW3 model implementation considers closed boundaries in both Atlantic Ocean and Dardanelles strait.  
 226 The river runoff inputs consist of monthly climatological data for 39 major rivers (characterized by an average discharge larger  
 227 than 50 m<sup>3</sup>/s) with a prescribed constant salinity at river mouth (Delrosso, 2020) evaluated by means of sensitivity experiments  
 228 and listed in Table A.4. More realistic and time varying river salinity values (at least for major rivers) will be evaluated in  
 229 future modeling evolutions using an estuary box model, such as the one presented in Verri et al. (2020), coupled to the  
 230 hydrodynamic model.

### 231 2.1.3 The data assimilation component

232 A 3D-variational data assimilation scheme, called OceanVar, initially developed by Dobricic and Pinardi (2008) and further  
 233 improved for a wide range of ocean data assimilation applications (Storto et al., 2015) is coupled to NEMO.

234 The OceanVar scheme aims to minimise the cost function as described in the following Eq. (1):

$$235 J = \frac{1}{2} \delta x^T B^{-1} \delta x + \frac{1}{2} (H \delta x - d)^T R^{-1} (H \delta x - d), \quad (1)$$

237 where  $\delta x = x - x_b$ , and  $x$  is the unknown ocean state, equal to the analysis  $x_a$  at the minimum of  $J$ ,  $x_b$  is the background state,  
 238  $d = y - H(x_b)$  is the misfit between an observation  $y$  and its modelled correspondent mapped onto the observation space to  
 239 the observation location by the observation operator,  $H$ .

241 In OceanVar, the background error covariance matrix is considered as  $B = VV^T$ , where  $V$  is a sequence of linear operators:  
 242  $V = V_\eta V_H V_V$ . Multivariate EOFs (Empirical Orthogonal Functions, described in Dobricic et al., 2006 and Pistoia et al., 2017)  
 243 compose the vertical component operator,  $V_V$ . EOFs are computed in every grid point for the sea surface height, temperature  
 244 and salinity using a three-year simulation in order to capture the mesoscale eddy variability that is assumed to represent the  
 245 unbalanced component of the background error covariance. The horizontal covariances,  $V_H$ , are modelled by an iterative  
 246 recursive filter (Dobricic and Pinardi, 2008; Storto et al., 2014). In order to assimilate altimeter observations, the dynamic height  
 247 operator,  $V_\eta$ , developed in Storto et al. (2011) is used. A reference level of 1000 m is used for this operator so SLA along track  
 248 observations over water shallower than this depth are not assimilated.

249 The observational error covariance matrix,  $R$ , is estimated following Desroziers et al. (2005) relationship. The assimilated  
 250 observations include along-track altimeter sea level anomaly from six satellites and in-situ vertical temperature and salinity  
 251 profiles from Argo floats. The SLA tracks provided by nadir altimeters are assimilated by subsampling every second  
 252 observation to reduce the spatial correlation between consecutive measurements. A special quality control procedure is applied  
 253 to the Argo data before they are assimilated. It consists of removing not good quality profiles, rejecting observations with

**Deleted:** The general circulation model lateral open boundary conditions (LOBC) in the Atlantic Ocean are

**Deleted:** provided by the Copernicus Global Analysis and Forecast products (Lellouche et al., 2018) at 1/12° horizontal resolution and 50 vertical levels.

**Deleted:** The river runoff inputs consist of monthly climatological data for 39 major rivers (characterised by an average discharge larger than 50 m<sup>3</sup>/s) with a prescribed constant salinity at river mouth (Delrosso, 2020) and listed in Table A.4.

**Formatted:** Font: (Default) Times New Roman, Font colour: Text 1

**Deleted:** )

**Formatted:** Font colour: Text 1

**Formatted:** Font colour: Text 1

**Formatted:** Font: (Default) Times New Roman

**Formatted:** Font: (Default) Times New Roman

**Formatted:** Font: (Default) Times New Roman

**Formatted:** Font: (Default) Times New Roman

**Deleted:** ) (

**Deleted:** :

**Deleted:** ,

**Deleted:** ,.

**Deleted:** A reference level of 1000 m is used for this operator so SLA along track observations shallower than this depth are not assimilated....

**Formatted:** Font: (Default) Times New Roman, Font colour: Text 1

271 negative temperature and/or salinity, temperature higher than 45°C and salinity higher than 45 PSU, removing profiles with  
272 gaps in the observations of more than 40 m in the first 300 m depth (to avoid possible inconsistencies in the thermocline),  
273 profiles with observations provided only below 35 m depth and observations in the 1<sup>st</sup> model layer (0-2 m). Moreover, a  
274 background quality check is implemented to reject observations whose square departure exceeds the sum of the observational  
275 and background-error variances 64 times in case of SLA and 25 times in case of in-situ temperature and salinity. The quality  
276 checks are applied to each individual observation of each Argo vertical profile and for each altimeter track. The misfits are  
277 computed at the observation time by applying the FGAT (First Guess at the Appropriate Time) procedure and the corrections  
278 to the background are applied once a day to the restart file using observations within a one-day time window.

Deleted: 45°C

Deleted: 45PSU

Deleted: 40m

Deleted: 300m

Deleted: 35m

Deleted: 2m

Formatted: Font: Not Italic

Deleted: ¶

Deleted: The misfits are computed at the observation time by applying the FGAT (First Guess at the Appropriate Time) procedure and the corrections to the background are applied once a day, using observations within a one-day time window.

## 279 2.2. The wind wave component

### 280 2.2.1. Numerical model description

281 The WAV component consists of two nested wave model implementations: the first grid covers the whole Mediterranean Sea  
282 at 1/24° horizontal resolution and it is nested within a coarser resolution wave model grid at 1/6° horizontal resolution  
283 implemented over the Atlantic Ocean (Figure 2).

284 The wave model is based on the state-of-the-art third generation WAM Cycle 4.6.2 which is a modernised and improved  
285 version of the well-known and extensively used WAM Cycle 4 wave model (WAMDI Group, 1988; Komen et al., 1994).  
286 WAM solves the wave transport equation explicitly without any presumption on the shape of the wave spectrum. Its source  
287 terms include the wind input, whitecapping dissipation, nonlinear transfer, and bottom friction. The wind input term is adopted  
288 from (Snyder et al., 1981). The whitecapping dissipation term is based on (Hasselmann, 1974) whitecapping theory. The wind  
289 input and whitecapping dissipation source terms of the present cycle of the wave model are a further development based on  
290 Janssen's quasi-linear theory of wind-wave generation (Jansen, 1989; Jansen, 1991). The nonlinear transfer term is a  
291 parameterization of the exact nonlinear interactions (Komen et al., 1984 and Hasselmann et al., 1985). Lastly, the bottom friction  
292 term is based on the empirical JONSWAP model of (Hasselmann et al., 1973).

Deleted: AMDI

293 The bathymetric map has been constructed using the GEBCO 30arc-second bathymetric data set for the Mediterranean Sea  
294 model and the ETOPO 2 data set (U.S. Department of Commerce, National Oceanic and Atmospheric Administration, National  
295 Geophysical Data Centre, 2006. 2-minute Gridded Global Relief Data) for the North Atlantic model. In both cases mapping  
296 on the model grid was done using bi-linear interpolation accompanied by some degree of isotropic Laplacian smoothing. This  
297 bathymetry is different from the one used for the PHY component, optimized for the specific quality of the wave products.

298 The wave spectrum is discretized using 32 frequencies, which cover a logarithmically scaled frequency band from 0.04177 Hz  
299 to 0.8018 Hz (covering wave periods ranging from approximately 1 s to 24 s) at intervals of  $df/f = 0.1$  and 24 equally spaced  
300 directions (15 degrees bin). The WAV model component runs in shallow water mode considering wave refraction due to depth  
301 and currents in addition to depth-induced wave breaking. Modifications from default values of WAM 4.6.2 have been  
302 performed in the input source functions as a result of a tuning procedure. Specifically, the value of the wave age shift parameter

Deleted: as proposed by

Deleted: )

Deleted: (

318 (ZALP) in the wind input source function was set to 0.011 (0.008 is the default) for the Mediterranean model and the tunable  
319 whitecapping dissipation coefficients  $C_{DS}$  and  $\delta$  were altered from their default values to become  $C_{DS}=1.33$  (2.1 default) and  
320  $\delta = 0.5$  (default value was 0.6). Finally, a limitation to the high-frequency part of the wave spectrum corresponding to the  
321 Cy43r1 ECMWF wave forecasting system (ECMWF, 2016) was also implemented and tested in order to reduce the wave  
322 steepness at very high wind speeds.

### 323 324 2.2.2. Model initialization, external forcing and boundary conditions

325 The WAV component is forced with 10 m above sea surface analysis and forecast ECMWF winds at 1/8° dissemination  
326 resolution. The temporal resolution is 6 h for the analysis, 3 h for the first 3 days of the forecast and 6 h for the rest of the  
327 forecast cycle. From year 2021, a higher spatial (1/10° for both analysis and forecast) and temporal (hourly for forecast days  
328 1-3, 3-hourly for days 4-6 and 6-hourly for days 7-10) resolution dataset is used to force the WAV component. The wind is  
329 bi-linearly interpolated onto the model grids. Sea ice coverage fields used by the North Atlantic wave model are also obtained  
330 from ECMWF. With respect to currents forcing, the WAV model is forced by daily averaged surface currents obtained from  
331 Copernicus Marine Service Med MFC at 1/24° resolution and the North Atlantic model is forced by daily averaged surface  
332 currents obtained from the Copernicus global physical model at 1/12° resolution. The WAV component runs one cycle per day  
333 operating in analysis (for 24 hours in the past - previous day) and forecast (for 10 days in the future) modes. During the analysis  
334 phase, model background is blended through data assimilation with available SWH satellite observations at 3-hourly intervals  
335 and forced with ECMWF analyses 6-hourly winds and daily averaged surface currents.

336 The Mediterranean Sea model receives a full wave spectrum at 5-min intervals at its Atlantic Ocean open boundary from the  
337 WAM implementation in the North Atlantic. The latter model is considered to have all its four boundaries closed assuming no  
338 wave energy propagation from the adjacent seas. This assumption is readily justified for the north and west boundaries of the  
339 North Atlantic model considering the adjacent topography which restricts the development and propagation of swell into the  
340 model domain.

### 341 342 2.2.3 The wave data assimilation component

343 The assimilation module of the WAV component is based on the data assimilation scheme of WAM Cycle 4.6.2 which consists  
344 of an Optimal Interpolation (OI) of the along-track Significant Wave Height (SWH) observations retrieved by altimetry and  
345 then re-adjusting the wave spectrum at each grid point accordingly. This assimilation approach was initially developed by  
346 Lionello et al. (1992) and consists of two steps. First, a best guess (analysed) field of significant wave height is determined by  
347 OI with appropriate assumptions regarding the error covariance matrix. One of the key issues is the specification of the  
348 background error covariance matrix, for the waves called P, and the observation error covariance matrix, R. The first is defined  
349 as in the following Eq. (2):

**Deleted:** The WAV component is forced with 10 m above sea surface wind fields obtained from the ECMWF Integrated Forecasting System (IFS) at 1/8° dissemination resolution. The temporal resolution of the wind forcing is 3 h for the first 3 days of the forecast and 6 h for the rest of the forecast cycle.

**Deleted:** Sea ice coverage fields are also obtained from ECMWF at the same horizontal resolution (1/8°) and are updated daily.

**Deleted:** Global wave model

**Formatted:** Font: (Default) Times New Roman, Font colour: Text 1



358  $P = \exp\left(\frac{d_{ij}}{l_c}\right),$  (2)

359 while the second is Eq. (3):

360  $R = \frac{\sigma_o^2}{\sigma_b^2},$  (3)

363 where  $i$  and  $j$  are the model grid points in the longitudinal and latitudinal directions respectively,  $d$  is the distance of the  
364 observation location to the grid point,  $l_c$  is the field correlation length, while  $\sigma_o^2$  and  $\sigma_b^2$  stand for the observation and model  
365 errors, respectively. In the above expressions the error is considered as being homogeneous and isotropic. We use  $R=1$  and the  
366 correlation length  $l_c$  equal to 3 deg (~300 km).

367 Finally, the weights assigned to the observations are the elements of the gain matrix  $K$  as presented in Eq. (4):

368  $K = PH^T[HPH^T + R]^{-1}$  (4)

371 where  $H$  is the observation operator that projects the model solution to the observation location. For the current version of  
372 Med-waves, the OI analysis procedure is applied only to altimeter along-track SWH measurements although wind at 10 m  
373 measurements can be assimilated as well. Prior to OI procedure, quality checked SWH observations which are available in a  
374  $\pm 1.5$  hours time window are collocated with the closest model grid point and averaged.

375 During the second step, the analysed significant wave height field is used to retrieve the full dimensional wave spectrum from  
376 a first-guess spectrum provided by the model itself, introducing additional assumptions to transform the information of a single  
377 wave height spectrum into separate corrections for the wind sea and swell components of the spectrum. Two-dimensional wave  
378 spectra are regarded either as wind sea spectra, if the wind sea energy is larger than 3/4 times the total energy, or, if this  
379 condition is not satisfied, as swell. If the first-guess spectrum is mainly wind-sea, the spectrum is updated using empirical  
380 energy growth curves from the model. In case of swell, the spectrum is updated assuming the average wave steepness provided  
381 by the first-guess spectrum is correct, but the wind is not updated.

382 Prior to assimilation, all altimeter SWH observations are subject to a quality control procedure. Every day the system is  
383 scheduled to simulate 264 hours: 24 hours in the past (analysis) blending through data assimilation model results with all  
384 satellite SWH observations available followed by 240 hours forecast. The assimilation step adopted for the current version of  
385 the Med-waves system equals to 3 hours.

## 386 2.3 Mediterranean biogeochemical component

### 387 2.3.1. Numerical model description

388 The BIO component consists of the Biogeochemical Flux Model (BFM, Vichi et al., 2007) coupled with the transport  
389 (OGSTM) module (Salon et al., 2019). Advection, vertical and horizontal diffusion and the sinking term for the  
390 biogeochemical tracers (Foujols et al., 2000) are solved by the OGSTM module that uses daily 3D velocity, diffusivities and

Formatted: Font: (Default) Times New Roman

Formatted: Font: (Default) Times New Roman

Deleted:

Formatted: Font: (Default) Times New Roman

Formatted: Font: (Default) Times New Roman

Deleted: 10m

393 2D atmospheric fields provided by the PHY component through the offline coupling scheme (Figure 1). A source splitting  
394 numerical time integration is used to couple advection and diffusion to the biochemical tracer rates.  
395 BFM describes the biogeochemical cycles of carbon, nitrogen, phosphorus, silicon and oxygen through the dissolved inorganic  
396 and the particulate living and non-living organic compartments (Lazzari et al., 2012; Lazzari et al., 2016). The model includes  
397 four phytoplankton functional groups (i.e., diatoms, flagellates, picophytoplankton and dinoflagellates), four zooplankton  
398 groups (i.e., carnivorous, and omnivorous mesozooplankton, heterotrophic nanoflagellates and microzooplankton) and  
399 heterotrophic bacteria. Among the nutrients, dissolved inorganic nitrogen is simulated in terms of nitrate and ammonia. The  
400 non-living dissolved organic compartment includes labile, semi-labile and refractory organic matter. A carbonate system  
401 component (Cossarini et al., 2015) includes alkalinity (ALK), dissolved inorganic carbon (DIC) and particulate inorganic  
402 carbon (PIC) as prognostics variables, computes CO<sub>2</sub> air-sea gas exchange according to Wanninkhof (2014) and provides  
403 diagnostics variables such as pH, CO<sub>2</sub> concentration and calcite saturation horizon.

### 404 405 **2.3.2. Model initialization, external forcing and boundary conditions**

406 Initial condition of nutrients (nitrate, ammonia, silicate and phosphate), oxygen and carbonate variables (DIC and alkalinity)  
407 consist of 16 climatological profiles homogeneously applied in each of the sub-regions represented in Figure 3.  
408 Climatological profiles are computed from the EMODnet dataset (Buga et al., 2018). The other biogeochemical state variables  
409 (phytoplankton, zooplankton and bacteria biomasses) are initialised in the photic layer (0–200 m) according to the standard  
410 BFM values. A 5-year hindcast is run using the first year (i.e. 2017) in perpetual mode. The model has two open lateral  
411 conditions: in the Atlantic Ocean and at the Dardanelles Strait. The model has two open lateral conditions: in the Atlantic  
412 Ocean and in the Dardanelles Strait. Nutrients, oxygen, DIC and alkalinity in the Atlantic (i.e., boundary at lon=9°W) are  
413 provided through seasonally varying climatological profiles derived from Word Ocean Atlas (WOA 2018) and literature  
414 (Alvarez et al., 2014) and a Newtonian dumping is applied. The Newtonian dumping is set between the longitudes 9°W and  
415 6.5°W with a time scale relaxation term linearly varying from 1/24 1/d at 9°W to 90 1/d at 6.5°W. A Dirichlet-type scheme  
416 with constant concentration values of nutrients, DIC and alkalinity derived from literature (Yalcin et al., 2017; Tugrul et al.,  
417 2002; Souvermezoglou et al., 2014; Copin-Montegut, 1993; Schneider et al., 2007; Krasakopoulou et al., 2017) is applied at  
418 the Dardanelles Strait. The concentrations are also tuned to provide input fluxes from Black Sea to the Mediterranean Sea  
419 consistent with published estimates (Deliverable of Perseus, 2020; Yalcin et al., 2017; Tugrul et al., 2002; Copin-Montegut,  
420 1993). A radiative condition is set for the other BFM tracers.  
421 Terrestrial inputs include 39 rivers consistently with the PHY component. Annual nutrients input are about 46500 10<sup>6</sup> molN/y  
422 and 881 10<sup>6</sup> molP/y (Salon et al., 2019). Carbon and alkalinity inputs are 9300 10<sup>9</sup> gC/y and 800 10<sup>9</sup> mol/y, respectively.  
423 Estimates are derived considering typical concentrations per freshwater mass in macro coastal areas of the Mediterranean Sea  
424 (Copin-Montegut, 1993; Meybeck and Ragu, 1995; Kempe et al., 1991) and the river water discharges from the PERSEUS  
425 dataset (Deliverable of Perseus, 2012 as before). Annual atmospheric nutrient depositions are 81300 10<sup>6</sup> molN/y and 1194 10<sup>6</sup>  
426 molP/y for nitrogen and phosphorus, respectively (Ribera d'Alcalá et al., 2003). Spatially constant values of atmospheric pCO<sub>2</sub>

**Formatted:** Font: (Default) Times New Roman, Font colour: Text 1

**Deleted:** Climatological profiles from EMODnet (Buga et al., 2018) are used to initialize nutrients (nitrate, ammonia, silicate and phosphate), oxygen and carbonate variables (DIC and alkalinity) in each of the areas represented in Fig. 3.

**Deleted:** Nutrients, oxygen, DIC and alkalinity in the Atlantic are provided through seasonally varying climatological profiles derived from Word Ocean Atlas (WOA 2018) and literature (Alvarez et al., 2014) and Newtonian dumping is applied.

**Deleted:** e

**Deleted:** 9300109

**Formatted:** Superscript

are derived from the 1992-2018 time series of the ENEA Lampedusa station (Trisolino et al., 2021) with the 2019 and 2020 values extrapolated by linear trend.

### 2.3.3 The biogeochemical data assimilation component

The BIO component features a variational data assimilation scheme (3DVarBio) which is based on the minimization of the cost function (Eq. 1) (Teruzzi et al., 2014). Minimization is computed iteratively in a reduced space using an efficient parallel PETSc/TAO solver (Teruzzi et al., 2019) and the background error covariance matrix,  $B$ , is factored as  $B = VV$ , where  $V$  is a sequence of linear operators:  $V = V_h V_v V_n$ . The horizontal error covariance operator ( $V_h$ ) is a gaussian filter and includes non-uniform and direction-dependent length scale correlation radius to account for anisotropic coastal assimilation (Teruzzi et al., 2018) and vertical profile assimilation (Cossarini et al., 2019). The vertical error covariance operator ( $V_v$ ) is based on a set of 0-200 m 200m vertical error profiles obtained using an empirical orthogonal functions (EOFs) decomposition of a 20-year long pre-existing biogeochemical simulation. EOFs are computed monthly for the 16 subregions with the actual vertical resolution and rescaled at each grid-point considering the ratio between observation and model variances (Teruzzi et al., 2018). The biogeochemical error covariance operator ( $V_n$ ) is designed to preserve the ratios among phytoplankton functional types and their internal carbon to nutrient quotas (Teruzzi et al., 2014) and supports monthly and spatial varying covariances between dissolved inorganic nutrients (Teruzzi et al., 2021). In the most recent BIO model configuration (Teruzzi et al., 2021; Cossarini et al., 2019), the assimilated biogeochemical observations are satellite multi-sensor (MODIS, VIIRS and OLCI) surface chlorophyll data (Volpe et al., 2019) and quality-controlled BGC-Argo nitrate and chlorophyll profiles (Schmechtig et al., 2018; Johnson et al., 2018). Ocean colour data are interpolated from original 1km resolution to the 1/24° model resolution.

### 2.4 Systems evolutions

The Mediterranean has been the site of major forecasting research activities since the late nineties (Pinardi and Woods, 2001, Pinardi et al., 2003; Pinardi and Coppini, 2010). Before 2008, only the PHY and BIO components were present. The PHY component was based on the Ocean Parallels (OPA) code (Madec et al., 1998) with the highest available horizontal and vertical resolution of 1/16° degrees (approx. 6.5 km) in horizontal and 72 vertical levels, with closed lateral boundaries, only 7 major rivers and implementing a weekly 3D-VAR assimilation scheme (Dobricic et al., 2007) assimilating temperature and salinity vertical profiles, Sea Level Anomaly (SLA) along with track altimeter data, moreover a non-solar heat flux correction was imposed through a nudging along the whole day with Sea Surface Temperature (SST) satellite gridded data.

A major upgrade of the PHY component was achieved in 2009 by implementing a version of the numerical model NEMOv3.1 including LOBC in the Atlantic Ocean (Oddo et al., 2009) and moving to a daily assimilation cycle. The first exchanges with a wave model were implemented in 2010 when the PHY component was coupled hourly with WAM receiving the surface drag coefficient to better represent the wind stress. In 2013 the whole operational modelling system was updated by implementing an upgraded 2-way on-line coupled system based on NEMOv3.4 and WW3 (Clementi et al., 2017a) allowing for a more consistent exchange between the two models. The following year the PHY general circulation module was improved by

**Deleted:** Atmospheric pCO<sub>2</sub> mean annual concentrations are from the ENEA Lampedusa (Trisolino et al., 2021) station with the present-day values extrapolated by linear regression.

**Formatted:** Subscript

**Formatted:** Subscript

**Formatted:** Subscript

**Formatted:** Font: (Default) Times New Roman, Font colour: Text 1

**Deleted:** The BIO component features a variational data assimilation scheme (3DVarBio) which is based on the minimization of the cost function (Eq. 1) (Teruzzi et al., 2014). Minimization is computed iteratively in a reduced space using an efficient parallel PETSc/TAO solver (Teruzzi et al., 2019) and the background error covariance matrix,  $B$ , is factorised in a sequence of linear operators, as in the PHY component, that accounts for the vertical error covariance of the biogeochemical fields, the horizontal error covariance, and the error covariance among the biogeochemical variables.

The horizontal error covariance operator is a gaussian filter and includes non-uniform and direction-dependent length scale correlation radius to account for anisotropic coastal assimilation (Teruzzi et al., 2018) and vertical profile assimilation (Cossarini et al., 2019). The vertical error covariance operator is based on a set of vertical error profiles obtained using an empirical orthogonal functions (EOFs) decomposition of a pre-existing biogeochemical simulation. EOFs are computed monthly for the 16 subregions and rescaled at each grid-point considering the ratio between observation and model variances (Teruzzi et al., 2018). The biogeochemical error covariance operator is designed to preserve the ratios among phytoplankton functional types and their internal carbon to nutrient quotas (Teruzzi et al., 2014) and supports monthly and spatial varying covariances between dissolved inorganic nutrients (Teruzzi et al., 2021).

**Formatted:** Font: (Default) Times New Roman, Font colour: Text 1, English (UK), Pattern: Clear

**Deleted:** In the most recent configuration (Teruzzi et al., 2021, Cossarini et al., 2019), the assimilated biogeochemical observations are satellite multi-sensor (MODIS, VIIRS and OLCI) surface chlorophyll data (Volpe et al., 2019) and quality-controlled Argo-BGC nitrate and chlorophyll profiles (Schmechtig et al., 2018; Johnson et al., 2018).

**Deleted:** .

**Deleted:** PArallels

**Deleted:** (approx.

**Deleted:** .

508 accounting for the effect of atmospheric pressure effect (in addition to wind and buoyancy fluxes) and an explicit linear free  
509 surface formulation using a time splitting scheme (Oddo et al., 2014), while the assimilation scheme was enhanced thanks to  
510 the assimilation of Tailored Altimetry Products for Assimilation Systems (TAPAS) SLA data allowing for the application of  
511 specific corrections of the altimetric original signal (Dobricic et al., 2012).

512 The PHY component delivered in 2015 included the nesting in the Atlantic Ocean through daily analysis and forecast fields  
513 from the global system, while one year later the assimilation scheme was enhanced including the computation of monthly and  
514 grid point EOFs and vertical observational errors varying with depth.

515 Another major PHY component evolution was achieved in 2017 when the resolution of the operational system was increased  
516 to 1/24° degrees (approx. 4 km) horizontal and 141 vertical levels using the z-star vertical coordinate system, a non-linear free  
517 surface formulation and the NEMOV3.6 version and 39 rivers were introduced. From year 2019 the Dardanelles Strait inflow  
518 was set as a lateral open boundary condition (instead as a river runoff climatological input) allowing for a daily update of the  
519 fluxes, and an improved nudging with the satellite sea surface temperature was included by correcting the heat fluxes only  
520 close to midnight.

521 The WAV component was developed and released for the first time in 2017 based on WAM Cycle 4.5.4 providing on a daily  
522 basis 5 days wave forecasts and simulations for the Mediterranean Sea at 1/24° horizontal resolution (Ravdas et al., 2018)  
523 nested within a North Atlantic model at 1/6° resolution and forced with ECMWF 10 m winds and PHY component surface  
524 currents. In March 2018 the system was upgraded by incorporating the data assimilation component to utilise available track  
525 SWH satellite observations from Sentinel-3A and Jason-3. In 2019, the wave model was upgraded to Cycle 4.6.2 and the  
526 duration of the forecasts were extended to 10 days. Additionally, a limitation to the high frequency part of the wave spectrum  
527 was applied while modifications from default values were introduced in the input source and dissipation functions: ZALP was  
528 set to 0.011 and  $C_{Ds}$  and  $\delta$  became 1.33 and 0.5 respectively.

529 In 2009, the first pre-operational version of the BIO component featured early versions of OGSTM transport model and BFM  
530 model (Lazzari et al., 2010). The spatial resolution was 1/8°, which required a subsampling of the PHY component fields from  
531 the 1/16° resolution. The Atlantic boundary was closed with a nudging term for nutrients and the land nutrients input included  
532 the three major Mediterranean rivers (i.e., Po, Rhone and Nile) and the Dardanelles was treated as a river. BFM used constant  
533 daily averaged irradiance to force photosynthesis (Lazzari et al., 2010).

534 Horizontal resolution aligned with the physical model in 2013 and was refined to 1/24° in 2017. Full alignment between the  
535 PHY and BIO components in terms of same horizontal and vertical resolutions, bathymetry, boundaries (number and position  
536 of rivers) was introduced in 2018 and remained a standard that mitigates possible approximation errors related to the use of  
537 daily output of the eddy-resolving ocean general circulation model to force the transport of tracers (Salon et al., 2019).  
538 Additionally, nutrient and carbon land input from 39 rivers were introduced in 2017, open boundary conditions at Dardanelles  
539 Strait in 2019 and in the Atlantic Ocean in 2020 (Salon et al., 2019).

Deleted: 10m

Deleted: The

542 Since 2008, three major improvements of the BFM model have been integrated (i) the addition of the carbonate system to  
543 predict alkalinity, ocean acidity and CO<sub>2</sub> air-sea exchanges in 2016 (Cossarini et al., 2015), (ii) the revision of nutrient  
544 formulation of phytoplankton in 2018 (Lazzari et al., 2016) and, (iii) in 2020, the introduction of the day-night cycle in light-  
545 dependent formulation of phytoplankton (Salon et al., 2019) and of the novel light extinction coefficient (Terzic et al., 2021).

546 A major system evolution and quality improvement was achieved in 2013 with the inclusion of the assimilation of satellite  
547 chlorophyll through a variational scheme with prescribed background error covariance (Teruzzi et al., 2014). Assimilation  
548 method was improved in 2018 to include coastal component (i.e., non-uniform and direction-dependent horizontal covariance;  
549 Teruzzi et al., 2018) and in 2019 to integrate new observations (i.e., BGC-Argo float profiles) including new parameterization  
550 for the vertical and biogeochemical background error covariance (Cossarini et al., 2019).

551 In terms of operational product delivery, the BIO component has produced daily 10-day forecasts and weekly 7-day analysis  
552 since 2020, fully aligned with the PHY component (Salon et al., 2019). Before that, the system produced 7-day analysis and a  
553 7-day forecast once per week since 2013, while a second cycle of 7-day forecasts was added each week in 2015.

### 554 3. Quality assessment

555 The evaluation of the quality of the Med-MFC is given here only for the analysis products, leaving the assessment of the  
556 forecast skill for future work. One overarching driver for the Med-MFC evolution is the continuous improvement of the  
557 numerical model and data assimilation modules with respect to a well-defined set of goodness indices established for all the  
558 European regional Seas (Hernandez et al., 2009). Ocean model uncertainties emerge from sources of errors relevant to the  
559 ocean state, including physics, biogeochemistry, and sea ice, as well as errors in the initial state and boundary conditions (i.e.  
560 atmospheric forcing and lateral open boundary conditions). Model uncertainties in ocean physics have a significant impact in  
561 all other system components as, for example, in biogeochemistry and sea ice (Alvarez Fanjul et al., 2022). Our results describe  
562 the quality of the Med-MFC products presenting the statistics and accuracy numbers based on a reference simulation produced  
563 to calibrate and validate the operational forecasting systems, whereas the analysis of model uncertainty sources is outlined in  
564 the discussion part also referring to previous specific publications.

#### 565 3.1. PHY component skill

566 The skill of the physical component is assessed over a 3-year period from 2018 to 2020 (Clementi et al., 2019). The evaluation  
567 is done by means of Estimated Accuracy Numbers (EANs) which consist of the root mean square differences (RMSD) and  
568 bias (model minus observations) of daily mean of model outputs against satellite and in-situ observations. EANs are evaluated  
569 using daily mean of model estimates interpolated on the available observations in that day: this goodness score is somewhat  
570 approximated especially at the surface where daily variability is large, but this is a score used by many forecasting systems  
571 (Ciliberti et al., 2022; Toledano et al., 2022; Sotillo et al., 2021; Najy et al., 2020) and we will show it for reference purposes.  
572 We also use misfits, which are the difference between the model solutions and the observations at the observational time during

**Deleted:** Since 2008, three major improvements of the BFM model included the addition of the carbonate system to predict alkalinity, ocean acidity and CO<sub>2</sub> air-sea exchanges in 2016 (Cossarini et al., 2015), the revision of nutrient formulation of phytoplankton in 2018 (Lazzari et al., 2016) and, in 2020, the introduction of the day-night cycle in light-dependent formulation of phytoplankton (Salon et al., 2019) and of the novel light extinction coefficient (Terzic et al., 2021).

**Deleted:** Teruzzi

**Deleted:** Argo-BGC

**Formatted:** Font: (Default) Times New Roman, Font colour: Text 1, English (UK), Pattern: Clear

**Deleted:** Med-MFC

**Deleted:** Med-MFC

**Formatted:** Font: (Default) Times New Roman, Font colour: Text 1

**Formatted:** Font: (Default) Times New Roman, Font colour: Text 1

585 the forward model integration, for this assessment. The misfits provide quasi-independent and more accurate skill assessment  
586 since they are calculated before the variational analysis and at the observational time. In EAN, the daily mean analyses are  
587 interpolated on daily available observations: this goodness score is somewhat approximated especially at the surface where  
588 daily variability is large, but this is a score used by many forecasting systems and we will show it for reference purposes.  
589 Table 2 summarises the EAN of 3D model temperature and salinity daily mean values compared to in-situ observations, in  
590 particular Argo floats and CTD profiles averaged over the three reference years. Model temperature shows small positive and  
591 negative biases depending on the depth, with the largest error (maximum value of the period is 0.85°C) in the sub-surface  
592 layers between 10 and 60 m, decreasing with depth. Salinity is characterised by an almost general negative small bias, meaning  
593 generally lower salinities than measured, along the whole water column except for the first layer. The salinity RMSD mean  
594 value is generally lower than 0.2 PSU, the error is larger in the first layers and decreases significantly below 150 m. The  
595 comparison with other Copernicus Marine Service forecasting systems EAN values presented in the Quality Information  
596 Document (QUID), considering that the validation periods are different, shows that the Mediterranean temperature and salinity  
597 quality in terms of RMSD are aligned with all the other Copernicus forecasting systems. In particular the sea surface  
598 temperature, averaged RMSD with respect to satellite data ranges from 0.48°C in the North West Shelf (derived from the QUID  
599 of the product NORTHWESTSHELF\_ANALYSIS\_FORECAST\_PHY\_004\_013 <https://doi.org/10.48670/moi-00054>) to  
600 0.8°C in the Baltic Sea (derived from the QUID of the product BALTICSEA\_ANALYSISFORECAST\_PHY\_003\_006  
601 <https://doi.org/10.48670/moi-00010>), while the 3D mean temperature RMSD with respect to in-situ data ranges from 0.4°C in  
602 the Mediterranean and North West Shelf to 0.7°C in the Black Sea (derived from the QUID of the product BLKSEA  
603 ANALYSISFORECAST\_PHY\_007\_001 [https://doi.org/10.25423/cmcc/blksea\\_analysisforecast\\_phy\\_007\\_001\\_eas4](https://doi.org/10.25423/cmcc/blksea_analysisforecast_phy_007_001_eas4)) and the  
604 salinity mean RMSD varies from 0.1 PSU in the Mediterranean and North West Shelf to 0.3 PSU in the Iberia-Biscay-Ireland  
605 area (derived from the QUID of the product IBI\_ANALYSISFORECAST\_PHY\_005\_001 <https://doi.org/10.48670/moi-00027>). The sea level anomaly skill is also aligned with the ones of other operational systems within the Copernicus Marine  
606 Service when compared with satellite altimeter observations (from 2.2 cm in the Black Sea to 9 cm in the North West Shelf  
607 area).  
608  
609 The other goodness index is computed as weekly mean root mean square error and bias using temperature and salinity misfits,  
610 that are computed at FGAT. The misfits are more precise to account for surface errors since the observations are compared  
611 with the model at the exact time of the day when observations are taken. This index is represented as a depth-time Hovmoller  
612 diagram in Figure 4. The temperature error is seasonal (Figure 4a), with maximum values of ~1.8 °C, in the range of 30-60 m  
613 depth corresponding to the depth of the mixed layer and the seasonal thermocline during the stratified season, from June to  
614 November. The error is reduced to an average value of around 0.4 °C, during the vertically mixed season from December to  
615 May. The temperature misfits (Figure 4c) indicate an overall overestimation of the temperature, except for the subsurface  
616 layers, during winter and spring.  
617 The salinity error (Figure 4b) is defined by two main structures: one that is constant throughout the year down to about 150 m  
618 and the seasonal amplification during summer, as for the temperature errors. The maximum errors reach values of 0.35 PSU

**Deleted:** The skill of the physical analysis fields is assessed over a 3 years period from 2018 to 2020 comparing model results (Clementi et al., 2019) to satellite and in-situ observational datasets by means of root mean square differences (RMSD) and bias (model minus observations) of daily mean analysis outputs, so called Estimated Accuracy Number (EAN) and misfits, calculated at observation time during the forward model integration and evaluated on a sub-set of observations corresponding to the ones assimilated by the system.

**Deleted:** (Ciliberti et al., 2022; Toledano et al., 2022; Sotillo et al., 2021, Najy et al., 2020)

**Deleted:** Table 2 summarises the EAN of 3D model temperature and salinity daily mean values compared to in situ observations, in particular Argo floats and CTD profiles average over the three reference years. Model temperature is generally warmer than observations, i.e., it shows a positive bias, with the largest error (maximum value of the period is 0.8°C) in the sub-surface layers between 10 and 60 m, decreasing with depth. Salinity is characterised by a negative bias, meaning generally lower salinities than measured, along the whole water column. The salinity RMSD yearly mean values is lower than 0.22 PSU, the error is larger in the first layers and decreases significantly below 150 m.

**Deleted:** )

**Deleted:** SST

**Formatted:** Font colour: Text 1

**Formatted:** Font colour: Text 1

**Formatted:** Font: Not Italic

**Formatted:** Font colour: Text 1

**Deleted:** 1PSU

**Deleted:** 3PSU

**Formatted:** Font colour: Text 1

**Deleted:** 2cm

**Deleted:** 9cm

**Deleted:** 8°C

**Deleted:** 4°C

**Formatted:** Font: (Default) Times New Roman, Font colour: Text 1

**Deleted:** The temperature bias (Figure 4c), as already shown in Table 2 for EAN, indicates an overall overestimation of the temperature except for the subsurface during winter and spring. The positive bias could be caused by an overestimation of the downward shortwave radiation flux which is estimated according to Reed (1977) formula, as already discussed in (Byun et al., 2007) and (Pettenuzzo et al., 2010).

**Formatted:** Font: (Default) Times New Roman, Font colour: Text 1

655 in the summer period and decrease to 0.025 PSU below ~150 m. We argue that the background error, uniform throughout the  
656 year, could be due to inaccurate advection of salinity in different sub-areas of the Mediterranean Sea. Moreover, the model  
657 salinity bias is generally negative, i.e., the model salinity is lower than the observations (Figure 4d). This could be related to  
658 the larger Atlantic water inflow with respect to literature (Soto-Navaro et al., 2010) at Gibraltar as reported in Table 3 and to  
659 inaccurate mixing at Gibraltar due to the lack of tides.

660 Sea surface temperature (SST) and sea level anomaly (SLA) skills are evaluated comparing them with satellite observations:  
661 model daily mean SST is compared to SST satellite L4 gridded data at 1/16° resolution (Buongiorno Nardelli et al., 2018)  
662 while SLA is compared to along with track satellite altimeter observations (Taburet et al., 2019) in terms of model misfits.

663 Table 4 presents the RMSD and bias values computed for SST as well as SLA RMSD averaged in the Mediterranean Sea and  
664 over the 16 sub-regions (see Figure 3). Considering SST, the RMSD values range between 0.47 °C and 0.69 °C (mean  
665 Mediterranean Sea error is 0.54 °C) and the bias is generally positive, possibly caused by an overestimation of the downward  
666 shortwave radiation flux which is estimated according to Reed (1977) formula, as already discussed in (Byun et al. (, 2007)  
667 and Pettenuzzo et al. (2010). The SLA error ranges between 2.3 cm and 5.3 cm (mean error is 3.8 cm), The SLA skill scores  
668 vary in different regions, this could be related to the spatial coverage of the observations (not homogeneous in the basin) and  
669 on the limit of the 1000 m assimilation depth (due to the dynamic height operator which assumes a level-of-no-motion to  
670 compute the sea level increments from temperature and salinity increments, see section 2.1.3).

671 The time variability of the model SLA accuracy is also provided by means of weekly model misfits evaluated for each available  
672 satellite altimeter and averaged in the whole Mediterranean Sea as shown in Figure 5. The error ranges between 2.5 cm and  
673 5.5 cm (maximum error with respect to Cryosat) with a large variability among the different satellites, with a generalised  
674 increase of error during Autumn and Winter seasons.

### 675 3.2. WAV component skill

676 The quality of the wave analysis and forecast product is assessed over a three-year period from January 2018 to December  
677 2020. The skill of the Mediterranean wave model is assessed by considering inter-comparisons of the model solution during  
678 the 24-h analysis phase with available in-situ (SWH and mean wave period from wave buoys) and remotely sensed (SWH)  
679 observations. As the latter are ingested into the model through data assimilation, the model first guess SWH (i.e. model  
680 background) is used instead of model analysis.

681 Significant wave height (SWH) and mean wave period (MWP) measurements are used for data validation from 28 wave buoys  
682 in the Mediterranean Sea (lower panel of Figure 7). Data quality control procedures have been applied to the in-situ  
683 observations (Copernicus Marine In-Situ Team, 2020) and measurements associated with a bad quality flag are not taken into  
684 consideration.

685 Figure 6 depicts scatter plots of the evaluation of the observed SWH and MWP against measurements obtained from the 28  
686 buoys. For the immense number of match-up data (within the range 0 – 1.25 m), the model overestimates SWH with respect  
687 to the buoy measurements (left-hand side panel). Additionally, the model underestimates SWH during more energetic events

**Formatted:** Font: (Default) Times New Roman, Font colour: Text 1

**Formatted:** Font: (Default) Times New Roman, Font colour: Text 1

**Formatted:** Font: (Default) Times New Roman, Font colour: Text 1

**Deleted:** Table 4 presents the EAN RMSD values computed for SST and misfit SLA RMSD averaged in the Mediterranean Sea and over the 16 sub-regions, presented in Figure 3. Considering SST, the EAN RMSD values range between 0.47 °C and 0.69°C (mean Mediterranean Sea error of 0.54 °C), while the SLA error ranges between 2.3 cm and 5.3 cm (mean error is 3.8 cm).

**Deleted:** The quality of the analysis varies in different regions depending on the spatial distribution of the observations (for SLA) in addition to the model inaccuracies.

**Formatted:** Font: (Default) Times New Roman, Font colour: Text 1

**Deleted:** Model analysis and first-guess (i.e. just before data assimilation) outputs are compared to in-situ and satellite observations respectively.

**Deleted:** Figure 6 lower panel).

( $>1.25$  m), except for the range 5.5-6.2 m. For large wave heights, model results underestimate SWH compared to the buoys, which agrees with past findings for the Mediterranean Sea (Ardhuin et al., 2007; Korres et al., 2011). Negative SWH BIAS can be attributed to errors in the forcing or inaccurate wave growth and dissipation at high wind speeds (Pineau-Guillou et al., 2018). The dashed orange line (i.e. the  $45^\circ$  ref. line) in the Quantile-Quantile (QQ) plot stands for the unit gradient line. We observe that model results follow the dashed orange line very closely, meaning the model produces well the distribution of SWH observations. Although for higher waves ( $> 1.25$  m) the model tends to underestimate SWH (except for the range 5.5-6.2 m), it overproduces very large wave heights (100th, 99.97th, 99.96th, 99.95th percentiles); hence a deviation from the orange dashed reference line in the QQ plot becomes prominent for very high waves. Concerning MWP, the model systematically underestimates it (right-hand side panel). Despite the overall modelled MWP underestimation (BIAS =  $-0.314$  s), the system tends to overestimate MWP for high percentiles/very long waves (hence we observe the deviation of the Q-Q plot from the unit gradient line for very high periods). Seasonal results (not shown) for both variables SWH and MWP indicated that the model adequately captures the seasonal variability. For SWH, RMSD values vary from 0.154 m in summer to 0.231 m in winter. Nevertheless, SI is higher in summer (0.26) than during the other seasons. Additionally, the highest Pearson correlation coefficient (CORR) is observed in winter (0.963, while the lower one is equal to 0.932 and it is observed in summer). The metrics reveal that the model follows better the observations in winter than during the other months since the former is associated with more well-defined weather patterns and higher waves. A similar conclusion has been reached also by other studies (e.g. Ardhuin et al., 2007) for the Mediterranean Sea. Summer and autumn are characterised by higher SI values (0.244 and 0.260 respectively), while lower values are obtained for winter and spring (0.231 and 0.227 respectively). Finally, small positive BIAS values are met for all seasons, with the highest values found in summer (0.012 m). Regarding mean wave period, RMSD varies from 0.610 s in summer to 0.66 s in winter and BIAS is negative for all seasons. SI does not present significant seasonal variability, with the highest value encountered in summer. Finally, CORR for MWP is higher than 0.8 in all seasons (values are within the range 0.859 – 0.878, while during summer CORR equals 0.792). These metrics demonstrate that the model wave period (similarly to the wave height) correctly follows the observations in well-defined weather conditions characterised by higher waves and longer periods, agreeing with past studies (Cavaleri and Sclavo, 2006; Ravdas et al., 2018).

The qualification metrics for the different buoy locations in Figure 6 are plotted in Figure 7 (upper panel). RMSD at the different buoy locations varies from 0.13 m to 0.31 m. Scatter Index (SI) varies from 0.17 at buoy 3732621 to 0.35 at the buoys of Malaga and SARON (Aegean Sea). In general, SI values above the mean value for the whole Mediterranean Sea (0.24) are obtained at wave buoys located near the coast, particularly if these are sheltered by land masses on their north-northwest (e.g. western French coastline), and/or within enclosed basins characterised by a complex topography such as the Aegean Sea. As explained in several studies (Ravdas et al., 2018), in these cases, the spatial resolution of the wave model is often not adequate to resolve the fine bathymetric features whilst the spatial resolution of the forcing wind forcing is incapable to reproduce the fine orographic effects, introducing errors to the wave analysis. The Pearson correlation coefficient (CORR) mostly follows the pattern of variation of SI (in this figure we present the CORR deviation from unity). CORR ranges from 0.87 at SARON

**Deleted:** Figure 6 depicts scatter plots of the evaluation of the observed SWH and MWP against measurements, obtained from the 28 buoys. The figure reveals small SWH underestimation by the model mainly for very small wave heights ( $< 0.6$  m). A prevalence of model overestimation is obtained for waves above about 2m, which becomes more pronounced for higher waves. Regarding MWP, the model underestimates the observations for  $MWP < 7$  s whilst model overestimation is observed for higher periods.

**Deleted:** Equivalent seasonal results (not shown) revealed that the performance of the model is better in winter than in summer which agrees with other studies (Cavaleri and Sclavo, 2006; Ravdas et al., 2018).

**Formatted:** Font: (Default) Times New Roman, Font colour: Text 1

**Deleted:** Fig.

**Deleted:** is

**Deleted:** model



750 in the Aegean Sea to 0.97 at the deep-water buoy 6100196 offshore Spain, which is well-exposed to the prevailing north-  
751 westerly winds in the region. The BIAS varies from -0.13 m at buoy 3732621 (located north of Crete) to 0.13 m at buoy  
752 6100021 located near the French coast. Its sign varies, with positive and negative values computed at almost the same number  
753 of locations respectively. Figure 8 (right) shows the scatter plot between the first guess SWH and satellite observations. Here  
754 the initial guess SWH refers to the model SWH before data assimilation, thus meaning semi-independent model data. In  
755 addition, a scatter plot resulting from the comparison of the ECMWF forcing wind speeds (U10) and satellite measurements  
756 of U10 is shown in Figure 8 (left). It is seen that ECMWF forcing overestimates U10 with respect to observations, throughout  
757 most of U10 range while some underestimation is observed for high wind speeds (14 – 19 m/s). An overall ECMWF  
758 overestimation of 3% is computed. On the other hand, the SWH model underestimation is about 6%. Compared to the  
759 equivalent results obtained from the model-buoy comparison, a smaller scatter (by about 7%) with a larger overall bias is  
760 associated with the model-satellite comparison, i.e. open ocean waves. SI values compare well at the more exposed wave  
761 buoys in the Mediterranean Sea.

762 Figure 9 maps statistics of the comparison of model first-guess and satellite observations of SWH for the different sub-regions  
763 of the Mediterranean Sea. The Aegean and Alboran Seas have relatively high SI values (0.21). The highest value of SI is  
764 obtained for the North Adriatic Sea (0.26) followed by the South Adriatic (0.23). The lowest values (0.13-0.15) are found in  
765 the Levantine Basin, the Ionian Sea, and the Southwest Mediterranean Sea. Relatively low values (0.16) are also found west  
766 of the islands of Sardinia and Corsica. As discussed above, the error is due to inaccuracies associated with orographic winds  
767 and/or local sea breezes and the missing representation of the complicated bathymetry in the fetch-limited, enclosed regions.  
768 SWH negative bias is present in all sub-regions.

769 Finally, inter-compared to ECMWF, UK MetOffice and DMI (Danish Meteorological Institute) wave forecasting systems for  
770 a different year (2014), Med-waves shows a better skill in terms of SWH with RMS errors for the Western Med buoys equal  
771 to 0.227 m (0.234 m for ECMWF; 0.281 m for UK MetOffice) and 0.201 m for the central and eastern Mediterranean (0.227  
772 m for ECMWF; 0.268 m for DMI).

### 774 3.3. BIO component skill

775 The BIO component state variables can be validated at three different uncertainty levels providing a “degree of confirmation”  
776 (Oreskes et al., 1994) of different scales of variability based on the availability of reference data.

777 Near real time satellite and BGC-Argo float data provide a rigorous skill performance validation data set down to the scales of  
778 the week and mesoscale dynamics for a limited set of variables: chlorophyll, nitrate and oxygen. Dataset of historical  
779 oceanographic data (Socot dataset, Baker et al (2016); EMODnet data collection, Buga et al. (2018); Cossarini et al., (2017);  
780 Lazzari et al., 2016) are used to build a reference framework of sub-regions and annual and seasonal climatological profiles to  
781 validate model performance to simulate the basin wide gradients, the mean vertical profiles and the seasonal cycle. For this

**Deleted:** The Correlation coefficient (CORR) mostly follows the pattern of variation of the SI. It ranges from 0.87 at SARON in the Aegean Sea to 0.97 at the deep-water buoy 6100196 offshore Spain, which is well exposed to the prevailing north-westerly winds in the region....

**Deleted:** Overestimation at buoy 6100198 in the Alboran Sea is part of a general overestimation of the wave heights in the Atlantic and Alboran regions as will be seen later in the comparison with satellite observations.¶

**Deleted:** It is seen that ECMWF is forcing underestimates observed U10 throughout the entire U10 range, even more so at high wind speeds....

**Deleted:** The model underestimates SWH for the lower range (< 2.5 m) and overestimates SWH for larger waves.

**Deleted:** 234m

**Deleted:**

**Deleted:** 201m

**Deleted:** 227m

**Deleted:** ),

**Deleted:** (

**Deleted:** ))

803 data set it is possible to have nutrients, such as nitrate, phosphate, ammonia and silicate, as well as dissolved oxygen, dissolved  
804 inorganic carbon, alkalinity and surface pCO<sub>2</sub>.

805 Lastly, a third level of validation regards those variables whose observability level is very scarce (e.g., phytoplankton biomass)  
806 or based on indirect estimations (e.g., primary production, air-sea CO<sub>2</sub> fluxes). Only confirmation of the range of variability  
807 and a general uncertainty estimation can be provided for those variables (see for example the validation of model primary  
808 production in (von Schuckmann et al., 2020; Cossarini et al., 2020).

809 Considering the 2018-2020 reference period, the chlorophyll is very well reproduced by the BIO component, both in terms of  
810 seasonal cycle and spatial gradient at surface (Figure 10) and in terms of vertical profiles at the BGC-Argo float positions  
811 (Table 5). Uncertainty of surface chlorophyll is lower than 0.03 mg/m<sup>3</sup> with larger values registered in winter and western sub-  
812 regions where the variability and the chlorophyll values are higher (Figure 10a and b). Regarding profiles, chlorophyll values  
813 and vertical shapes driven by mesoscale dynamics are simulated with a high level of accuracy by the model (Salon et al., 2019;  
814 Cossarini et al., 2019, 2021). Daily values of RMSD and of Pearson correlation are computed between satellite and model  
815 output maps, then averaged over the two periods (Figure 10c and d). The plot of RMSD (Figure 10c) shows that higher errors  
816 are registered in the western sub-regions and in winter when chlorophyll levels and variability are higher. On the other hand,  
817 spatial correlation values are moderate and high in all sub-regions (i.e., values always above 0.5 except for a few sub-regions),  
818 with summer values better than winter values. Considering the number of grid points in each sub-regions, all values in Figure  
819 10d should be considered significantly non-zero at the 0.05 level. Indeed, Salon et al. (2019) show how, using novel metrics,  
820 the BIO component reproduces with high level of accuracy not only the concentrations in the euphotic layer, but also the  
821 seasonal evolution of the shape of the profiles. The depth of the deep chlorophyll maximum during summer and of the surface  
822 bloom during winter, as well as the depth of the nitracline and the depth of the maximum oxygen layer, which results from the  
823 interaction of physical and biogeochemical processes, are reproduced with an uncertainty of the  $O(10^1)$  meters (Table 5).  
824 However, the conclusions about mesoscale accuracy of the BIO component should be taken with caution since the BGC-Argo  
825 observations are still relatively few in number (about 1 over 8 w.r.t. the Argo floats have biochemical sensors) and unevenly  
826 spaced (e.g., southern Mediterranean Sea is less observed than northern areas).

827 As explained above, an additional verification of biogeochemical variables can be achieved for additionally 7 variables (not  
828 considering chlorophyll) and two other derived variables with climatological data. An example of such comparison is shown  
829 in Figure 11 for the carbonate system variables. Average maps and profiles of Alkalinity and DIC in selected sub-regions in  
830 the zonal directions (coloured lines) are well superimposed to the range of variability of the historical in-situ data (grey shaded  
831 areas) demonstrating the capability of the BIO component to reproduce both horizontal basin-wide gradients and vertical  
832 profiles in the different areas. A slight overestimation of DIC and alkalinity (underestimation of alkalinity) is simulated in the  
833 Alboran sub-region in the upper 0-100 layer.

834 As a summary of the skill performance analysis, statistics based on RMSD for all the considered model variables (Table 6)  
835 reports the model uncertainty in reproducing the basin-wide values and gradients for the selected layers. Generally, larger  
836 errors are computed for the upper layers where the variability (both spatial and temporal) is higher. Ammonia reports high

Deleted: mmol

Formatted: Superscript

Deleted: (

Deleted: ..

Deleted: The depth of the deep chlorophyll maximum during summer and of the surface bloom during winter, as well as the depth of the nitracline and the depth of the maximum oxygen layer, which results from the interaction of physical and biogeochemical processes, are reproduced with an uncertainty of the order of a meter (Table 5)....

Deleted: Average maps and profiles of Alkalinity and DIC in selected sub-regions in the zonal directions (coloured lines) are well superimposed to the range of variability of the historical in-situ data (grey shaded areas) demonstrating the capability of the BIO component to reproduce both horizontal basin-wide gradients and vertical profiles in the different areas.

852 errors also in subsurface layers, which is due to a possible incorrect initialization of deep layers since the lack of data in 9 out  
853 of 16 sub-regions. These numbers, which respond to the request for a synthetic measurement of Copernicus Marine Service  
854 product accuracy (Hernandez et al., 2018), are consolidated by in deep skill performance analysis of BFM model in reproducing  
855 chlorophyll (Lazzari et al., 2012; Teruzzi et al., 2018), nutrients (Lazzari et al., 2016; Salon et al., 2019) and carbonate system  
856 variables (Cossarini et al., 2015).

Deleted: ,

857 Chlorophyll from Ocean Color is the most common variable used for validation and near real time assessment of operational  
858 biogeochemical models and allows for a comparison of the forecast skill performance among the Marine Copernicus systems.  
859 Results of surface chlorophyll skill scores show that the quality of the first day of forecast of the BIO component is in line  
860 with those of other Copernicus models<sup>1</sup> (Spruch et al., 2020; Vandenbulcke et al., 2022; McEwan et al., 2021; McGovern et  
861 al., 2020). In particular, the two proposed accuracy indexes (i.e., one minus scatter index and one minus the root mean square  
862 error normalised on variability) of the MED model equal to 34% and 47%, which are within the ranges of the other Copernicus  
863 systems: 11%-38% and 13%-73% for the two skill scores, respectively (Spruch et al., 2020; Vandenbulcke et al., 2022;  
864 McEwan et al., 2021; McGovern et al., 2020).

Deleted: ,

Deleted: ,

865 For other biogeochemical variables, a direct comparison of the accuracy among Copernicus models is not straightforward,  
866 given the different protocols for metrics computation, the representativeness of the available observations and the large range  
867 of variability of observed values of biogeochemical variables among the European seas. Nevertheless, a rough comparative  
868 assessment of the quality of Marine Copernicus biogeochemical models can be provided using published estimated **EA**Ns,  
869 **normalized by** the typical values of the variables (McEwan et al., 2021; Feudale et al., 2021; Spruch et al., 2020; Melsom and  
870 Yumruktepe, 2021; McGovern et al., 2020; Vandenbulcke et al., 2021) to derive a common index of relative uncertainty. As  
871 for examples, relative uncertainty of oxygen of the MED system is of the order of 2% which is in line with the other Copernicus  
872 systems, except for Baltic and Black Seas systems, which show slightly higher relative errors. For nutrients, nitrate and  
873 phosphate uncertainties of the MED are about 50% and 35% which are similar or slightly better than most of the other  
874 Copernicus marine biogeochemical systems (i.e., ranges of 30-75% and 30-50% for nitrate and phosphate, respectively).  
875 Finally, the relative uncertainty of pH simulated by the MED system is less than 0.5% while other Copernicus systems report  
876 relative errors of the order of 1-2%.

Deleted: accuracy numbers (

Deleted: )

Deleted: and

877 Beside the aforementioned comparison, it is worth to report that the MED biogeochemical system exhibits some  
878 distinguishable features: the continuous monitoring of the forecast skill of surface chlorophyll since the beginning of the  
879 operational biogeochemical system dating back to 2010 (Salon et al., 2019), a large number of validated variables with in-situ  
880 data (i.e., up to 10 variables, Table 6), the thorough use of **BGC-Argo** observations for near real time **forecast** validation (Salon  
881 et al., 2019; Cossarini et al., 2021; <https://medeaf.ogs.it/nrt-validation>, last visit August 2022).

Deleted: -BGC

Deleted: ,

Formatted: Font colour: Text 1

<sup>1</sup> Product Quality Dashboard, Green Ocean section, <https://pqd.mercator-ocean.fr/>, accessed 15 July 2022.

### 3.4. ECMWF forcing skill

A calibration/validation system of the ECMWF forcing fields used by the Med-MFC operational systems has been developed using in-situ ground meteorological observations (METAR stations) and numerical model data from ECMWF (see Figure 12). Four well-established statistical indices for validating 2 m temperature, dew point temperature, air pressure and wind speed have been defined: (a) Bias, (b) RMS Error, (c) Nash-Sutcliffe Model Efficiency Coefficient, (d) Correlation Coefficient. The atmospheric forcing Cal/Val system will become publicly available and an example of this validation is provided in figure 12 showing daily mean wind speed time series from a METAR station (blue line) and ECMWF (red line) in the area of the Gulf of Lion during the year 2019 as well as time series of main skill metrics.

## 4. Conclusions and Future Perspectives

In this paper, the Med-MFC components (PHY, BIO and WAV) have been described providing an overview of their technical specifications. The PHY component provides 3D currents, temperature, salinity with the BIO and WAV components daily, with daily mean values. This approximation is flexible enough that improvements can be carried out separately on the three components, considering different levels of maturity of the numerical modelling parametrizations, the data assimilation components and the validation data sets. A different data assimilation system is run for each component making the best use of all available data from satellite and in-situ observations, the effort is to assimilate as much data as possible and use background or model uncertainties to account for the missing couplings. The 3 components accuracy has been evaluated for a common three-year period, from January 2018 to December 2020.

The PHY component has been validated comparing model data with respect to in-situ and satellite observations showing a good accuracy in representing the spatial pattern and the temporal variability of the temperature, salinity and sea level in the Mediterranean Sea. In particular, the model has a warm surface temperature bias of +0.12 °C when compared to satellite SST. The temperature error along the water column has a clear seasonal signal with the largest errors at the depth of the surface mixed layer and the seasonal thermocline. The model error in salinity is higher in the first layers and decreases significantly below 150 m. The SLA presents a mean average error of 3.8 cm on the three-year averaged period for the whole basin.

The WAV component was extensively validated for the 3-year period using all available in-situ and satellite observations in the Mediterranean Sea. All statistical values calculated and presented here showed a very good system performance. It is concluded that the Mediterranean SWH is accurately simulated by the WAV component. The typical SWH difference with observations (RMSE) over the whole basin is 0.21 m (0.197 m for in-situ and 0.228 m for satellite observations) with a bias ranging from -0.137 m to -0.005 m, when the comparison is against the in-situ observations, and from -0.088 m to 0.131 m when the comparison is with satellites. The scatter index (SI) exhibits low values (13%-17%) over the majority of the basin and relatively higher values (18%-21%) over the Aegean, Alboran, Ligurian and East Levantine Sea, with the highest SI value encountered in the North Adriatic Sea (26%). As explained, the occurrence of higher SI values is mainly related to the quality

Formatted: English (UK)

Formatted: English (UK)

Formatted: English (UK)

Deleted: Med-MFC

Deleted: ,

Deleted: Wav

Deleted: The system is offline coupled and the

Deleted: exchanges

Deleted: WAC

Deleted: Three

Deleted: are

Deleted: Jan

Deleted: Dec.

Formatted: Font: (Default) Times New Roman, Font colour: Text 1

Deleted: The PHY component shows a warm bias at surface of +0.7°C compared to satellite SST. The RMSD has a clear seasonal signal with the largest errors due to the depth of the surface mixed layer and the seasonal thermocline. The model salinity is higher in the first layers and decreases significantly below 150 m. The analysis SLA presents an average error of 3.8cm on a three-year average.

Formatted: Font: (Default) Times New Roman, Font colour: Text 1

Deleted: 202

Deleted:

Deleted:

Deleted: 214

Deleted:

Deleted: 004

Deleted: 0031

Deleted: 15

Deleted: %-22

Deleted: South Adriatic Seas (

Deleted: equal to 28% occurs

Deleted: ).

949 of ECMWF winds in fetch-limited areas of the basin where the orographic effects play an important role and the difficulties  
950 of wave models to appropriately resolve complicated bathymetry and coastline.

951 Overall, the quality of the WAV component stems from the ECMWF wind forcing that drives the wave dynamics, data  
952 assimilation, forcing from Med-PHY surface currents and improved parameterization of wave wind source and dissipation  
953 terms of WAM model. In particular, the WAV component assimilates satellite altimetry data with a well calibrated stand-alone  
954 OI scheme and implements regular updates and improved parameterization independently from the other components. Given  
955 that wind forcing quality has a substantial influence on the model response, a considerable part of the wave product uncertainty,  
956 especially under high winds or extreme conditions, is related to the wind forcing uncertainty and can be substantially improved  
957 by undertaking the ensemble approach in wave forecasting. The lower accuracy of the wave product in semi-enclosed regions  
958 of the Mediterranean Sea (e.g. Adriatic and Aegean Seas) can be related to the current spatiotemporal resolution of the wind  
959 forcing. Near the coast, unresolved topography by the wind and wave models and fetch limitations causes the wave model  
960 performance to deteriorate. In particular, the WAV component assimilates satellite altimetry data with a well calibrated stand-  
961 alone OI scheme and implements regular updates and improved parameterization independently from the other components.  
962 Given that wind forcing quality has a substantial influence on the model response, a considerable part of the wave product  
963 uncertainty, especially under high winds or extreme conditions, is related to the wind forcing uncertainty and can be  
964 substantially improved by undertaking the ensemble approach in wave forecasting. The lower accuracy of the wave product  
965 in semi-enclosed regions of the Mediterranean Sea (e.g. Adriatic and Aegean Seas) can be related to the current spatiotemporal  
966 resolution of the wind forcing. Near the coast, unresolved topography by the wind and wave models and fetch limitations cause  
967 the wave model performance to deteriorate.

968 The BIO system has defined a validation framework (Salon et al., 2019) based on multivariate (e.g., more than 10 variables)  
969 and multilevel metrics that include GODAE class 1 and class 4 statistics and process-oriented metrics. Particularly interesting,  
970 the present validation framework includes also near real time observations (i.e. satellite and BGC-Argo) that show  
971 average errors in the 0-200 m layer of 0.04 mg/m<sup>3</sup>, 0.4 mmol/m<sup>3</sup> and 16.8 mmol/m<sup>3</sup> for chlorophyll, nitrate and oxygen,  
972 respectively. Thus, the validation framework represents a robust benchmark for the future improvements of the Mediterranean  
973 BIO model. Indeed, as detailed in Salon et al. (2019) and Cossarini et al. (2021), critical sources of the BIO model errors  
974 include unresolved Atlantic boundary conditions as well as land-sea and atmospheric-sea forcing uncertainty in model  
975 parameterization and inconsistency of coupled physical-biogeochemical processes.

976 The value and reliability of the Med-MFC systems is demonstrated by the several downscaling coastal model systems and  
977 downstream applications that use its outputs operationally. The CYCOFOS – Cyprus Coastal Ocean Forecasting and Observing  
978 System (Zodiatis et al., 2003), which is a sub-regional forecasting and observing system in the Eastern Mediterranean  
979 Levantine Basin, uses the Med-MFC output to set its boundary conditions. The Med-MFC outputs are used asfor initial and  
980 lateral boundary conditions by the physical and wave ocean system MITO, which provides 5-day forecasts at resolution up to  
981 1/48° (Napolitano et al., 2022). The Southern Adriatic Northern Ionian coastal Forecasting System (SANIFS), which is a  
982 coastal-ocean operational system providing short-term forecasts since September 2014 (Federico et al., 2017). It is built on the

**Formatted:** Font: (Default) Times New Roman, Font colour: Text 1

**Deleted:** Overall, the quality of the WAV component stems out of the weakly coupled offline coupling between PHY and WAV. In particular, the WAV component assimilates data with a well calibrated stand-alone OI scheme using satellite altimetry data and implements regular updates and improved parameterization independently from the other components.

**Formatted:** Font: (Default) Times New Roman, Font colour: Text 1

**Formatted:** Font: (Default) Times New Roman, Font colour: Text 1

**Deleted:** The BIO system has defined a validation framework (Salon et al., 2019) based on the near real time observations (i.e., satellite and Argo) showing average errors in the 0-200m layer of 0.04 mg/m<sup>3</sup>, 0.4 mmol/m<sup>3</sup> and 16.8 mmol/m<sup>3</sup> for chlorophyll, nitrate and oxygen, respectively.

**Formatted:** English (UK)

**Formatted:** English (UK)

**Formatted:** English (UK)

**Formatted:** English (UK)

994 unstructured-grid finite-element three-dimensional hydrodynamic SHYFEM model and is based on a downscaling approach  
995 starting from the large-scale system Med-MFC which provides the open-sea fields.  
996 The CADEAU physical-biogeochemical forecast system of the Northern Adriatic Sea (Bruschi et al., 2021) is based on a high  
997 resolution (up to 700 m/700m) application of the MITgcm-BFM model (Cossarini et al., 2017) targeting water quality and  
998 eutrophication and uses the daily Med-MFC products for initialization and to constrain the southern boundary.  
999 In addition, the GUTTA-VISIR system, which can be defined as a tactical, global-optimization, single-objective, deterministic  
1000 model system for ship route planning (Mannarini et al., 2015 and 2016; Mannarini and Carelli, 2019), uses the analysis and  
1001 forecast wave and current fields from the Med-MFC in conjunction with wind fields from ECMWF.  
1002 Since 2008 the Med-MFC components have been continuously upgraded and substantially improved. The system evolution  
1003 will continue also in the future following the main drivers of the three components; the Copernicus Marine Service users.  
1004 Considering the PHY system, the users need finer spatial scales and higher time frequencies of the products especially for  
1005 improving the representation of the coastal scale and limited area processes in nested models, thus providing a unique  
1006 opportunity to model the coastal areas at the resolution of few hundred meters using nesting schemes as demonstrated in  
1007 Federico et al. (2017) and Trotta et al. (2021) among the others. Users also require higher accuracy in storm surge forecasting,  
1008 which can be achieved by including the explicit representation of the tidal forcing to resolve non-linear interactions between  
1009 astronomical and internal tides with the baroclinic circulation. An upgrade of lateral open boundary conditions in the Atlantic  
1010 and the Black Sea would provide better evaluation of the transport at Gibraltar on one side, and improved dynamics in the  
1011 north Aegean Sea on the other. Higher frequency river runoff data from hydrological models, as well as more accurate salinity  
1012 values at river mouths, would provide better salinity skill not only along the coastal areas but in the whole basin. Another  
1013 important goal for the future is to assimilate Argo and drifter trajectories (Nelson et al., 2016) and gliders (Dobricic et al.,  
1014 2009) data as well as sea level anomaly in coastal areas. Finally, the future should consider ensemble forecasting to recast the  
1015 deterministic forecast within a probabilistic framework assessing the modeling uncertainties (Pinardi et al., 2011; Millif et al.,  
1016 2009; Thoppil et al., 2021; Barton et al., 2021). Another important goal for the future is to assimilate Argo and drifter  
1017 trajectories (Nelson et al., 2016) and gliders (Dobricic et al., 2009), as well as sea level anomaly in coastal areas.  
1018 User needs for the future evolution of the WAV component indicate the increase of the frequency of the wave analyses, making  
1019 available larger data sets such as the wave spectra and dedicated products (like the directional spread at peak frequency and  
1020 different parts of the wave spectrum). The required increased accuracy in wave height and mean periods predictions can be  
1021 mainly achieved by improving the quality of the wind forcing which is the main driving force of wave models. Bias correction  
1022 of ECMWF winds and further downscaling of ECMWF forecasts is expected to improve winds and consequently wave product  
1023 quality especially in semi-enclosed areas (e.g. Adriatic, Aegean) and near the coast. Assimilation upgrades with the ingestion  
1024 of multi-mission significant wave heights at 5Hz and in-situ wave heights measurements from HF Radars will improve  
1025 accuracy in coastal areas of the Mediterranean Sea while the inclusion of spectral information in the near future (e.g. CFOSAT  
1026 wave spectrum) will further improve the prediction of the sea state. Finally the development of a WAV ensemble prediction

**Formatted:** English (UK)

**Formatted:** Font: (Default) Times New Roman, Font colour: Text 1,

**Formatted:** English (UK)

**Deleted:** Med-MFC

**Deleted:** ,

**Formatted:** Font: (Default) Times New Roman, Font colour: Text 1

**Deleted:** Considering the PHY component, the user needs finer spatial scales and higher time frequencies of the products. User require also higher accuracy in storm surge forecasting including tidal forcing and improved representation of lateral open boundary conditions (e.g., rivers, nesting in the Atlantic and the Black Sea). The Med-MFC offers a unique opportunity to model the coastal areas at the resolution of few hundred meters using nesting schemes (Federico et al., 2017, Trotta et al. 2021). Finally, the future should consider ensemble forecasting to recast the deterministic forecast in within a probabilistic framework (Pinardi et al. 2011, Millif et al. 2009, Thoppil et al. 2021; Barton et al., 2021).

**Formatted:** Font: (Default) Times New Roman, Font colour: Text 1

**Deleted:** Another important goal for the future is to assimilate Argo and drifter trajectories (Nelson et al., 2016) and gliders (Dobricic et al., 2009) as well as tidal coastal station at sea level.

**Formatted:** Font: (Default) Times New Roman, Font colour: Text 1

**Formatted:** Font: (Default) Times New Roman, Font colour: Text 1

based on ECMWF operational ensemble winds is expected to improve the existing accuracy of the deterministic forecast at lead times beyond 48 hours providing in parallel uncertainty estimates of wave parameters. User requirements for the BIO component developments include improved quality and products tailored for ecosystem and coastal applications. The validation results have contributed to identify ameliorable model process representations and model parameter estimates that can be improved. These include better representation of vertical nutrient and plankton dynamics, a greater number of phytoplankton functional types and zooplankton compartments to describe the diversity of the plankton community and the different energy and matter pathways in the ecosystem. In addition, the integration of optics and biogeochemistry, including novel hyperspectral and high-resolution radiometric data, can be used to better represent photosynthesis and light-related processes and to calibrate parameters of important ecosystem processes (Lazzari et al., 2021). Assimilation of new in-situ profile sensors and variables (e.g., BGC-Argo Float and Glider) will help increase the reliability of BIO products, especially along the water column (Cossarini et al., 2019). Higher quality vertical dynamics can be achieved through better representation of vertical model error covariances by ensemble (Carrassi et al., 2018) or joint physical-biogeochemical data assimilation techniques. Finally, revising nutrient and carbon inputs from rivers (e.g., from monthly climatologies to daily observations or model predictions) will allow better resolution of coastal dynamics and coastal-offshore patterns in critical areas.

**Author Contributions:** G.C. (Coppini) and E.C. coordinated the preparation of the paper in collaboration with G.C. (Cossarini) and G.K. E.C., G.C. (Cossarini) G.K., P.L., A.T., G.B., J.P., A.C.G., A.A., R.E., A.C., D.D., S.M., A.N., N.P., M.R. contributed to the system and models development; V.L., A.G., L.F., C.A., V.D., A.M., A.C.G, A.Z., C.O., E.C. contributed to the model validation and assessment; R.L., M.D., A.M., A.B., G.L.C., contributed to the operational activities. All authors contributed to the final version of the paper.

**Funding:** This work has been funded through the EU Copernicus Marine Med-MFC Service Contact n.74.

**Acknowledgments:** This study has been conducted using EU Copernicus Marine Service Information. Within the Copernicus Marine Service of the Med-MFC, CMCC is in charge of the coordination of the service and responsible for the Physics (ocean circulation) Production Unit, OGS is responsible for the BIO (biogeochemical) Production Unit and HCMR is responsible for the Wave Production Unit. The authors thank CINECA (Italian supercomputer centre) for the technical support provided in the biogeochemical component production workflow.

**Conflicts of Interest:** The authors declare no conflict of interest

**Formatted:** Font: (Default) Times New Roman, Font colour: Text 1

**Deleted:** Extreme waves forecasting requires also a probabilistic approach. The required increased accuracy can be achieved by improving the quality of the wind forcing using downscaled ECMWF forecasts and assimilating additional satellite (wave spectrum from SAR) or higher frequency in-situ wave measurements. Also, for the WAV component, the development of a WAB ensemble prediction system will be necessary.

**Formatted:** Font: (Default) Times New Roman, Font colour: Text 1

**Formatted:** Font: (Default) Times New Roman, Font colour: Text 1

**Formatted:** Font: (Default) Times New Roman, Font colour: Text 1

**Formatted:** Font: (Default) Times New Roman, Font colour: Text 1

**Formatted:** Font: (Default) Times New Roman, Font colour: Text 1

**Formatted:** Font: (Default) Times New Roman, Font colour: Text 1

**Formatted:** English (UK)

**Formatted:** Font: (Default) Times New Roman, Font colour: Text 1

**Deleted:** In the light of the user needs and requirements, the BIO component validation framework helped to identify strengths and weaknesses of the model system for future developments. In the BIO component case, future upgrades should be related to the development of the BFM biogeochemical model process representations and model parameter estimation. This includes increasing the number of phytoplankton functional types and zooplankton compartments to describe diversity of the plankton community and the different energy and matter pathways across the ecosystem. Additionally, the integration of optics and biogeochemistry including new coupled modelling and novel hyperspectral and high-resolution radiometric data will be beneficial for calibrating parameters of key ecosystem processes (Lazzari et al., 2021). Regarding the BIO component assimilation framework, the future developments should consider the assimilation of biochemical variables from new sensors such as novel satellite and in situ Argo and Gliders (Cossarini et al., 2019) and the evolution of the 3DVarBio towards hybrid-3Dvar or ensemble-3Dvar methods (Carrassi et al., 2018) and joint physical-biogeochemical data assimilation...

**Deleted:** ),

**Deleted:** Med-MFC

**Deleted:** MED-MFC

**Deleted:** WAVE

1104

1105 **Appendix A**

1106

1107

1108

Table A1. List of the NEMO and WW3 numerical setup for the PHY component.

Parameter	Value
NEMO model version	3.6
Horiz. Resolution	1/24°
Vertical discretization	141 z levels with partial cells
Vertical coordinates	<del>Z-star</del>
Time-step	240 s
Number of barotropic iterations	100
Free-surface formulation	Non-Linear free surface with split-explicit free surface
Air-sea fluxes	MFS-Bulk formulae
Atmospheric Pressure	Yes
Wave coupling	Neutral drag coefficient
Runoff	Surface boundary condition with specific treatment at river mouth and prescribed river salinity
Sea Surface Restoring T/S	only for temperature
Solar radiation penetration	2-band exponential penetration (insert the decay length and the transmission coeff)
Lateral momentum B.C.	No-slip
Lateral Open B.C.	Flather open boundary condition for barotropic currents, Orlansky for total currents and tracers
Bottom B.C	Non-linear friction with logarithmic formulation
Equation of State	EOS-80
Tracer Advection	Up-stream/MUSCL

Formatted Table

Deleted: zstar



Tracers Horiz. Diffusivity	Bi-Laplacian coeff = $-1.2.e8$ [m4/s]
Momentum Horiz. Viscosity	Bi-Laplacian coeff = $-2e.8$ [m4/s]
Momentum Advection	Vector form (energy and enstrophy cons. scheme)
Turbulent vertical viscosity scheme	Richardson number dependent formulation following Pacanowsky Philander (1981) and Lermousiaux (2001) adjustment
Background Vertical Visc.	$1.2e-6$ [m2/s]
Background Vertical Diff.	$1.0e-7$ [m2/s]
Vertical time stepping scheme	Implicit
WW3 model version	3.14
Horiz. Resolution	$1/24^\circ$
Number of frequencies	30
Number of directions	24
Time-step (global)	240 s
Wind input term	Janssen's quasi-linear theory (Jansen, 1989; Jansen, 1991)
Wave dissipation term	Hasselmann (1974) according to Komen et al. (1984)
Non-linear wave-wave interaction term	Discrete Interaction Approximation (DIA, Hasselmann et al., 1985)
Coupling with NEMO	Sea surface currents, sea surface temperature

Formatted: Superscript

Deleted: .,

**Table A2.** List of the WAM model set up for the WAV component.

Parameter	Value
WAM model version	Cycle 4.6.2
Horiz. Resolution	$1/24^\circ$

Formatted Table

Geographical domain	18.125°W - 36.2917°E 30.1875°N - 45.9792°N.
Depth map	GEBCO 30arc-second
Number of frequencies	32
Number of directions	24
Time-step (propagation)	60 s
Time-step (sources)	360 s
Deep/Shallow mode	Shallow
<u>10 m</u> winds	ECMWF <u>10 m</u> analyses and forecast winds
$C_{Ds}, \delta$	1.33, 0.5
ZALP	0.011
Surface currents coupling	Offline coupled with <u>Med-MFC</u> NRT daily surface currents
Data assimilation	Optimal Interpolation method / Altimeter satellite data provided by Copernicus Marine Service are assimilated in the wave model.

**Deleted:** 10m

**Deleted:** 10m

**Deleted:** Med-MFC

1114

1115

**Table A3.** List of the OGSTM-BFM model set up for the BIO component.

Parameter	Value
OGSTM model version	4.1
BFM model version	5.0
3DVarBio version	3.3
Horiz. Resolution	1/24o
Geographical domain	9.0°W - 36.2917°E 30.1875°N - 45.9792°N.
OGSTM: physical forcing	U, V, W, eddy diffusivity, SSH
OGSTM: timestep	450 s
OGSTM: off-line coupling frequency	1 d
OGSTM: advection scheme	Smolarkiewicz
OGSTM: horizontal diffusion	Bi-Laplacian coefficient $-3.e9$ [m <sup>4</sup> /s]
OGSTM: vertical diffusion scheme	implicit 2nd order
BFM parameters for Phytoplankton, Zooplankton, Bacteria, DOM and POM formulation	as in (Lazzari et al., 2012) and 2016
BFM light: type of model	instantaneous light from short wave radiation, light at the centre of the grid cell
BFM light: Fraction of Photosynthetically Available Radiation	0.40
BFM light: conversion W/m <sup>2</sup> to moli quanta/m <sup>2</sup> /s	1./0.217 Watt / umol photons
BFM light: background extinction coeff.	0.0435 1/m
BFM light: specific attenuation coefficient of particulate	0.001 m <sup>2</sup> /mgC

Formatted Table

BFM carbonate system: solver using total alkalinity and DIC	SolveSAPHE v1.0.1 routines (Munhoven, 2013)
BFM carbonate system: K <sub>0</sub> , solubility of CO <sub>2</sub> in the water (K Henry)	Weiss 1974
BFM carbonate system: k <sub>1</sub> and k <sub>2</sub> constants for carbonic acid	Mehrbach et al. (1973) refit, by Lueker et al. (2000) (total scale)
BFM carbonate system: K <sub>b</sub> constant for boric acid	Millero p.669 (1995) using data from Dickson (1990) (total scale)
BFM carbonate system: k <sub>1p</sub> , k <sub>2p</sub> and k <sub>3p</sub> constants of phosphoric acid	Millero (1974)
BFM carbonate system: K <sub>si</sub> constant of orthosilicic acid	Millero (1995)
BFM carbonate system: K <sub>w</sub> of water dissociation	Millero (1995)
BFM carbonate system: k <sub>s</sub> of sulfuric acid	Dickson (1990)
BFM carbonate system: k <sub>f</sub> of folic acid	Perez & Fraga (1987) recom. by Dickson et al., (2007)
BFM carbonate system: air-sea exchange model	Wannikoff et al., 2014
3DVarBio: max depth of assimilation	<del>200 m</del>
3DVarBio: n. of vertical EOFs	26
3DVarBio: horizontal correlation radius	variable in X and Y; average 15 km (Teruzzi et al., 2018)
3DVarBio: solver for cost function J	quasi-Newton L-BFGS minimizer
3DVarBio: Minimum gradient of J	1.0E-11
3DVarBio: Percentage of initial gradient	0.01
3DVarBio: n. of interactions of recursive filter	4

Deleted: 200m

1121  
1122

1124  
1125  
1126  
1127

**Table A.4.** River sources implemented as freshwater inputs in the physical and biogeochemical models, including river name, the annual mean runoff and the imposed salinity at river mouth.

<b>River Name</b>	<b>Mean annual Runoff [m3/s]</b>	<b>Salinity at river mouth [psu]</b>
Ebro	432	30
Rhone	1707	25
Po	1519	18
Buna-Bojana	675	15
Seman	201	15
Vjosa	183	15
Nile	475	8
Aude	59	15
Arno	88	15
Tevere	181	15
Volturno	63	15
Medjerda	59	15
Reno	67	15
Adige	232	15
Brenta	163	15
Piave	129	15
Livenza	96	15
Tagliamento	79	15
Isonzo	175	15
Lika	84	15
Krka	57	15
Neretva	239	15
Trebisnjica	93	15
Mati	99	15
Shkumbini	54	15
Arachtos	75	15
Acheloos	106	15
Pineios	67	15
Axios	97	15
Struma	81	15
Maritza	166	15
Gediz	53	15
Buyuk Menderes	106	15
Köprüçay/Eurimedonte	85	15
Manavgat	122	15
Goksu	203	15
Seyhan	200	15
Ceyhan	231	15
Orontes	94	15

1128  
1129

**Formatted:** Justified, Line spacing: 1,5 lines

**Deleted:** ¶

**Formatted:** Font: (Default) Times New Roman

**Formatted Table**

1131

Deleted: ¶

Page Break

1132 **References**

1133 Adani, M., Dobricic, S., and Pinardi N.: Quality Assessment of a 1985–2007 Mediterranean Sea Reanalysis. *J. Atmos. Oceanic Technol.*, 28, 569–589., doi:10.1175/2010JTECHO798.1, 2011.

Deleted: .

1136 Alves, J.-H.G.M.: Numerical modeling of ocean swell contributions to the global wind-wave climate. *Ocean Model.* 11, 98–122. doi:10.1016/j.ocemod.2004.11.007, 2006.

Deleted: .

1139 Álvarez, M., Sanleón-Bartolomé, H., Tanhua, T., Mintrop, L., Luchetta, A., Cantoni, C., et al.: The CO<sub>2</sub> system in the Mediterranean Sea: a basin wide perspective. *Ocean Sci.* 10, 69–92. doi: 10.5194/os-10-69-2014, 2014.

Deleted: .

Formatted: Font: (Default) Times New Roman, 10 pt, Font colour: Text 1, English (UK)

1141 [Alvarez Fanjul, E., Ciliberti, S., and Baharel, P.: Implementing Operational Ocean Monitoring and Forecasting Systems. Paris, France, IOC-UNESCO, 376pp. & Annexes. \(GOOS-275\). DOI: https://doi.org/10.48670/ETOOFShttps://doi.org/10.48670/ETOOFS, 2022.](https://doi.org/10.48670/ETOOFS)

Formatted: Font: (Default) Times New Roman, 10 pt, Font colour: Text 1, English (UK)

Deleted: ¶

1146 Ayoub, N., Le Traon, P.-Y., and De Mey: P. A description of the Mediterranean surface variable circulation from combined ERS-1 and Topex/Poseidon altimetric data. *J. of Mar. Syst.* 18 (1–3), 3–40, 1998.

Deleted: .

Deleted: ¶

1149 Arduin, F., Bertotti, L., Bidlot, J. R., Cavaleri, L., Filipetto, V., Lefevre, J. M., and Wittmann, P.: Comparison of wind and wave measurements and models in the Western Mediterranean Sea. *Ocean Eng.* 34, 526–541, <https://doi.org/10.1016/j.oceaneng.2006.02.008>, 2007.

Moved down [1]: M.,

Moved down [2]: P.,

Deleted: Harasawa, S., Kozyr, A., Nojiri, Y., O'Brien, K.

1153 Artuso, F., Chamard, P., Piacentino, S., Sferlazzo, D. M., De Silvestri, L., Di Sarra, A., and Monteleone, F.: Influence of transport and trends in atmospheric CO<sub>2</sub> at Lampedusa. *Atmospheric Environment*, 43(19), 3044–3051, 2009.

Deleted: Schuster, U., Telszewski, M., Tilbrook, B., Wada, C., Akl, J., Barbero, L., Bates, N. R., Boutin, J., Bozec, Y., Cai, W.-J., Castle, R. D., Chavez, F.

1156 Bakker, D. C. E., Pfeil, B., Smith, K., Hankin, S., Olsen, A., Alin, S. R., Cosca, C., et al.: An update to the Surface Ocean CO<sub>2</sub> Atlas (SOCAT version 2), *Earth Syst. Sci. Data*, 6, 69–90, doi:10.5194/essd-6-69-2014, 2014.

Deleted: Chen, L., Chierici, M., Currie, K., De Baar, H. J. W., Evans, W., Feely, R. A., Fransson, A., Gao, Z., Hales, B., Hardman-Mountford, N. J., Hoppema, M., Huang, W.-J., Hunt, C. W., Huss, B., Ichikawa, T., Johannessen, T., Jones, E. M., Jones, S., Jutterstrom, S., Kitidis, V., Körtzinger, A., Landschützer, P., Lauvset, S. K., Lefèvre, N., Manke, A. B., Mathis, J. T., Merlivat, L., Metzl, N., Murata, A., Newberger, T., Omar, A. M., Ono, T., Park, G.-H., Paterson, K., Pierrot, D., Rios, A. F., Sabine, C. L., Saito, S., Salisbury, J., Sarma, V. V. S. S., Schlitzer, R., Sieger, R., Skjelvan, I., Steinhoff, T., Sullivan, K. F., Sun, H., Sutton, A. J., Suzuki, T., Sweeney, C., Takahashi, T., Tjiputra, J., Tsurushima, N., Van Heuven, S. M. A. C., Vandemark, D., Vlahos, P., Wallace, D. W. R., Wanninkhof, R. and Watson, A. J

Formatted: Font colour: Text 1

1159 Barton N.E, Metzger J., C. A. Reynolds, B. Ruston, C. Rowley, O. M. Smedstad, J. A. Ridout, A. Wallcraft, S. Frolov, P. Hogan, M. A. Janiga, J. F. Shriver, J. McLay, P. Thoppil, A. Huang, W. Crawford, T. Whitcomb, C. H. Bishop, L. Zamudio, M. Phelps: The Navy's Earth System Prediction Capability: A new global coupled atmosphere-ocean-sea ice prediction system designed for daily to subseasonal forecasting. Barton N., Metzger E. J., Reynolds, C. A., Ruston, B., Rowley, C., Smedstad, O. M., et al.: The Navy's Earth System Prediction Capability: A new global coupled atmosphere-ocean-sea ice prediction system designed for daily to subseasonal forecasting. *Earth Space Sci.* 8, e2020EA001199, 2021.

Moved down [3]: Earth Space Sci.

Moved down [4]: 8, e2020EA001199, 2021.

1166 Bergamasco, A. and Malanotte-Rizzoli, P.: The circulation of the Mediterranean Sea: a historical review of experimental investigations, *Adv. Oceanogr. Limnol.* 1:1, 11–28, DOI: 10.1080/19475721.2010.491656, 2010.

Deleted:

1169 Brassington, G. B.: Forecast Errors, Goodness, and Verification in Ocean Forecasting. *Journal of Marine Research*, Volume 75, Number 3, pp. 403–433(31). <https://doi.org/10.1357/002224017821836851>, 2017.

Moved (insertion) [1]

1172 Bruschi, A., Lisi, I., De Angelis, R., Querin, S., Cossarini, G., Di Biagio, V., et al.: Indexes for the assessment of bacterial pollution in bathing waters from point sources: The northern Adriatic Sea CADEAU service. *Journal of Environmental Management*, 293, 112878, 2021.

Deleted: ¶

Moved (insertion) [3]

Moved (insertion) [4]

1176 Byun, D. S. and Pinardi, N.: Comparison of Marine Insolation Estimating methods in the Adriatic Sea, *Ocean Sci. J.* 42(4), 211–222, 2007.

Deleted: .

Formatted: Font colour: Text 1

Deleted: .

1212 Buongiorno Nardelli, B., Tronconi, C., Pisano, A., and Santoleri, R.: High and Ultra-High resolution processing of satellite  
1213 Sea Surface Temperature data over Southern European Seas in the framework of MyOcean project, *Rem. Sens. Env.*, 129, 1-  
1214 16, doi:10.1016/j.rse.2012.10.012, 2013.

1215

1216 Buga, L., Sarbu, G., Fryberg, L., Magnus, W., Wesslander, K., Gatti, J., et al.: EMODnet Chemistry Eutrophication and  
1217 Acidity aggregated datasets v2018, <https://doi.org/10.6092/EC8207EF-ED81-4EE5-BF48-E26FF16BF02E>, 2018.

1218

1219 Canu, D., Ghermandi, A., Nunes, P., Lazzari, P., Cossarini, G., and Solidoro, C.: Estimating the value of carbon  
1220 sequestration ecosystem services in the Mediterranean Sea: An ecological economics approach, *Global Environmental*  
1221 *Change*. 32. 10.1016/j.gloenvcha.2015.02.008, 2015.

1222

1223 Carrassi, A., Bocquet, M., Bertino, L., and Evensen, G.: Data assimilation in the geosciences: An overview of methods, issues,  
1224 and perspectives, *Wiley Interdisciplinary Reviews: Climate Change*, 9(5), e535, 2018.

1225

1226 Cavaleri, L. and Scilavo, M.: The calibration of wind and wave model data in the Mediterranean Sea, *Coast. Eng.* 53, 613–  
1227 627, 2006.

1228

1229 Cessi, P., Pinardi, N., and Lyubartsev, V.: Energetics of Semiclosed Basins with Two-Layer Flows at the Strait, *J. Phys.*  
1230 *Oceanogr.*, 44, 967–979. doi: 10.1175/JPO-D-13-0129.1, 2014.

1231

1232 Ciliberti, S.A., Jansen, E., Coppini, G., Peneva, E., Azevedo, D., Causio, S., et al.: The Black Sea Physics Analysis and  
1233 Forecasting System within the Framework of the Copernicus Marine Service. *J. Mar. Sci. Eng.*, 10, 48.  
1234 <https://doi.org/10.3390/jmse10010048>, 2022.

1235

1236 Clementi, E., Oddo, P., Drudi, M., Pinardi, N., Korres, G., and Grandi, A.: Coupling hydrodynamic and wave models: first  
1237 step and sensitivity experiments in the Mediterranean Sea, *Oc. Dyn.*, doi: <https://doi.org/10.1007/s10236-017-1087-7>, 2017a.

1238

1239 Clementi, E., Pistoia, J., Delrosso, D., Mattia, G., Fratianni, C., Storto, A., et al.: A 1/24 degree resolution Mediterranean  
1240 analysis and forecast modelling system for the Copernicus Marine Environment Monitoring Service. Extended abstract to the  
1241 8th EuroGOOS Conference, Bergen, <http://eurogoos.eu/download/publications/EuroGOOS-2017-Conference->  
1242 [Proceedings.pdf](http://eurogoos.eu/download/publications/EuroGOOS-2017-Conference-), 2017b.

1243

1244 Clementi, E., Pistoia, J., Escudier, R., Delrosso, D., Drudi, M., Grandi, A., et al.: Mediterranean Sea Analysis and Forecast  
1245 (CMEMS MED-Currents EAS5 system, 2017-2020) [Data set], Copernicus Monitoring Environment Marine Service  
1246 (CMEMS), [https://doi.org/10.25423/CMCC/MEDSEA\\_ANALYSIS\\_FORECAST\\_PHY\\_006\\_013\\_EAS5](https://doi.org/10.25423/CMCC/MEDSEA_ANALYSIS_FORECAST_PHY_006_013_EAS5), 2019.

1247

1248 Copin-Montegut, C.: Alkalinity and carbon budgets in the Mediterranean Sea. *Global Biogeochemical Cycles*, 7(4), pp. 915-  
1249 925, 1993.

1250

1251 Copernicus Marine In-Situ Team and Copernicus In Situ TAC, Real Time Quality Control for WAVES, CMEMS-INS-  
WAVES-RTQC, <https://doi.org/10.13155/46607>, 2020.

1252

1253 Cossarini, G., Mariotti, L., Feudale, L., Teruzzi, A., D’Ortenzio, F., Tallandier, V., and Mignot A.: Towards operational 3D-  
1254 Var assimilation of chlorophyll Biogeochemical-Argo float data into a biogeochemical model of the Mediterranean Sea,  
1255 *Ocean Model*, 133, 112–128, <https://doi.org/10.1016/j.ocemod.2018.11.005>, 2019.

1256

1257 Cossarini, G., Querin, S., Solidoro, C., Sannino, G., Lazzari, P., Di Biagio, V., and Bolzon, G.: Development of  
1258 BFMCOUPLER (v1.0), the coupling scheme that links the MITgcm and BFM models for ocean biogeochemistry  
simulations, *Geosci. Model Dev.*, 10, 1423–1445, <https://doi.org/10.5194/gmd-10-1423-2017>, 2017.

1259

1260 Cossarini G., Lazzari P., and Solidoro, C.: Spatiotemporal variability of alkalinity in the Mediterranean Sea, *Biogeosciences*,  
1261 12, 1647–1658, <https://doi.org/10.5194/bg-12-1647-2015>, 2015.

1262

Formatted: English (UK)

Formatted: English (UK)

Deleted: Leroy, D., Iona, S., Larsen, M., Koefoed Romer, J., Ostrem, A.K., Lipizer, M., Giorgiotti, A: Data from:

Deleted: .

Formatted: English (UK)

Formatted: English (UK)

Deleted: .

Formatted: English (UK)

Deleted: .

Formatted: English (UK)

Deleted: .

Deleted: .

Formatted: English (UK)

Formatted: English (UK)

Deleted: .

Deleted: .

Deleted: Stefanizzi, L., Creti, S., Lecci, R., Lima, L., Ilicak, M., Pinardi, N., Palazov, A

Formatted: Font colour: Text 1

Deleted: .

Formatted: Font colour: Text 1

Deleted: Ciliberti, S., Lemieux, B., Fenu, E., Simoncelli, S., Drudi, M., Grandi, A., Padeletti, D., Di Pietro, P., Pinardi, N

Formatted: English (UK)

Formatted: English (UK)

Deleted: .

Formatted: English (UK)

Formatted: Font colour: Text 1

Deleted: Lecci, R., Creti, S., Ciliberti, S., Coppini, G., Masina, S., Pinardi, N.:

Deleted: .

Formatted: Font colour: Text 1

Formatted: Font colour: Text 1

Deleted: .

Formatted: Font colour: Text 1

Formatted: Font colour: Text 1

1282 Cossarini G., Bretagnon M., Di Biagio V., Fanton d'Andon O., Garnesson P., Mangin A., and Solidoro C.: Primary  
 1283 production, Copernicus Marine Service Ocean State Report, Issue 3, J. Oper. Oceanogr., 12:sup1, s88–s91; DOI:  
 1284 10.1080/1755876X.2020.1785097, 2020.  
 1285  
 1286 Cossarini, G., Feudale, L., Teruzzi, A., Bolzon, G., Coidessa, G., Solidoro, C., Di Biagio, V., Amadio, C., Lazzari, P.,  
 1287 Brosich, A. and Salon, S.: High-resolution reanalysis of the Mediterranean Sea biogeochemistry (1999–2019). *Frontiers in*  
 1288 *Marine Science*, 8, 1537, 2021.  
 1289  
 1290 Deliverable D4.6: SES land-based runoff and nutrient load data (1980 2000), edited by Bouwman L. and van Apeldoorn D.,  
 1291 2012 PERSEUS H2020 grant agreement n. 287600.  
 1292  
 1293 Delrosso, D.: Numerical modelling and analysis of riverine influences in the Mediterranean Sea, PhD Thesis, Alma Mater  
 1294 Studiorum Università di Bologna. DOI 10.6092/unibo/amsdottorato/9392, 2020.  
 1295  
 1296 Desroziers, G., Berre, L., Chapnik, B., and Poli, P.: Diagnosis of observation, background and analysis-error statistics in  
 1297 observation space, *Q.J.R. Meteorol. Soc.* 131: 3385–3396. doi: 10.1256/qj.05.108, 2005.  
 1298  
 1299 Dobricic, S. and Pinardi, N.: An oceanographic three-dimensional variational data assimilation scheme, *Ocean modelling*,  
 1300 22: 89-105 (2008), doi:10.1016/j.ocemod.2008.01.004, 2008.  
 1301  
 1302 Dobricic, S., Pinardi, N., Adani, M., Tonani, M., Fratianni, C., Bonazzi, A., and Fernandez, V.: Daily oceanographic  
 1303 analyses by the Mediterranean basin scale assimilation system, *Ocean Sciences*, 3, 149-157, doi:10.5194/os-3-149-2007,  
 1304 2007.  
 1305  
 1306 Dobricic, S., Dufau C., Oddo P., Pinardi N., Pujol I., and Rio M.-H.: Assimilation of SLA along track observations in the  
 1307 Mediterranean with an oceanographic model forced by atmospheric pressure, *Ocean Sci.*, 8, 787-795, doi:10.5194/os-8-787-  
 1308 2012, 2012.  
 1309  
 1310 Dobricic, S., Pinardi, N., Testor, P., and Send, U.: Impact of data assimilation of glider observations in the Ionian Sea  
 1311 (Eastern Mediterranean), *Dynamics of Atmospheres and Oceans*, 50, 78-92, doi:10.1016/j.dynatmoce.2010.01.001, 2010.  
 1312  
 1313 ECMWF IFS Documentation CY43R1, Part VII: ECMWF Wave Model, *Book chapter*, ECMWF, 2016.  
 1314  
 1315 Escudier, R., Clementi, E., Omar, M., Cipollone, A., Pistoia, J., Aydogdu, A., et al.: Mediterranean Sea Physical Reanalysis  
 1316 (CMEMS MED-Currents) (Version 1) [Data set], Copernicus Monitoring Environment Marine Service (CMEMS),  
 1317 [https://doi.org/10.25423/CMCC/MEDSEA\\_MULTITYEAR\\_PHY\\_006\\_004\\_E3R1](https://doi.org/10.25423/CMCC/MEDSEA_MULTITYEAR_PHY_006_004_E3R1), 2020.  
 1318  
 1319 Escudier, R., Clementi, E., Cipollone, A., Pistoia, J., Drudi, M., Grandi, A., et al.: A High Resolution Reanalysis for the  
 1320 Mediterranean Sea, *Front. Earth Sci.* 9:702285. doi: 10.3389/feart.2021.702285, 2021.  
 1321  
 1322 Federico, I., Pinardi, N., Coppini, G., Oddo, P., Lecci, R., and Mossa, M.: Coastal ocean forecasting with an unstructured  
 1323 grid model in the southern Adriatic and northern Ionian seas, *Nat. Hazards Earth Syst. Sci.*, 17, 45–59,  
 1324 <https://doi.org/10.5194/nhess-17-45-2017>, 2017.  
 1325  
 1326 Fennel, K., Gehlen, M., Brasseur, P., Brown, C.W., Ciavatta, S., Cossarini, G., et al.: Advancing Marine Biogeochemical  
 1327 and Ecosystem Reanalyses and Forecasts as Tools for Monitoring and Managing Ecosystem Health, *Front. Mar. Sci.*, 6,  
 1328 UNSP 89, doi: 10.3389/fmars.2019.00089, 2019.  
 1329  
 1330 Feudale, L., Bolzon, G., Lazzari, P., Salon, S., Teruzzi, A., Di Biagio, V., Coidessa, G., and Cossarini, G.: Mediterranean  
 1331 Sea Biogeochemical Analysis and Forecast (CMEMS MED-Biogeochemistry, MedBFM3 system) (Version 1) [Data set],  
 1332 Copernicus Monitoring Environment Marine Service (CMEMS),  
 1333 [https://doi.org/10.25423/CMCC/MEDSEA\\_ANALYSISFORECAST\\_BGC\\_006\\_014\\_MEDBFM3](https://doi.org/10.25423/CMCC/MEDSEA_ANALYSISFORECAST_BGC_006_014_MEDBFM3)  
 1334 2021 [https://doi.org/10.25423/CMCC/MEDSEA\\_ANALYSISFORECAST\\_BGC\\_006\\_014\\_MEDBFM3\\_2021](https://doi.org/10.25423/CMCC/MEDSEA_ANALYSISFORECAST_BGC_006_014_MEDBFM3_2021).

Formatted: English (UK)

Deleted: . In:

Moved (insertion) [5]

Moved (insertion) [2]

Formatted: Font: Not Italic

Formatted: Font: Not Italic

Deleted: .

Deleted: .

Deleted: "

Deleted: .

Formatted: English (UK)

Deleted: .

Formatted: English (UK)

Formatted: English (UK)

Formatted: English (UK)

Formatted: Font colour: Text 1

Formatted: Font colour: Text 1

Formatted: Font: (Default) Times New Roman

Formatted: Font: (Default) Times New Roman

Deleted: Drudi, M., Grandi, A., Lyubartsev, V., Lecci, R., Creti, S., Masina, S., Coppini, G., Pinardi, N

Deleted: ].

Formatted: Font colour: Text 1

Deleted: Lyubartsev, V., Lecci, R., Aydogdu, A., Delrosso, D., Omar, M., Masina, S., Coppini, G., Pinardi, N

Formatted: English (UK)

Deleted: .

Deleted: Crise A., Edwards, C.A., Ford, D., Friedrichs, M.A.M., Gregoire, M., Jones, E., Kim, H.C., Lamouroux, J., Murtugudde, R., Perruche, C

Formatted: English (UK)

Deleted: .

Deleted: &

Deleted: ].

Deleted: ).

Formatted: English (UK)



|B54  
 |B55 **Flather, R. ARA.: A tidal model of the north-west European continental shelf, Mem. Soc. R. Sci. Liege, 10, pp. 141–164,**  
 |B56 **1976.**  
 |B57  
 |B58 ▼ **Fourrier M., Coppola L., Claustre H., D’Ortenzio F., Sauzède R., and Gattuso, J-P.: A Regional Neural Network Approach**  
 1359 **to Estimate Water-Column Nutrient Concentrations and Carbonate System Variables in the Mediterranean Sea: CANYON-**  
 1360 **MED. Front. Mar. Sci. 2020, 7, 620, 2021.**  
 1361  
 |B62 **Giesen, R., Clementi, E., Bajo, M., Federico, I., Stoffelen, A., and Santoleri R.: The November 2019 record high water levels**  
 1363 **in Venice, Italy. In: Copernicus Marine Service Ocean State Report, Issue 5, Journal of Operational Oceanography, 14:sup1,**  
 1364 **s140–s148; DOI: 10.1080/1755876X.2021.1946240, 2021.**  
 |B65  
 1366 ▲ **Gunther, H., Hasselmann, H., and Janssen, P.A.E.M.: The WAM model cycle 4, DKRZ report n. 4, 1993.**  
 1367  
 1368 **Janssen, P.A.E.M.: Wave induced stress and the drag of air flow over sea wave, J. Phys. Ocean., 19, 745-754, 1989.**  
 1369  
 1370 **Janssen, P.A.E.M.: Quasi-Linear theory of wind wave generation applied to wave forecasting, J. Phys. Ocean., 21, 1631-**  
 1371 **1642, 1991.**  
 1372  
 1373 **Johnson, K., Pasqueron De Fommervault, O., Serr, R., D’Ortenzio, F., Schmechtig, C., Claustre, H., and Poteau A.:**  
 |B74 **Processing Bio-Argo nitrate concentration at the DAC Level, Version 1.1, March 3rd, IFREMER for Argo Data**  
 |B75 **Management, 22pp. DOI: <http://doi.org/10.13155/46121>, 2018.**  
 1376  
 1377 **Hasselmann, K., On the spectral dissipation of ocean waves due to whitecapping, Boundary-Layer Meteorol., 126, 107 –**  
 1378 **127, 1974.**  
 1379  
 1380 **Hasselmann K., Allender J. H., and Barnett, T. P.: Computations and parameterizations of the nonlinear energy transfer in a**  
 |B81 **gravity wave spectrum. Part II: Parameterizations of the nonlinear energy transfer for application in wave models, J. Phys.**  
 1382 **Oceanogr., 15, 1378–1391, 1985.**  
 1383  
 |B84 **Hasselmann, K., Hasselmann, K., Barnett, T.P., Bouws, E., Carlson, H., Cartwright, D.E., et al.: Measurements of wind-**  
 1385 **wave growth and swell decay during the Joint North Sea Wave Project (JONSWAP), Dtsch. Hydrogr. Z., 8, 1–95, 1973.**  
 1386  
 |B87 **Hernandez, F., Bertino, L., Brassington, G., Chassignet, E., Cummings J., Davidson F., et al.: Validation and**  
 |B88 **intercomparison studies within GODAE, Oceanography 22(3): 128–143, <https://doi.org/10.5670/oceanog.2009.71>, 2009.**  
 1389  
 |B90 **Hernandez, F., Smith, G., Baetens, K., Cossarini, G., Garcia-Hermosa, I., Drevillon, M., et al.: Measuring Performances,**  
 1391 **Skill and Accuracy in Operational Oceanography: New Challenges and Approaches, New Frontiers in Operational**  
 1392 **Oceanography, E. Chassignet, A. Pascual, J. Tintoré, and J. Verron, Eds., GODAE OceanView, 759-796,**  
 1393 **doi:10.17125/gov2018.ch29, 2018.**  
 1394  
 |B95 **Katsafados, P., Papadopoulos, A., Korres, G., and Varlas, G.: A fully coupled Atmosphere–Ocean Wave modeling system**  
 1396 **(WEW) for the Mediterranean Sea: interactions and sensitivity to the resolved scales and mechanisms, Geosci. Model Dev.,**  
 1397 **9, 161–173, 2016.**  
 1398  
 |B99 **Kempe, S., Pettine M., and Cauwet, G.: Biogeochemistry of european rivers, In Degensempe & Richey eds, biogeochemistry**  
 1400 **of Major World Rivers, SCOPE 42 John Wiley 169-211, 1991.**  
 1401  
 1402 **Komen, G.J., Hasselmann, S., and Hasselmann, K.: On the existence of a fully developed windsea spectrum, J. Phys. Ocean.,**  
 1403 **14, 1271-1285, 1984.**  
 1404  
 1405 **Komen, G. J., Cavaleri, L., Donelan, M., Hasselmann, K., Hasselmann, S., and Janssen, P.: Dynamics and modelling of**  
 |H06 **ocean waves, Cambridge University Press, Cambridge, 1994.**

**Formatted:** Font: (Default) Times New Roman, Font colour: Text 1, English (UK)

**Deleted:** ¶

**Formatted:** Font: (Default) Times New Roman

**Deleted:** .

**Formatted:** Font colour: Text 1

**Deleted:** .

**Deleted:** Enke, K., Ewing, J.A., Gienapp, H., Hasselmann, D.E., Kruseman, P., Meerburg, A., Müller, P., Olbers, D.J., Richter, K., Sell, W., Walden, H

**Deleted:** Drévilion, M., G. Garric, M. Kamachi, J.-M. Lellouche, R. Mahdon, M.J. Martin, A. Ratsimandresy, and C. Regnier;

**Deleted:** .

**Deleted:** Maksymczuk, J., Melet, A., Regnier, C., Von Schuckman, K...

**Deleted:**

**Deleted:** .

1420 Korres, G., Papadopoulos, A., Katsafados, P., Ballas, D., Perivoliotis, L., and Nittis, K.: A 2-year intercomparison of the  
1421 WAM-Cycle4 and the WAVEWATCH-III wave models implemented within the Mediterranean Sea, *Mediterranean Marine*  
1422 *Science*, 12(1), 129-152, *Mediterranean Marine Science*, 12(1), 129–152,  
1423 <https://doi.org/10.12681/mms.57><https://doi.org/10.12681/mms.57>, 2011.

1424 Krasakopoulou, E., Souvermezoglou, E., Giannoudi, L., and Goyet, C.: Carbonate system parameters and anthropogenic CO<sub>2</sub>  
1425 in the North Aegean Sea during October 2013. *Continental Shelf Research*, 149, 69-81, 2017.

1426 Lazzari, P., Teruzzi, A., Salon, S., Campagna, S., Calonaci, C., Colella, S., Tonani, M., and Crise, A.: Pre-operational short-  
1427 term forecasts for the Mediterranean Sea biogeochemistry, *Ocean Sci.*, 6, 25–39, <https://doi.org/10.5194/os-6-25-2010>, 2010.

1428 Lazzari, P., Solidoro, C., Ibello, V., Salon, S., Teruzzi, A., Branger, K., Colella, S., and Crise, A.: Seasonal and inter-annual  
1429 variability of plankton chlorophyll and primary production in the Mediterranean Sea: a modelling approach, *Biogeosciences*  
1430 2012, 9:217–233, doi:10.5194/bg-9-217-2012, 2012.

1431 Lazzari, P., Solidoro, C., Salon, S., and Bolzon, G.: Spatial variability of phosphate and nitrate in the Mediterranean Sea: a  
1432 modelling approach, *Deep-Sea Res. Pt. I*, 108, 39–52, <https://doi.org/10.1016/j.dsr.2015.12.006>, 2016.

1433 Lazzari, P., Álvarez, E., Terzić, E., Cossarini, G., Chernov, I., D'Ortenzio, F., and Organelli, E.: CDOM Spatiotemporal  
1434 Variability in the Mediterranean Sea: A Modelling Study, *J. Mar. Sci. Eng.*, 9(2), 176, 2021.

1435 Lionello, P., H. Gunther, and P. A. E. M., Janssen: Assimilation of altimeter data in a global third generation wave model, *J.*  
1436 *Geophys. Res.*, 97C, 14 453–14 474, 1992.

1437 Lellouche, J.-M., Greiner, E., Le Galloudec, O., Garric, G., Regnier, C., Drevillon, M., et al.: Recent updates on the  
1438 Copernicus Marine Service global ocean monitoring and forecasting real-time 1/12° high resolution system, *Ocean Sci.*  
1439 Discuss. doi: <https://doi.org/10.5194/os-2018-15>, 2018.

1440 Lermusiaux, O.F.J.: Evolving the subspace of the three-dimensional multiscale ocean variability: Massachusetts Bay, *Journal*  
1441 *of Marine Systems* 29, 385–422, [https://doi.org/10.1016/S0924-7963\(01\)00025-2](https://doi.org/10.1016/S0924-7963(01)00025-2) 2001.

1442 Le Traon, P. Y., Reppucci, A., Alvarez Fanjul, E., Aouf, L., Behrens, A., Belmonte, M., et al.: From Observation to  
1443 Information and Users: The Copernicus Marine Service Perspective, *Front. Mar. Sci.* 6:234. doi: 10.3389/fmars.2019.00234,  
1444 2019.

1445 Levy, M., Estubier, A., and Madec, G.: Choice of an advection scheme for biogeochemical models. *Geophys. Res. Lett.*, 28,  
1446 Madec, G. and the NEMO system Team, NEMO Ocean Engine, Scientific Notes of Climate Modelling Center (27) - ISSN  
1447 1288-1619, Institut Pierre-Simon Laplace (IPSL) 2019, <http://doi.org/10.5281/zenodo.1464816> 2001

1448 Madec, G., Delecluse, P., Imbard, M., and Levy, C.: OPA8.1 Ocean general Circulation Model reference manual. Note du  
1449 Pole de modelisation, Institut Pierre-Simon Laplace (IPSL), France, 11, 1998.

1450 Maderich, V., Ilyin, Y., and Lemesko, E.: Seasonal and interannual variability of the water exchange in the Turkish Straits  
1451 System estimated by modelling, *Mediterr. Mar. Sci.*, [S.I.], v. 16, n. 2, p. 444-459, ISSN 1791-6763,  
1452 doi:<http://dx.doi.org/10.12681/mms.1103>, 2015.

1453 Mannarini, G. and Carelli, L.: VISIR-1. b: Ocean surface gravity waves and currents for energy-efficient navigation,  
1454 *Geoscientific Model Development*, 12(8), 3449-3480, 2019.

1455 Marchesiello, P., McWilliams, J.C., and Shchepetkin, A.: Open boundary conditions for long-term integration of regional  
1456 oceanic models, *Ocean modelling*, 3, 1–2, pp. 1–20, 2001.

Formatted: Font colour: Text 1, Highlight

Deleted: :

Formatted: Font colour: Text 1

Deleted: :

Deleted: :

Deleted: :

Formatted: Italian

Formatted: Font colour: Text 1

Formatted: Italian

Deleted: :

Formatted: Font: Not Italic, Italian

Formatted: Italian

Formatted: Font: (Default) Times New Roman, Italian

Formatted: Italian

Deleted: :

Deleted: Benkiran, M., Testut, C.E., Bourdalle-Badie, R., Gasparin, F., Hernández, O., Levier, B., Drillet, Y., Remy, E., Le Traon, P.Y

Deleted: :

Formatted: Font colour: Text 1

Deleted: :

Formatted: Font colour: Text 1

Deleted: Bentamy, A., Bertino, L., Brando, V., Kreiner, M.B., Benkiran, M., Carval, T., Ciliberti, S.A., Claustre, H., Clementi, E., Coppini, G., Cossarini, G., De Alfonso Alonso-Muñoz, M., Delamarche, A., Dibarbour, G., Dinessen, F., Drevillon, M., Drillet, Y., Faugere, Y., Fernández, V., Fleming, A., Garcia-Hermosa, M.I., Sotillo, M.G., Garric, G., Gasparin, F., Giordan, C., Gehlen, M., Gregoire, M.L., Guinehut, S., Hamon, M., Harris, C., Hernandez, F., Hinkler, J.B., Hoyer, J., Karvonen, J., Kay, S., King, R., Lavergne, T., Lemieux-Dudon, B., Lima, L., Mao, C., Martin, M.J., Masina, S., Melet, A., Buongiorno Nardelli, B., Nolan, G., Pascual, A., Pistoia, J., Palazov, A., Piolle, J.F., Pujol, M.I., Pequignot, A.C., Peneva, E., Pérez Gómez, B., Petit de la Villeon, L., Pinardi, N., Pisano, A., Pouliquen, S., Reid, R., Remy, E., Santoleri, R., Siddorn, J., She, J., Staneva, J., Stoffelen, A., Tonani, M., Vandenbulcke, L., von Schuckmann, K., Volpe, G., Wettre, C., and Zacharioudaki, A

Deleted: :

Deleted: :

Formatted: Font colour: Text 1

Deleted: :

Formatted: Font: (Default) Times New Roman, Font colour: Text 1, English (UK)

Deleted: ¶

Formatted: Font: (Default) Times New Roman

1501 McEwan, R., Kay, S., and Ford, D.: Quality Information Document of  
1502 NWSHELF\_ANALYSISFORECAST\_BGC\_004\_002. Marine Copernicus Service.  
1503 <https://catalogue.marine.copernicus.eu/documents/QUID/CMEMS-NWS-QUID-004-002.pdf>,  
1504 accessed 15 July 2022, 2021.

1505  
1506 McGovern, J.V., Dabrowski, T., Pereiro, D., Gutknecht, E., Lorente, P., Reffray, G., Aznar, R., and Sotillo, M.G.: Quality  
1507 Information Document of IBI\_ANALYSISFORECAST\_BGC\_005\_004. Marine Copernicus Service.  
1508 <https://catalogue.marine.copernicus.eu/documents/QUID/CMEMS-IBI-QUID-005-004.pdf>, accessed 15 July 2022, 2020.

1509  
1510 Melsom, A. and Yumruktepe, C.: Quality Information Document of ARTIC\_ANALYSIS\_FORECAST\_BIO\_002\_004.  
1511 Marine Copernicus Service. <https://catalogue.marine.copernicus.eu/documents/QUID/CMEMS-ARC-QUID-002-004.pdf>,  
1512 accessed 15 July 2022, 2021.

1513  
1514 Meybeck, M. and Ragu, A.: River Discharges to the Oceans: An Assessment of suspended solids, major ions and nutrients  
1515 UNEP STUDY, 1995.

1516  
1517 Milliff, R., Bonazzi, A., Wikle, C.K., Pinardi, N., and Berliner, L. M.: Ocean ensemble forecasting. Part I: Ensemble  
1518 Mediterranean winds from a Bayesian hierarchical model. *Q. J. R. Meteorol. Soc.* 137: 858–878. DOI:10.1002/qj.767, 2011.

1519  
1520 Nagy, H., Lyons, K., Nolan, G., Cure, M., and Dabrowski, T.: A Regional Operational Model for the North East Atlantic:  
1521 Model Configuration and Validation. *J. Mar. Sci. Eng.*, 8, 673. <https://doi.org/10.3390/jmse8090673>, 2020.

1522  
1523 [Napolitano, E., Iacono, R., Palma, M., Sannino, G., Carillo, A., Lombardi, E., Pisacane, G. and Struglia, M.V.: MV \(2022\)](#)  
1524 [MITO: A new operational model for the forecasting of the Mediterranean sea circulation.](#) *Front. Energy Res.* 10:941606.  
1525 [doi: 10.3389/fenrg.2022.941606](https://doi.org/10.3389/fenrg.2022.941606), 2022.

1526  
1527 Oddo, P., Adani, M., Pinardi, N., Fratianni, C., Tonani, M., and Pettenuzzo, D.: A Nested Atlantic-Mediterranean Sea  
1528 General Circulation Model for Operational Forecasting. *Ocean Sci.*, 5, 461–473, doi:10.5194/os-5-461-2009, 2009.

1529  
1530 Oddo, P., Bonaduce, A., Pinardi, N., and Guarneri, A.: Sensitivity of the Mediterranean sea level to atmospheric pressure  
1531 and free surface elevation numerical formulation in NEMO, *Geosci. Model Dev.*, 7, 3001–3015. doi:10.5194/gmd-7-3001-  
1532 2014, 2014.

1533  
1534 [Orlanski, I.: A simple boundary condition for unbounded hyperbolic flows.](#) *Journal of computational physics*, 21.3, pp. 251–  
269, 1976.

1535  
1536 Pacanowski, R. C., and Philander, S. G. H.: Parameterization of vertical mixing in numerical models of tropical  
1537 oceans. *Journal of Physical Oceanography*, 11, 1443–1451. [https://doi.org/10.1175/1520-0485\(1981\)011<1443:POVMIN>2.0.CO;2](https://doi.org/10.1175/1520-0485(1981)011<1443:POVMIN>2.0.CO;2), 1981.

1538  
1539 Pettenuzzo, D., Large, W. G., and Pinardi, N.: On the corrections of ERA-40 surface flux products consistent with the  
1540 Mediterranean heat and water budgets and the connection between basin surface total heat flux and NAO. *J. Geophys. Res.*,  
1541 115 (C6), doi:10.1029/2009JC005631, URL <http://dx.doi.org/10.1029/2009JC005631>, 2010.

1542  
1543 Pinardi, N., Arneri, E., Crise, A., Ravaoli, M., and Zavatarelli, M.: "The physical, sedimentary and ecological structure and  
1544 variability of shelf areas in the Mediterranean Sea" *The Sea*, Vol. 14 (A. R. Robinson and K. Brink Eds.), Harvard  
1545 University Press, Cambridge, USA 1243-1330, 2006.

1546  
1547 Pinardi, N., and Coppini, G.: Preface "Operational oceanography in the Mediterranean Sea: the second stage of  
1548 development", *Ocean Sci.*, 6, 263–267, <https://doi.org/10.5194/os-6-263-2010>, 2010.

1549  
1550 Pinardi, N., Zavatarelli, M., Adani, M., Coppini, G., Fratianni, C., Oddo, P., et al.: Mediterranean Sea large-scale low-  
1551 frequency ocean variability and water mass formation rates from 1987 to 2007: A retrospective analysis. *Prog. Oceanogr.*,  
1552 132, 318–332, <https://doi.org/10.1016/j.pocean.2013.11.003>, 2015.

Deleted: .:

Deleted: .:

Deleted: .:

Deleted: .:

Deleted: .:

Deleted: .:

Deleted: .:

Deleted: .:

Formatted: Font: Times New Roman, 10 pt, Font colour: Text 1, Pattern: Clear

Formatted: Font: Times New Roman, 10 pt, Font colour: Text 1, Pattern: Clear

Formatted: Font: Times New Roman, 10 pt, Font colour: Text 1, Pattern: Clear

Deleted: ¶

Formatted: English (UK)

Deleted: .:

Formatted: English (UK)

Formatted: English (UK)

Formatted: Font: (Default) Times New Roman, Font colour: Text 1, English (UK)

Formatted: Font: (Default) Times New Roman, Font colour: Text 1, English (UK)

Deleted: ¶

Formatted: Font colour: Text 1

Deleted: .:

Formatted: Font colour: Text 1

Formatted: English (UK)

Formatted: Font colour: Text 1

Formatted: English (UK)

Deleted: Simoncelli, S., Tonani, M., Lyubartsev, V., Dobricic, S., Bonaduce, A

Deleted: .:

Formatted: Font colour: Text 1

1566 Pinardi, N., Lermusiaux, P., F. J.; Brink Kenneth, H., Preller Ruth, H.: The Sea: The science of ocean predictions. *Journal of*  
1567 *Marine Research*, Volume 75, Number 3, May 2017, pp. 101-102(2), [10.1357/002224017821836833](https://doi.org/10.1357/002224017821836833), 2017.

1568  
1569 Pinardi, N., Cessi, P., Borile, F., [and](#) Wolfe, C.L.: The Mediterranean Sea Overturning Circulation. *J. Phys. Oceanogr.*, 49,  
1570 1699–1721, doi: 10.1175/JPO-D-18-0254.1, 2019.

1571  
1572 [Pineau-Guillou, L., Arduin, F., Bouin, M.-N., Redelsperger, J.-L., Chapron, B., Bidlot, J.-R., and Quilfen Y.: Strong winds](#)  
1573 [in a coupled wave-atmosphere model during a North Atlantic storm event: evaluation against observations, \*Quarterly Journal\*](#)  
1574 [of the Royal Meteorological Society, 144\(711\), Part B, 317-332.](#)  
1575 <https://doi.org/10.1002/qj.3205><https://doi.org/10.1002/qj.3205>, 2018.

1576  
1577 Pistoia, J., Clementi, E., Delrosso, D., Mattia, G., Fratianni, C., Drudi, M., [et al.](#): Last improvements in the data assimilation  
1578 scheme for the Mediterranean Analysis and Forecast system of the Copernicus Marine Service. Extended abstract to the 8th  
1579 EuroGOOS Conference 2017, Bergen, <http://eurogoos.eu/download/publications/EuroGOOS-2017-Conference->  
1580 [Proceedings.pdf](#), 2017.

1581  
1582 Ramirez-Romero, E., Jordà, G., Amores, A., Kay, S., Segura-Noguera, M., Macias, D.M., Maynou, F., Sabatés, A., and  
1583 Catalán, I.A.: Assessment of the Skill of Coupled Physical–Biogeochemical Models in the NW Mediterranean. *Front. Mar.*  
1584 *Sci.* 7:497. doi: 10.3389/fmars.2020.00497, 2020.

1585  
1586 Ravdas, M., Zacharioudaki, A., [and](#) Korres, G.: Implementation and validation of a new operational wave forecasting system  
1587 of the Mediterranean Monitoring and Forecasting Centre in the framework of the Copernicus Marine Environment  
1588 Monitoring Service. *Nat. Hazards Earth Syst. Sci.*, 18, 2675-2695, <https://doi.org/10.5194/nhess-18-2675-2018>, 2018.

1589  
1590 Ribera d'Alcalà, M., Civitarese, G., Conversano, F., [and](#) Lavezza, R.: Nutrient ratios and fluxes hint at overlooked processes  
1591 in the Mediterranean Sea. *Journal of Geophysical Research*, 108(C9), 8106, doi:10.1029/2002JC001650, 2003.

1592  
1593 Robinson, A.R., Leslie, W.G., Theocharis, A., [and](#) Lascartos, A.: Mediterranean Sea Circulation. *Encyclopedia of Ocean*  
1594 *Sciences*, pp 1689-1705, <https://doi.org/10.1006/rwos.2001.0376>, 2001.

1595  
1596 [Lazzari, P., Teruzzi, A., Solidoro, C., Crise, A.: Marine Ecosystem forecasts: skill performance of the CMEMS](#)  
1597 [Mediterranean Sea model system. \*Ocean Sci. Discuss.\*, 1–35, <https://doi.org/10.5194/os-2018-145>, 2019.](#)

1598  
1599 [Salon, S., Cossarini, G., Bolzon, G., Feudale, L., Lazzari, P., Teruzzi, A., et al.: Novel metrics based on Biogeochemical](#)  
1600 [Argo data to improve the model uncertainty evaluation of the CMEMS Mediterranean marine ecosystem forecasts. \*Ocean\*](#)  
1601 [Science, 15\(4\), 997-1022, 2019.](#)

1602  
1603 Schneider, A., Wallace, D. W. R., and Kortzinger, A.: Alkalinity of the Mediterranean Sea, *Geophys. Res. Lett.*, 34, L15608,  
1604 doi:10.1029/2006GL028842, 2007.

1605  
1606 [Schmechtig, C., Poteau, A., Claustre, H., D'Ortenzio, F., Dall'Olmo, G., and Boss, E.: Processing Bio-Argo particle](#)  
1607 [backscattering at the DAC level. <https://doi.org/10.13155/39468>, 2018.](#)

1608  
1609 Semedo, A., Sušelj, K., Rutgersson, A., and Sterl, A.: A global view on the wind sea and swell climate and variability from  
1610 EERA-40. *J. Clim.* 24 1461–79, 2011.

1611  
1612 [Simoncelli, S., Masina, S., Axell, L., Liu, Y., Salon, S., Cossarini, G., et al.: MyOcean regional reanalyses: overview of](#)  
1613 [reanalyses systems and main results. \*Mercator Ocean J\* 54: Special issue on main outcomes of the MyOcean2 and MyOcean](#)  
1614 [follow-on projects. <https://www.mercator-ocean.fr/wpcontent/uploads/2016/03/JournalMO-54.pdf>, 2016.](#)

1615  
1616 Simoncelli, S., Fratianni, C., Pinardi, N., Grandi, A., Drudi, M., Oddo, P., [and](#) Dobricic, S.: Mediterranean Sea Physical  
1617 Reanalysis (CMEMS MED-Physics) (Version 1) [Data set]. Copernicus Monitoring Environment Marine Service  
1618 (CMEMS). [https://doi.org/10.25423/MEDSEA\\_REANALYSIS\\_PHYS\\_006\\_004](https://doi.org/10.25423/MEDSEA_REANALYSIS_PHYS_006_004), 2019.

Formatted: Font colour: Text 1

Deleted: .

Formatted: Font colour: Text 1

Deleted: Grandi, A., Padeletti, D., Di Pietro, P., Storto, A., Pinardi, N

Deleted: .

Formatted: Font colour: Text 1

Deleted: .

Formatted: English (UK)

Formatted: Font colour: Text 1

Formatted: English (UK)

Formatted: English (UK)

Deleted: .

Formatted: English (UK)

Formatted: Font colour: Text 1

Deleted: .

Salon, S., Cossarini, G., Bolzon, G.,

Moved up [5]: Feudale, L.,

Formatted: Font: (Default) Times New Roman, Font colour: Text 1

Formatted: English (UK)

Formatted: English (UK)

Deleted: .

Formatted: Font colour: Text 1

Formatted: English (UK)

Deleted: Bertino, L., Xie, J., Samuelsen, A., Levier, B.,

Formatted: English (UK)

Formatted: English (UK)

Deleted: .

Formatted: English (UK)

Formatted: English (UK)

Deleted: .

Deleted: .

Formatted: Font colour: Text 1

Formatted: Font colour: Text 1

1634  
1635 Siokou-Frangou, I., Christaki, U., Mazzocchi, M.G., Montresor, M., Ribera d'Alcal, M., Vaqu, D., and Zingone, A.:  
1636 Plankton in the open Mediterranean Sea: a review, *Biogeosciences*, 7 (5):1543–1586, 2010.

1637  
1638 Snyder, R. L., Dobson, F. W., Elliot, J. A., and Long, R. B.: Array measurements of atmospheric pressure fluctuations above  
1639 surface gravity waves, *J. Fluid Mech.*, 102, 1–59, 1981.

1640  
1641 [Sotillo, M. G., Garcia-Hermosa, I., Drévuillon, M., Régnier, C., Szczypta, C., Hernandez, F., Melet, A., and Le Traon, P.Y.:](#)  
1642 [Communicating CMEMS Product Quality: evolution & achievements along Copernicus-1 \(2015- 2021\), \*Mercator Ocean\*](#)  
1643 [Journal #57, <https://marine.copernicus.eu/it/node/19306><https://marine.copernicus.eu/it/node/19306>, 2021.](#)

1644  
1645 Souvermezoglou, E., Krasakopoulou, E., and Pavlidou, A.: Temporal and spatial variability of nutrients and oxygen in the  
1646 North Aegean Sea during the last thirty years. *Mediterranean Marine Science*, 15/4, 805-822, 2014.

1647  
1648 Spruch L., Verjovkina, S., Jandt, S., Schwichtenberg, F., Huess, V., Lorkowski, I., and Lagema, P.: Quality Information  
1649 Document of BALTICSEA\_ANALYSIS\_FORECAST\_BIO\_003\_007. Marine Copernicus Service.  
1650 <https://catalogue.marine.copernicus.eu/documents/QUID/CMEMS-BAL-QUID-003-007.pdf>, accessed 15 July 2022, 2020.

1651  
1652 Storto, A., Masina, S., and Navarra, A.: Evaluation of the CMCC eddy-permitting global ocean physical reanalysis system  
1653 (C-GLORS, 1982-2012) and its assimilation components, *Quarterly Journal of the Royal Meteorological Society*, 142, 738–  
1654 758, doi: 10.1002/qj.2673, 2015.

1655  
1656 Taburet, G., Sanchez-Roman, A., Ballarotta, M., Pujol, M.-I., Legeais, J.-F., Fournier, F., Faugere, Y., and Dibarboure, G.:  
1657 DUACSDT2018: 25years of reprocessed sea level altimetry products, *Ocean Sci.*, 15, 1207–1224,  
1658 <https://doi.org/10.5194/os-15-1207-2019>, 2019.

1659  
1660 Terzic, E., Salon, S., Solidoro, C., Cossarini, G., Teruzzi, A., Miro, A., and Lazzari, P.: Impact of interannually variable  
1661 diffuse attenuation coefficients for downwelling irradiance on biogeochemical modelling, *Ocean Modell.*, OCEMOD-D-20-  
1662 00012R2, 2021.

1663  
1664 Teruzzi, A., Dobricic, S., Solidoro, C., and Cossarini, G.: A 3D variational assimilation scheme in coupled transport  
1665 biogeochemical models: Forecast of Mediterranean biogeochemical properties, *J. Geophys. Res. Oceans*, 119, 200–217,  
1666 <https://doi.org/10.1002/2013JC009277>, 2014.

1667  
1668 Teruzzi, A., Bolzon, G., Salon, S., Lazzari, P., Solidoro, C., and Cossarini, G.: Assimilation of coastal and open sea  
1669 biogeochemical data to improve phytoplankton modelling in the Mediterranean Sea, *Ocean Model.* 132, 46–60,  
1670 <https://doi.org/10.1016/j.ocemod.2018.09.007>, 2018.

1671  
1672 Teruzzi, A., Di Cerbo, P., Cossarini, G., Pascolo, E., and Salon, S.: Parallel implementation of a data assimilation scheme for  
1673 operational oceanography: the case of the OGSTM-BFM model system, *Comput. Geosci.*, 124, 103–114,  
1674 <https://doi.org/10.1016/j.cageo.2019.01.003>, 2019.

1675  
1676 Teruzzi, A., Bolzon, G., Feudale, L., and Cossarini, G.: Deep chlorophyll maximum and nutricline in the Mediterranean Sea:  
1677 emerging properties from a multi-platform assimilated biogeochemical model experiment, *Biogeosciences*, 18(23), 6147-  
1678 6166, 2021.

1679  
1680 Thoppil, P.G., Frolov, S., Rowley, C.D., Reynolds C. A., Jacobs G. A., E. Metzger J., et al.: Ensemble forecasting greatly  
1681 expands the prediction horizon for ocean mesoscale variability, *Commun Earth Environ* 2, 89  
1682 <https://doi.org/10.1038/s43247-021-00151-5>, 2021.

1683  
1684 Toledano, C., Ghantous, M., Lorente, P., Dalphinnet, A., Aouf, L., and Sotillo, M.G.: Impacts of an Altimetric Wave Data  
1685 Assimilation Scheme and Currents-Wave Coupling in an Operational Wave System: The New Copernicus Marine IBI Wave  
1686 Forecast Service, *J. Mar. Sci. Eng.* 10, 457, <https://doi.org/10.3390/jmse10040457>, 2022.

Deleted: .

Deleted: F. W.

Deleted: J. A.

Deleted: R. B.

Deleted: .

Deleted: .

Deleted: ¶

Sotillo, M.G., Campuzano, F., Guihou, K., Lorente, P., Olmedo, E., Matulka, A., Santos, F., Amo-Baladrón, M.A., Novellino, A.: River Freshwater Contribution in Operational Ocean Models along the European Atlantic Façade: Impact of a New River Discharge Forcing Data on the CMEMS IBI Regional Model Solution. *J. Mar. Sci. Eng.*, 9, 401. <https://doi.org/10.3390/jmse9040401>, 2021

Formatted: English (UK)

Formatted: English (UK)

Formatted: English (UK)

Formatted: English (UK)

Formatted: English (UK)

Formatted: English (UK)

Formatted: English (UK)

Deleted: .

Formatted: English (UK)

Deleted: .

Formatted: English (UK)

Formatted: Font colour: Text 1

Formatted: English (UK)

Deleted: .

Formatted: Font colour: Text 1

Deleted: .

Formatted: Font colour: Text 1

Deleted: .

Formatted: English (UK)

Formatted: Font colour: Text 1

Formatted: English (UK)

Formatted: English (UK)

Deleted: .

Formatted: English (UK)

Deleted: .

Deleted: .

Deleted: .

1710  
1711  
1712  
1713  
1714  
1715  
1716  
1717  
1718  
1719  
1720  
1721  
1722  
1723  
1724  
1725  
1726  
1727  
1728  
1729  
1730  
1731  
1732  
1733  
1734  
1735  
1736  
1737  
1738  
1739  
1740  
1741  
1742  
1743  
1744  
1745  
1746  
1747  
1748  
1749  
1750  
1751  
1752  
1753  
1754  
1755  
1756  
1757  
1758  
1759  
1760  
1761

Tonani, M., Balmaseda, M., Bertino, L., Blockley, E., Brassington, G., Davidson, F., **et al.**: Status and future of global and regional ocean prediction systems, *J Operational Oceanography* 8:201-220, doi:10.1080/1755876X.2015.1049892, 2015.

Tonani, M., Pinardi, N., Dobricic, S., Pujol, I., **and** Fratianni, C.: A high-resolution free-surface model of the Mediterranean Sea, *Ocean Sci.*, 4, 1-14, 2008.

Trisolino, P., di Sarra, A., Sferlazzo, D., Piacentino, S., Montealeone, F., Di Iorio, T., **et al.**: Application of a Common Methodology to Select in Situ CO2 Observations Representative of the Atmospheric Background to an Italian Collaborative Network, *Atmosphere*, 12, 246. <https://doi.org/10.3390/atmos12020246>, 2021.

Tugrul, S., Besiktepe, T., **and** Salihoglu, I.: Nutrient exchange fluxes between the Aegean and Black Seas through the Marmara Sea, *Mediterranean Marine Science*, 3/1, 33-42, 2002.

Vandenbulcke L., Capet A., **and** Grégoire M.: Quality Information Document of BLKSEA\_ANALYSIS\_FORECAST\_BIO\_007\_010, *Marine Copernicus Service*, <https://catalogue.marine.copernicus.eu/documents/QUID/CMEMS-BS-QUID-007-010.pdf>, accessed 15 July 2022, 2021.

Verri, G., Pinardi, N., Bryan, F., Tseng, Y., Coppini, G., and Clementi, E.: A box model to represent estuarine dynamics in mesoscale resolution ocean models, *Ocean Modelling*. <http://dx.doi.org/10.1016/j.ocemod.2020.101587>, <http://dx.doi.org/10.1016/j.ocemod.2020.101587>, 2020.

Vichi M., Lovato, T., Butenschön, M., Tedesco, L., Lazzari, P., Cossarini, G., **et al.**: The Biogeochemical Flux Model (BFM): Equation Description and User Manual, BFM version 5.2. BFM Report series N. 1, Release 1.2, June 2020, Bologna, Italy, <http://bfm-community.eu>, pp. 104, 2020.

Vichi, M., Lovato, T., Butenschön, M., Tedesco, L., Lazzari, P., Cossarini, G., Masina, S., Pinardi, N., Solidoro, C., **and** Zavatarelli, M.: The Biogeochemical Flux Model (BFM): Equation Description and User Manual, BFM version 5.2. BFM Report series N. 1, Release 1.2, June 2020, Bologna, Italy, <http://bfm-community.eu>, pp. 104, 2020.

Volpe, G., Colella, S., Brando, V. E., Forneris, V., Padula, F. L., Cicco, A. D., **et al.**: Mediterranean ocean colour Level 3 operational multi-sensor processing, *Ocean Science*, 15(1), 127-146, 2019.

von Schuckmann, K., Le Traon, P.-Y., Alvarez Fanjul, E., Axell, L., Balmaseda, M., Breivik, L.-A., **et al.**: The Copernicus Marine Environment Monitoring Service Ocean State Report, *Journal of Operational Oceanography*, 9:sup2, s235-s320, DOI: 10.1080/1755876X.2016.1273446, 2016.

von Schuckmann K., Le Traon, P.-Y., Smith, N., Pascual, A., Brasseur, P., Fennel, K., **et al.**: Copernicus Marine Service Ocean State Report, *Journal of Operational Oceanography*, 11:sup1, S1-S142, DOI: 10.1080/1755876X.2018.1489208, 2018.

von Schuckmann K., Le Traon, P.-Y., Smith, N., Pascual, A., Djavidnia, S., Gattuso, J.-P., **et al.**: Copernicus Marine Service Ocean State Report, Issue 3, *Journal of Operational Oceanography*, 12:sup1, S1-S123, DOI: 10.1080/1755876X.2019.1633075, 2019.

von Schuckmann, K., Le Traon, P.-Y., Smith, N., Pascual, A., Djavidnia, S., Gattuso, J.-P., **et al.**: Copernicus Marine Service Ocean State Report, Issue 4. *J.Op. Oceanogr.*, 13, <https://doi.org/10.1080/1755876X.2020.1785097>, 2020.

Zodiatis, G., Lardner, R., Lascaratos, A., Georgiou, G., Korres, G., and Syrimis, M.: High resolution nested model for the Cyprus, NE Levantine Basin, eastern Mediterranean Sea: implementation and climatological runs, *Ann. Geophys.*, 21, 221-236, <https://doi.org/10.5194/angeo-21-221-2003>, 2003.

**Deleted:** Drillet, Y., Hogan, P., Kuragano, T., Lee, T., Mehra, A., Paranathara, F., Tanajura, CAS, Wang, H

**Deleted:** .

**Deleted:** .

**Deleted:** Apadula, F., Heltai, D., Lanza, A., Vocino, A., Caracciolo di Torchiareolo, L., Bonasoni, P., Calzolari, F., Busetto, M., Cristofanelli, P

**Formatted:** English (UK)

**Formatted:** English (UK)

**Deleted:** .

**Formatted:** English (UK)

**Formatted:** English (UK)

**Deleted:** .

**Formatted:** English (UK)

**Formatted:** Font: (Default) Times New Roman

**Deleted:** .

**Deleted:** .

**Formatted:** Font: 10 pt, Font colour: Text 1, English (UK)

**Deleted:** ¶

**Formatted:** English (UK)

**Deleted:** Masina, S., Pinardi, N., Solidoro, C., Zavatarelli, M

**Deleted:** .

**Formatted:** English (US)

**Formatted:** Font: (Default) Times New Roman, Font colour: Text 1, Italian

**Deleted:** ¶

**Formatted:** English (US)

**Formatted:** English (UK)

**Deleted:** ... and Santoleri, R

**Deleted:** .

**Deleted:** [...]:

**Formatted:** English (UK)

**Formatted:** English (UK)

**Deleted:** [...]:

**Formatted:** English (UK)

**Deleted:** [...]:

**Formatted:** English (UK)

**Deleted:** [...]:

**Formatted:** Font colour: Text 1

1783 WAMDI Group. The WAM model—a third generation ocean wave prediction model. *J. Phys. Oceanogr.*, 18:1775–1810.  
1784 [https://doi.org/10.1175/1520-0485\(1988\)018<1775:TWMTGO>2.0.CO;2](https://doi.org/10.1175/1520-0485(1988)018<1775:TWMTGO>2.0.CO;2), 1988.

1785  
1786 Wanninkhof, R.: Relationship between wind speed and gas exchange over the ocean revisited. *Limnol. Oceanogr. Methods*  
1787 12, 351–362. <https://doi.org/10.4319/lom.2014.12.351>, 2014.

1788  
1789 [Weatherall, P., Marks, K. M., Jakobsson, M., Schmitt, T., Tani, S., Arndt, J. E., Rovere, M., Chaves, D., Ferrini, V. and](#)  
1790 [Wigley, R.: A new digital bathymetric model of the world's oceans, \*Earth and space Science\*, 2\(8\), 331-345, 2015.](#)

1791  
1792 Yalcin, B., Artuz, M.L., Pavlidou, A., Cubuk, S., [and](#) Dassenakis, M.: Nutrient dynamics and eutrophication in the Sea of  
1793 Marmara: data from recent oceanographic research. *Science of the Total Environment*, 601-602, 405-424, 2017.

1794  
1795 Young, I.R.: Seasonal variability of the global ocean wind and wave climate. *Int. J. Climatol.* 19, 931–950.  
1796 doi:10.1002/(SICI)1097-0088(199907)19:93.0.CO;2-O, 1999.

1797  
1798

Deleted: .

Formatted: Font colour: Text 1

Deleted: .

Deleted: .

Deleted: ¶

1804 **Figures**

1805

1806

1807

1808

1809

1810

1811

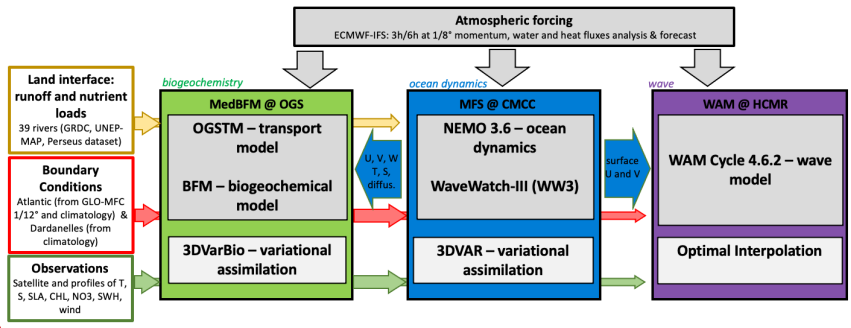


Figure 1: The **Med-MFC** core components and the off-line coupling scheme. The Blue arrow are the exchanged fields at daily frequency between the three components.

Formatted: English (UK)

Deleted: Med-MFC



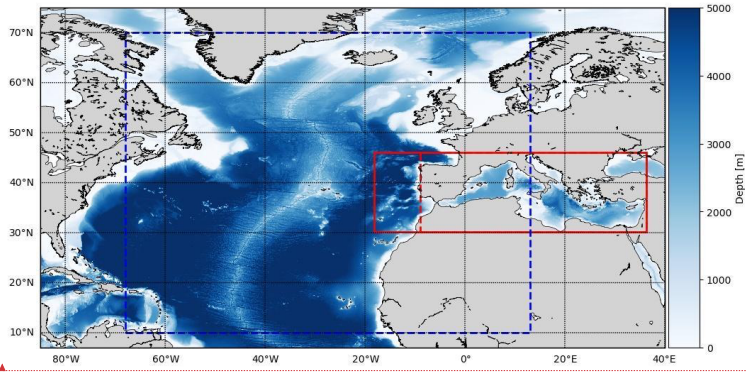


Figure 2. The solid red box presents the domain of the PHY and WAV Mediterranean components. For BIO the domain extends in the Atlantic as far as the dashed red line. The blue box presents one of the WAM domains, producing boundary conditions for the Mediterranean WAV component which extends only in the solid red box.

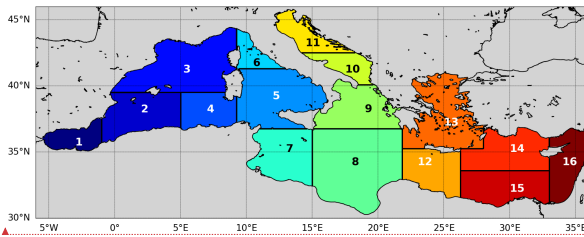
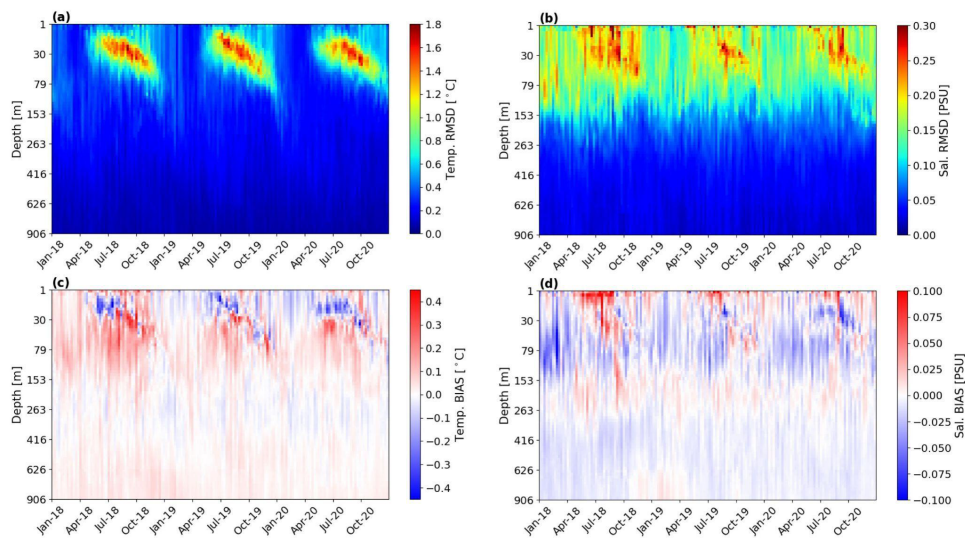


Figure 3 The Mediterranean Sea domain and sub-regions subdivision for analysis of the skill scores: Albanian (1), South-West Mediterranean-1 (2), North-West Mediterranean (3), South-West Mediterranean-2 (4), South Tyrrhenian (5), North Tyrrhenian (6), West Ionian (7), East Ionian (8), North-East Ionian (9), South Adriatic (10), North Adriatic (11), West Levantine (12), Aegean (13), North-Central Levantine (14), South-Central Levantine (15), East Levantine (16).

Formatted: English (UK)

Formatted: English (UK)



Formatted: English (UK)

1836

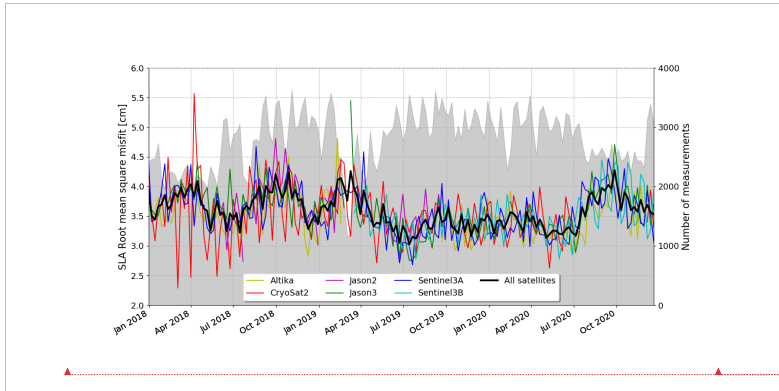
1837

1838

1839

**Figure 4** Hovmoller (Depth-Time) diagrams: (a) weekly RMS of temperature misfits, (b) weekly RMS salinity misfits, (c) weekly bias of temperature and (d) weekly bias of salinity, evaluated along the water column and averaged in the whole Mediterranean Sea.

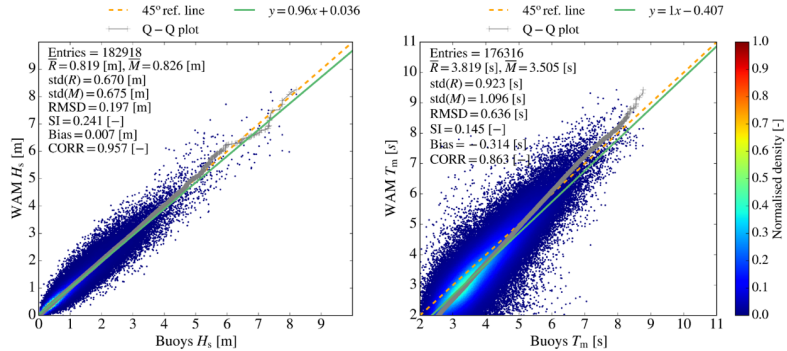
1840  
1841  
1842



1843 **Figure 5. Time Series of weekly mean RMS misfit error for SLA evaluated with respect to available satellite altimeters and averaged**  
1844 **in the whole Mediterranean Sea. Black bold line represents the mean error with respect to the whole set of satellites which are**  
1845 **separately shown with different colours. The grey area indicates the number of observations used for the validation.**

**Formatted:** English (UK)  
**Formatted:** Font: Times New Roman  
**Formatted Table**

1846



1847

1848

1849

1850

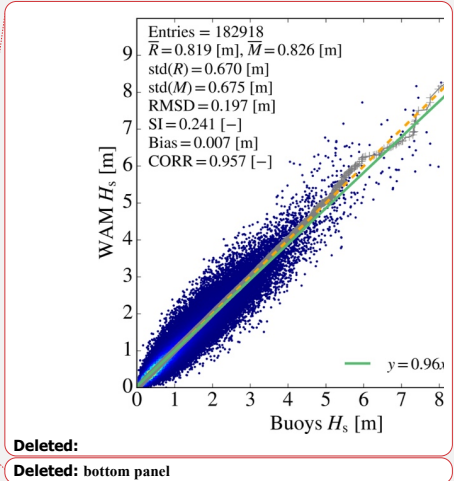
1851

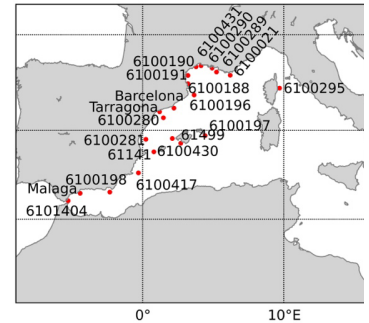
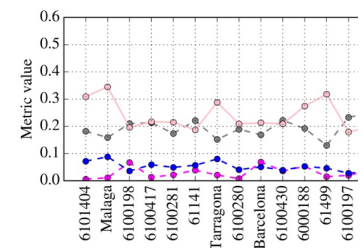
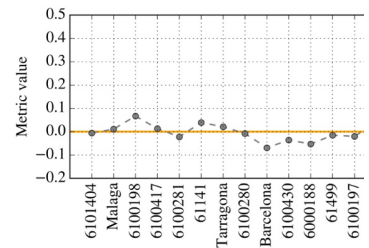
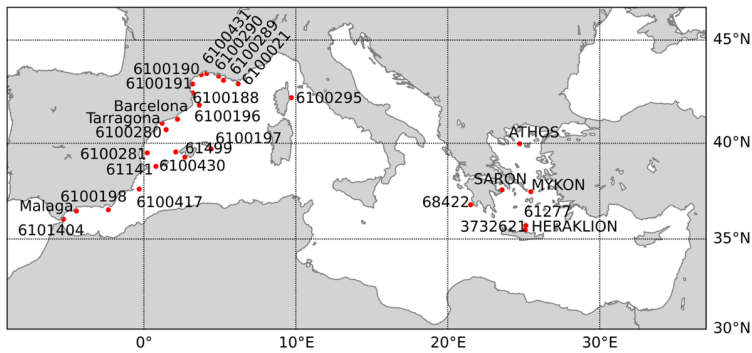
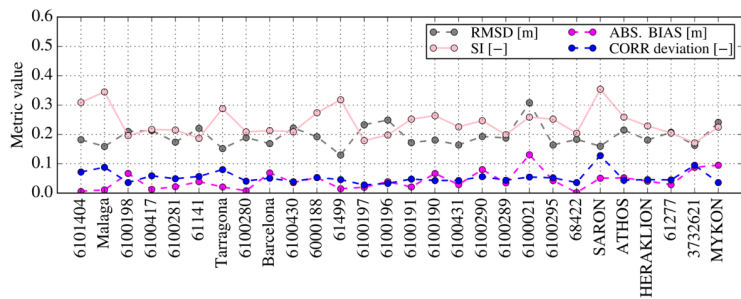
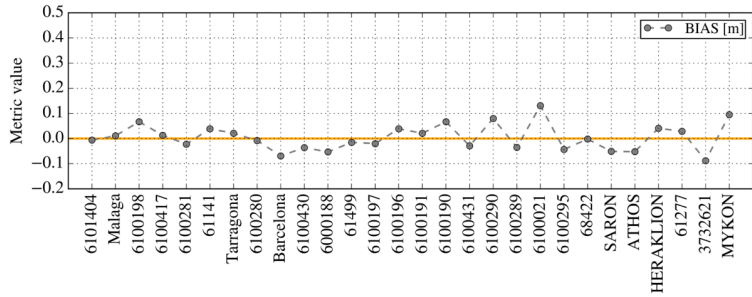
1852

1853

Figure 6. Scatter plots of: (left) significant wave height ( $H_s$ ); (right) mean wave period ( $T_m$ ) versus wave buoy observations, for the 28 stations of the Mediterranean Sea (bottom panel of Figure 2), for a three-year period (2018-2020). The graphs also include quantile-quantile plots (grey crosses), 45° reference lines (dashed orange line), and least-squares best fit lines (green line). On the top left of each picture statistical scores are given: entries refer to the number of data available for computing the statistics,  $\bar{R}$ ,  $\bar{M}$  refer to the observed and modelled value respectively,  $SI$  is the Scatter Index (defined as the standard deviation of model-observation differences relative to the observed mean), and  $CORR$  is the Pearson correlation coefficient.

1854





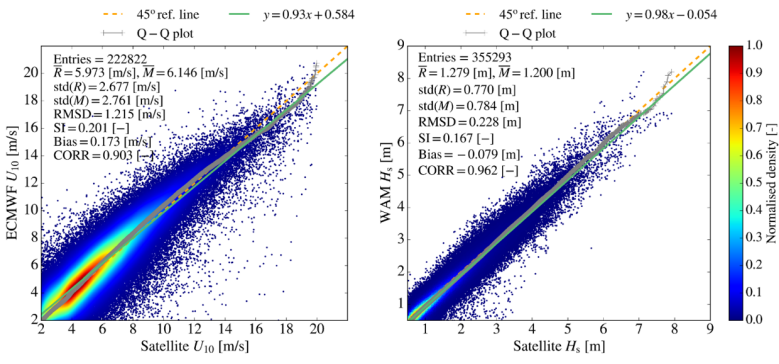
Deleted:

1857

1858  
1859  
1860  
1861

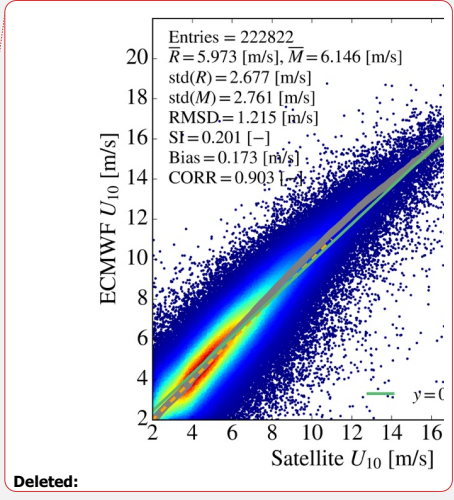
Figure 7. Significant wave height difference between model and observations (upper and middle graph) at the 28 buoy locations (lower panel) for a three-year period (2018-2020). For all locations, the performance of the model is evaluated against buoy data by means of bias, root mean square difference (RMSD), Scatter Index (SI), and deviations of the Pearson correlation coefficient from unity (CORR deviation).

1863  
1864  
1865  
1866  
1867  
1868  
1869  
1870



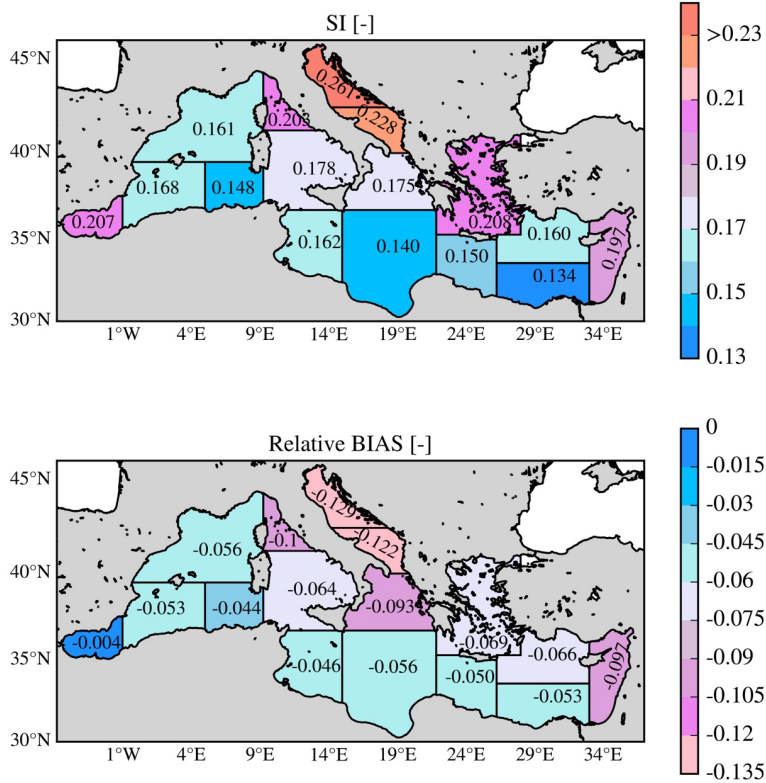
1871  
1872  
1873  
1874  
1875  
1876  
1877

Figure 8. Scatter plots of: ECMWF forcing wind speed U10 versus satellite U10 observations (left) and model significant wave height (Hs) versus satellite observations over the entire Mediterranean basin, for the three-year period (2018 – 2020).



Deleted:

1879  
1880

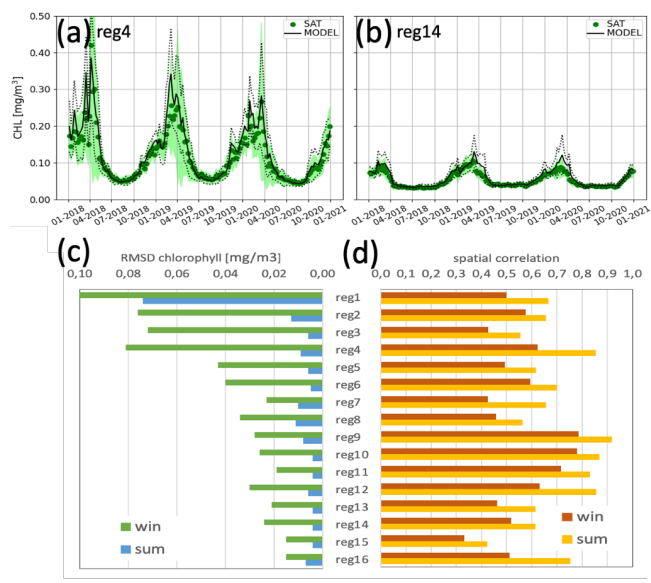


1881  
1882  
1883

Figure 9. SWH evaluation against satellite data: maps of Scatter Index (SI) (top) and Relative BIAS (bottom) over the Mediterranean Sea sub-regions (shown in Figure 3) for the three-year period (2018-2020).

1884  
1885  
1886  
1887

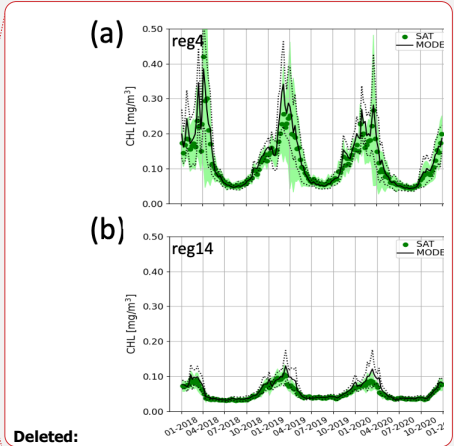
1888  
1889  
1890  
1891  
1892



1893  
1894  
1895  
1896  
1897  
1898

**Figure 10.** Timeseries of surface chlorophyll for centred composite 7-day satellite (green) and the model analysis (black) in two selected sub-regions (a and b). RMS of differences (c) and Pearson correlation (d) between maps of satellite and model forecast for the day before the assimilation in the 16 sub-regions of Figure Fig.5(c). Metrics are averaged over the winter (from Oct to Apr) and summer (from May to September) periods.

Formatted: Font: Times New Roman  
Formatted Table

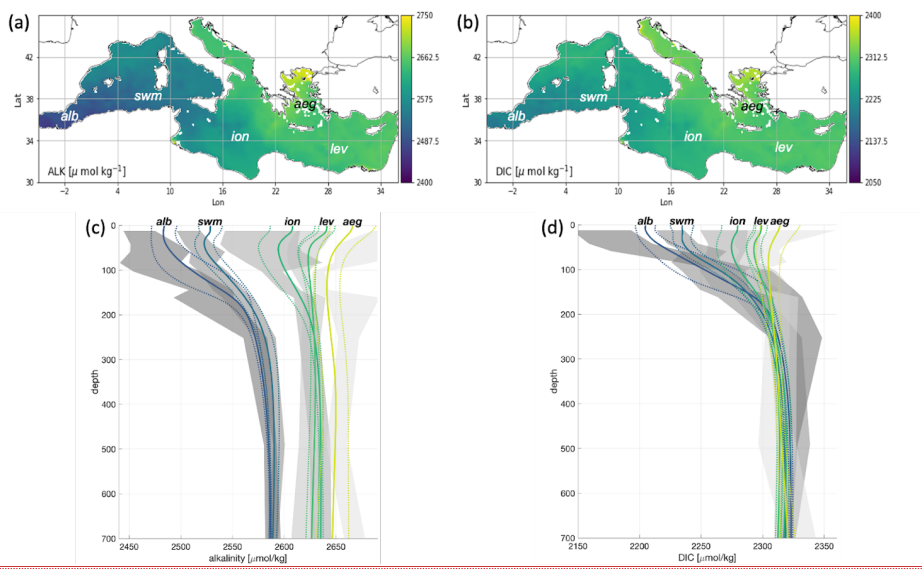


Deleted:  
Formatted: Font: Times New Roman  
Formatted: Font: (Default) Times New Roman, 9 pt, Bold, Font colour: Text 1

Deleted: Timeseries of surface chlorophyll for centred composite 7-day satellite (green) and the model forecast (black) in two selected sub-regions (a and b). Mean winter (from Oct to Apr) and summer (from May to September) RMS of the differences between satellite and model forecast for the day before the assimilation in the 16 sub-regions of Fig.5(c).

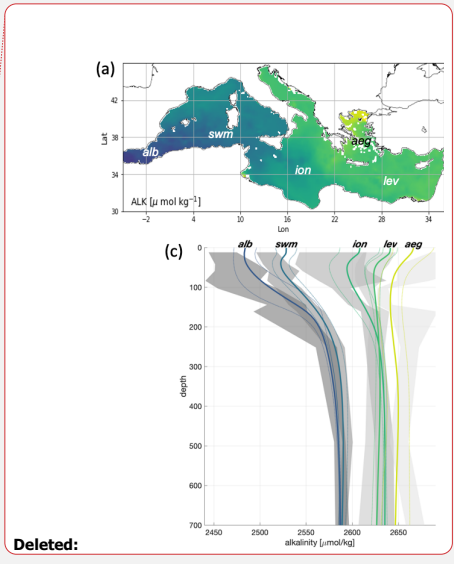


1906  
1907  
1908  
1909



1910  
1911  
1912  
1913  
1914  
1915

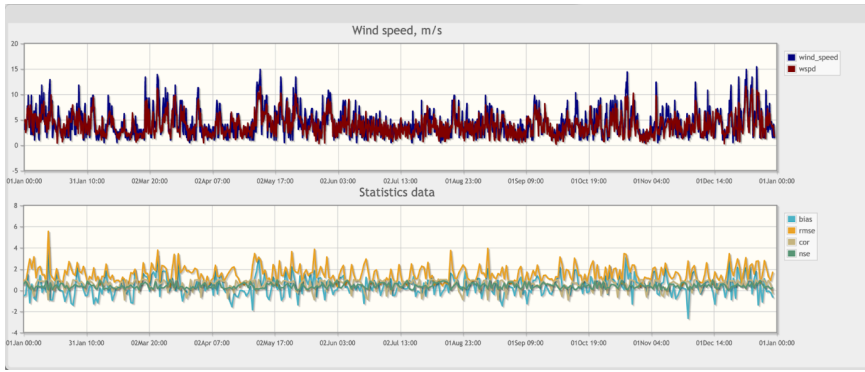
**Figure 11. Spatial distribution of modelled DIC (a) and alkalinity (b) and comparison of vertical profiles of DIC (c) and alkalinity (d) for model (average and range of variability, solid and dashed coloured lines, respectively) and Emodnet climatology (average and range of variability, black dots and lines and grey shaded areas, respectively) for selected macro areas. Climatological data are computed using historical data (Emodnet, 2018; Bakker 2014). The range of variability is the average  $\pm$  standard deviation.**



Deleted:

**Deleted:** spatial distribution of DIC (a) and alkalinity (b) and comparison of vertical profiles of DIC (c) and Alkalinity (d) for model (average and standard deviation coloured lines) and observed range of variability (grey shaded areas) for selected macro-areas. Climatological data are computed using historical data (Emodnet, 2018; Bakker 2014).

**Formatted:** Font: (Default) Times New Roman, 9 pt, Bold, Font colour: Text 1



1923  
 1924  
 1925 **Figure 12: Example of ECMWF wind speed validation with respect to METAR ground observations in 2019 in the area of the Gulf**  
 1926 **of Lion. Top panel: time series of daily mean wind speed time series from METAR station (blue line) and from ECMWF (red line).**  
 1927 **Bottom panel: time series of main skill metrics (bias, RMS Error (RMSE), Correlation Coefficient (cor), Nash-Sutcliffe Model**  
 1928 **Efficiency Coefficient (mse).**

1929  
1930  
1931  
1932

Tables

1933

Table 1 Changes in the Mediterranean forecasting components since 2008.

Year	Numerical Model Changes
<b>Physics component (PHY)</b>	
< 2008	1/16 deg., 72 vert. lev., OPA8.2 model (Madec et al., 1998) with closed lateral boundary conditions in the Atlantic (Tonani et al., 2008), 7 rivers (Ebro, Rhone, Nile, Po, Seman, Vjiose, Buna-Bojana), closed lateral boundary at Dardanelles strait, OceanVar (Dobricic et al., 2007) weekly assimilation
2009	As in 2008 with NEMOv3.1 with climatological lateral open boundary conditions in the Atlantic (Oddo et al., 2009), OceanVar with daily assimilation (Dobricic et al., 2007)
2010	As in 2009 with one-way offline coupling between NEMOv3.1 and WAM (wave)
2013	As in 2010 with two-way coupling between NEMOv3.4 and WW3 (Clementi et al., 2017a)
2014	As in 2013 but with surface atmospheric pressure forcing (Oddo et al., 2014), explicit linear free surface and SLA TAPAS(*) data assimilation (Dobricic et al., 2012)
2015	As in 2014 but with daily lateral open boundary conditions in the Atlantic
2016	As in 2015 but with monthly and grid point EOF and vertical observational error varying with depth in OceanVar
2017	1/24 deg., 141 vert. lev., NEMOv3.6 with nonlinear free surface and z-star coordinate system), 39 rivers (Table A.4)
2019	As in 2017 but with open lateral boundary conditions at the Dardanelles Strait, improved SST nudging
<b>Biogeochemistry component (BIO)</b>	
<2008	1/8 deg BFM offline coupled to PHY component
2009	Offline coupling to horizontal subsampled PHY component at 1/8 deg
2013	Coupling with 1/16 deg PHY component and Biogeochemical Data Assimilation (BDA) for Ocean Color derived Chlorophyll data (Teruzzi et al., 2014)
2015	Inclusion of the carbonate system in the model (Cossarini et al., 2015)
2017	Revision nutrient formulation in BFM (Lazzari et al., 2016) and coupling with 1/24 deg PHY component including z-star coordinate system
2018	BDA for Ocean Color coastal data (Teruzzi et al., 2018)
2019	Open lateral boundary condition at the Dardanelles Strait, revision daily light cycle in BFM (Salon et al., 2019)
2020	Open lateral boundary condition in the Atlantic Ocean and BDA with Argo biogeochemical data (Cossarini et al., 2019), and daily operational 10-days of forecast
<b>Wave component (WAV)</b>	
2017	1/24 deg WAM Cycle 4.5.4, one-way offline coupled to PHY component surface currents. Open boundary conditions from North Atlantic implementation of WAM model at 1/6 deg resolution.
2018	Implementation of data assimilation for along track Significant Wave Height (SWH) observations from Jason 3 and Sentinel 3a

Formatted Table

Formatted: Font: (Default) Times New Roman

Formatted: Font: (Default) Times New Roman

2019	WAM Cycle 4.6.2; assimilation of Cryosat-2 and Saral/Altika SWH observations tuning of wave age parameter; imposition of a limitation to the high frequency part of the spectrum based on Phillips spectrum.
2020	Assimilation of Sentinel-3b SWH observations

(\*) the Sea Level Anomaly (SLA) TAPAS product is produced to give information about the different corrections of the altimetric original signal.

Table 2. EAN estimates with in-situ observations. The differences (BIAS) and their square values (RMSD) are then averaged over the whole Mediterranean Sea region and 9 vertical layers for years 2018-2020.

Layer (m)	Temperature RMSD (°C)	Temperature bias (°C)	Salinity RMSD (PSU)	Salinity bias (PSU)
0-10	0.54	-0.02	0.19	0.01
10-30	0.82	-0.04	0.20	-0.01
30-60	0.85	0.04	0.19	-0.01
60-100	0.58	0.03	0.16	-0.02
100-150	0.41	-0.01	0.13	-0.01
150-300	0.28	-0.02	0.08	0.0000
300-600	0.18	0.00	0.05	-0.01
600-1000	0.09	-0.02	0.03	0.00
1000-2000	0.05	0.01	0.02	0.00

Table 3. Gibraltar mean and standard deviation volume transports [Sv] from the Med-PHY numerical system averaged in the period 2018-2020 compared to literature values (current meter observations from October 2004 to January 2009).

Gibraltar Transport	Model [2018-2020]	Literature	
		Soto-Navarro et al. (2010) [2004-2009]	al. Literature Candela (2001) [1994-1996]
Net	0.040±0.017	0.038 ± 0.007	0.04 (max: 0.26, min: 0.11)
Eastward	0.91±0.01	0.81 ± 0.06	1.01 (max: 1.12, min: 0.91)
Westward	0.87±0.06	0.78 ± 0.05	0.97 (max: 0.83, min: 1.11)

- Formatted Table ... [1]
- Formatted ... [2]
- Formatted ... [3]
- Formatted ... [6]
- Deleted: 0.02
- Deleted: -0.01
- Formatted ... [4]
- Formatted ... [5]
- Formatted ... [7]
- Formatted ... [8]
- Formatted ... [9]
- Formatted ... [12]
- Deleted: 0.04
- Deleted: 0.01
- Formatted ... [10]
- Formatted ... [11]
- Formatted ... [13]
- Formatted ... [14]
- Formatted ... [15]
- Formatted ... [16]
- Formatted ... [18]
- Deleted: -0.04
- Deleted: 0.01
- Formatted ... [17]
- Formatted ... [19]
- Formatted ... [20]
- Formatted ... [21]
- Formatted ... [22]
- Formatted ... [24]
- Deleted: -0.03
- Deleted: 0.02
- Formatted ... [23]
- Formatted ... [25]
- Formatted ... [26]
- Formatted ... [27]
- Formatted ... [28]
- Formatted ... [31]
- Deleted: 0.01
- Deleted: 0.01
- Formatted ... [29]
- Formatted ... [30]
- Formatted ... [32]
- Formatted ... [33]
- Formatted ... [34]
- Formatted ... [35]
- Formatted ... [38]
- Deleted: 0.02
- Deleted: 0.02
- Formatted ... [36]
- Formatted ... [37]
- Formatted ... [39]
- Formatted ... [40]
- Formatted ... [41]

1993

1994

1995

1996

1997

1998

1999

2000

2001

2002

Table 4. EAN RMSD and Bias of SST and SLA RMSD averaged in the whole Mediterranean Sea and 16 sub-regions (see Figure 3) for the period 2018-2020.

Region	Temperature RMSD (°C)	Temp. Bias (°C)	Sea Level Anomaly RMSD (cm)
MED SEA	0.54	0.12	3.8
REGION 1	0.69	-0.05	5.3
REGION 2	0.53	0.06	4.3
REGION 3	0.53	-0.01	3.2
REGION 4	0.55	0.15	5.1
REGION 5	0.47	0.13	3.1
REGION 6	0.49	0.15	3.5
REGION 7	0.51	0.22	5.0
REGION 8	0.55	0.16	3.8
REGION 9	0.51	0.14	3.4
REGION 10	0.58	0.20	2.3
REGION 11	0.63	0.08	NA
REGION 12	0.49	-0.01	4.0
REGION 13	0.59	0.14	3.6
REGION 14	0.57	0.16	3.3
REGION 15	0.53	0.13	4.4
REGION 16	0.52	0.24	3.1

**Deleted:** EAN RMSD of SST and SLA averaged in the whole Mediterranean Sea and 16 sub-regions (see Figure 3) for the period 2018-2020.

**Formatted:** Font: (Default) Times New Roman, Font colour: Text 1, English (UK)

**Formatted:** Font colour: Text 1, English (UK)

**Formatted Table**

**Formatted:** Font: (Default) Times New Roman, Font colour: Text 1

**Formatted:** Font: (Default) Times New Roman, Font colour: Text 1

**Formatted:** Font: (Default) Times New Roman, Font colour: Text 1

**Formatted:** Font: (Default) Times New Roman, Font colour: Text 1

**Formatted:** Font: (Default) Times New Roman, Font colour: Text 1

**Formatted:** Font: (Default) Times New Roman, Font colour: Text 1

**Formatted:** Font: (Default) Times New Roman, Font colour: Text 1

**Formatted:** Font: (Default) Times New Roman, Font colour: Text 1

**Formatted:** Font: (Default) Times New Roman, Font colour: Text 1

**Formatted:** Font: (Default) Times New Roman, Font colour: Text 1

**Formatted:** Font: (Default) Times New Roman, Font colour: Text 1

**Formatted:** Font: (Default) Times New Roman, Font colour: Text 1

**Formatted:** Font: (Default) Times New Roman, Font colour: Text 1

**Formatted:** Font: (Default) Times New Roman, Font colour: Text 1

**Formatted:** Font: (Default) Times New Roman, Font colour: Text 1

**Formatted:** Font: (Default) Times New Roman, Font colour: Text 1

**Formatted:** Font: (Default) Times New Roman, Font colour: Text 1

**Formatted:** Font: (Default) Times New Roman, Font colour: Text 1

2006  
2007  
2008  
2009

Table 5. RMS of the difference between MedBFM and Argo-BGC profiles for ecosystem metrics. RMSD of the metrics are computed for each profile, then averaged over time and space considering the 2017-2020 period. Sub-regions: swm (reg2+reg4), nwm (reg3), tyr (reg5+reg6), adr (reg10+reg11), ion (reg7+reg8+reg9) and lev (reg13+reg14+reg15+reg16).

	vertical metrics [units]	mean value [range]	RMSD					
			swm	nwm	tyr	adr	ion	lev
Chlorophyll	Average 0-200 m [mg/m3]	[0.01-1.5]	0.05	0.06	0.06	0.03	0.03	0.03
	Deep chlorophyll maximum depth [m]	80 [60-130]	10	11	7	6	16	18
	Mixed Bloom Winter depth [m]	40 [20-90]	25	39	35	29	16	27
Nitrate	Average 0-200 m [mmol/m3]	[0.1-8.0]	-	0.72	0.45	-	0.52	0.54
	Nitracline depth [m]	90 [70-150]	-	48	44	-	34	42
Oxygen	Average 0-200 m [mmol/m3]	220 [190-250]	11.5	8.5	7.9	10.8	4.7	5.7
	Maximum oxygen depth [m]	[60-120]	24	16	17	19	34	14

Deleted: ¶

Formatted Table

Deleted: 200m

Deleted: 200m

Deleted: 200m

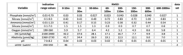
2010  
2011  
2012  
2013

2018  
 2019  
 2020  
 2021  
 2022  
 2023  
 2024  
 2025

Table 6. RMSD of the difference between model and climatological profiles at different depths evaluated in the 2017-2020 reference period. Statistics are computed using the 16 sub-regions in Figure 3. Reference datasets for validation (last column) are: (1) EMODnet data collections (Bugu et al., 2018) integrated with additional oceanographic cruises (Cossarini et al., 2015), and (2) Socat dataset (Baker et al 2014).

Variable	indicative range values	RMSD								data set
		0-10m	10-30m	30-60m	60-100m	100-150m	150-300m	300-600m	600-1000m	
Phosphate [mmol/m <sup>3</sup> ]	0.01-0.70	0.03	0.03	0.027	0.023	0.043	0.028	0.040	0.027	1
Nitrate [mmol/m <sup>3</sup> ]	0.1-9.0	0.42	0.41	0.49	0.72	0.83	0.72	1.09	0.83	1
Ammonia [mmol/m <sup>3</sup> ]	0.01-1.23	0.41	0.17	0.15	0.23	0.30	0.32	0.44	0.54	1
Silicate [mmol/m <sup>3</sup> ]	0.1-7.0	1.5	1.5	1.3	0.9	0.9	0.7	0.7	0.8	1
Oxygen [mmol/m <sup>3</sup> ]	190-260	5.9	5.7	6.4	4.2	5.2	4.3	8.6	5.8	1
DIC [μmol/kg]	2100-2400	42.2	37.6	28.1	17.1	16.7	7.7	9.9	3.8	1
Alkalinity [μmol/kg]	2360-2730	41.7	34.4	26.0	19.1	12.5	12.1	9.0	7.0	1
pH	7.0-8.2	0.04	0.03	0.03	0.02	0.01	0.01	0.01	0.01	1
pCO2 [μatm]	250-550	46								2

**Deleted:** RMSD of the difference between model and climatological profiles at different depths evaluated in the 2017-2020 reference period. Statistics are computed using the 16 sub-regions in Figure 3.

**Deleted:**  ... [59]

**Page 52: [1] Formatted Table    giovanni coppini    15/05/2023 12:23:00**

Formatted Table

▲  
**Page 52: [2] Formatted    giovanni coppini    15/05/2023 12:23:00**

Font: Times New Roman

▲  
**Page 52: [3] Formatted    giovanni coppini    15/05/2023 12:23:00**

Font: Times New Roman

▲  
**Page 52: [4] Formatted    giovanni coppini    15/05/2023 12:23:00**

Font: (Default) Times New Roman, Font colour: Text 1

▲  
**Page 52: [5] Formatted    giovanni coppini    15/05/2023 12:23:00**

Font: Times New Roman

▲  
**Page 52: [6] Formatted    giovanni coppini    15/05/2023 12:23:00**

Font: Times New Roman

▲  
**Page 52: [7] Formatted    giovanni coppini    15/05/2023 12:23:00**

Font: Times New Roman

▲  
**Page 52: [8] Formatted    giovanni coppini    15/05/2023 12:23:00**

Font: Times New Roman

▲  
**Page 52: [9] Formatted    giovanni coppini    15/05/2023 12:23:00**

Font: Times New Roman

▲  
**Page 52: [10] Formatted    giovanni coppini    15/05/2023 12:23:00**

Font: (Default) Times New Roman, Font colour: Text 1

▲  
**Page 52: [11] Formatted    giovanni coppini    15/05/2023 12:23:00**

Font: Times New Roman

▲  
**Page 52: [12] Formatted    giovanni coppini    15/05/2023 12:23:00**

Font: Times New Roman

▲  
**Page 52: [13] Formatted    giovanni coppini    15/05/2023 12:23:00**

Font: (Default) Times New Roman, Font colour: Text 1

▲  
**Page 52: [14] Formatted    giovanni coppini    15/05/2023 12:23:00**

Font: Times New Roman



Font: Times New Roman

▲  
**Page 52: [17] Formatted** giovanni coppini 15/05/2023 12:23:00

Font: Times New Roman

▲  
**Page 52: [18] Formatted** giovanni coppini 15/05/2023 12:23:00

Font: Times New Roman

▲  
**Page 52: [19] Formatted** giovanni coppini 15/05/2023 12:23:00

Font: (Default) Times New Roman, Font colour: Text 1

▲  
**Page 52: [20] Formatted** giovanni coppini 15/05/2023 12:23:00

Font: Times New Roman

▲  
**Page 52: [21] Formatted** giovanni coppini 15/05/2023 12:23:00

Font: Times New Roman

▲  
**Page 52: [22] Formatted** giovanni coppini 15/05/2023 12:23:00

Font: Times New Roman

▲  
**Page 52: [23] Formatted** giovanni coppini 15/05/2023 12:23:00

Font: Times New Roman

▲  
**Page 52: [24] Formatted** giovanni coppini 15/05/2023 12:23:00

Font: Times New Roman

▲  
**Page 52: [25] Formatted** giovanni coppini 15/05/2023 12:23:00

Font: (Default) Times New Roman, Font colour: Text 1

▲  
**Page 52: [26] Formatted** giovanni coppini 15/05/2023 12:23:00

Font: Times New Roman

▲  
**Page 52: [27] Formatted** giovanni coppini 15/05/2023 12:23:00

Font: Times New Roman

▲  
**Page 52: [28] Formatted** giovanni coppini 15/05/2023 12:23:00

Font: Times New Roman

▲  
**Page 52: [29] Formatted** giovanni coppini 15/05/2023 12:23:00

Font: (Default) Times New Roman, Font colour: Text 1

▲

**Page 52: [32] Formatted giovanni coppini 15/05/2023 12:23:00**

Font: (Default) Times New Roman, Font colour: Text 1

▲  
**Page 52: [33] Formatted giovanni coppini 15/05/2023 12:23:00**

Font: Times New Roman

▲  
**Page 52: [34] Formatted giovanni coppini 15/05/2023 12:23:00**

Font: Times New Roman

▲  
**Page 52: [35] Formatted giovanni coppini 15/05/2023 12:23:00**

Font: Times New Roman

▲  
**Page 52: [36] Formatted giovanni coppini 15/05/2023 12:23:00**

Font: (Default) Times New Roman, Font colour: Text 1

▲  
**Page 52: [37] Formatted giovanni coppini 15/05/2023 12:23:00**

Font: Times New Roman

▲  
**Page 52: [38] Formatted giovanni coppini 15/05/2023 12:23:00**

Font: Times New Roman

▲  
**Page 52: [39] Formatted giovanni coppini 15/05/2023 12:23:00**

Font: (Default) Times New Roman, Font colour: Text 1

▲  
**Page 52: [40] Formatted giovanni coppini 15/05/2023 12:23:00**

Font: Times New Roman

▲  
**Page 52: [41] Formatted giovanni coppini 15/05/2023 12:23:00**

Font: Times New Roman

▲  
**Page 52: [42] Formatted giovanni coppini 15/05/2023 12:23:00**

Font: Times New Roman

▲  
**Page 52: [43] Formatted giovanni coppini 15/05/2023 12:23:00**

Font: Times New Roman

▲  
**Page 52: [44] Formatted giovanni coppini 15/05/2023 12:23:00**

Font: Times New Roman

▲  
**Page 52: [45] Formatted giovanni coppini 15/05/2023 12:23:00**

Font: (Default) Times New Roman, Font colour: Text 1

Font: Times New Roman

▲  
**Page 52: [48] Formatted** giovanni coppini 15/05/2023 12:23:00

Font: Times New Roman

▲  
**Page 52: [49] Formatted** giovanni coppini 15/05/2023 12:23:00

Font: (Default) Times New Roman, Font colour: Text 1

▲  
**Page 52: [50] Formatted** giovanni coppini 15/05/2023 12:23:00

Font: Times New Roman

▲  
**Page 52: [51] Formatted** giovanni coppini 15/05/2023 12:23:00

Font: Times New Roman

▲  
**Page 52: [52] Formatted** giovanni coppini 15/05/2023 12:23:00

Font: Times New Roman

▲  
**Page 52: [53] Formatted** giovanni coppini 15/05/2023 12:23:00

Font: Times New Roman

▲  
**Page 52: [54] Formatted** giovanni coppini 15/05/2023 12:23:00

Font: Times New Roman

▲  
**Page 52: [55] Formatted** giovanni coppini 15/05/2023 12:23:00

Font: Times New Roman

▲  
**Page 52: [56] Formatted** giovanni coppini 15/05/2023 12:23:00

Font: Times New Roman

▲  
**Page 52: [57] Formatted** giovanni coppini 15/05/2023 12:23:00

Font: Times New Roman

▲  
**Page 52: [58] Formatted Table** giovanni coppini 15/05/2023 12:23:00

Formatted Table

▲  
**Page 55: [59] Deleted** giovanni coppini 07/05/2023 16:52:00  
▲